Universität Bremen

Characterization of the interactions between molecular chaperones and the amyloid protein Huntingtin throughout its aggregation pathway

Dissertation zur Erlangung des akademischen Grades des Doctor rerum naturalium (Dr. rer. nat.)

eingereicht im Fachbereich 02 Biologie/Chemie

der Universität Bremen

vorgelegt von

Merve Özel

March 2024

Reviewer 1: Prof. Dr. Janine Kirstein

Reviewer 2: Prof. Dr. Erich E. Wanker

Date of Defense: 02.05.2024

Table of Contents

0. Summary

Protein misfolding and subsequent aggregation characterize most neurodegenerative diseases and are associated with impaired protein homeostasis (proteostasis). As prominent components of the proteostasis network, molecular chaperones have been identified as modulators of protein aggregation. Understanding their mechanisms of action paves the way for their use as a therapeutic strategy against neurodegenerative diseases.

Huntington's disease (HD) is an inherited neurodegenerative disease caused by the abnormal expansion of CAG repeats in the first exon of the Huntingtin protein. Aggregation of the pathogenic HTTExon1 is suggested as the primary cause of neuronal deterioration.

Previously, it was shown that a trimeric chaperone complex composed of Hsc70, DNAJB1, and Apg2 can inhibit pathogenic HTTExon1 aggregation and disaggregate preformed HTTExon1 fibrils. As a member of the J-domain protein (JDP) family, and a co-chaperone of Hsc70, DNAJB1 is known to recognize protein substrates, to transfer them to Hsc70, and stimulate the ATPase activity of Hsc70. Recently, a binding interface between DNAJB1 and HTTExon1 has been identified and this work has contributed to the analysis of the effect of this binding site in HTTExon1 suppression and disaggregation activities by the trimeric chaperone complex. *In vitro* analyses showed that this binding site and unique features of DNAJB1 conferred specificity and functionality, distinguishing it from other JDPs.

Furthermore, association between the trimeric chaperones and HTTExon1 along its aggregation pathway was investigated. The data revealed that DNAJB1 and Hsc70 associate with aggregating HTTExon1 only in the presence of each other and an intact ATPase cycle, suggesting a cooperative association of these chaperones with HTTExon1 during aggregation. This association was found to be stable to detergent, suggesting that irreversible sequestration of chaperones in HTTExon1 aggregates is associated with the eventual failure of the trimeric chaperone complex in suppressing HTTExon1 aggregation.

0.1 Zusammenfassung

Proteinfehlfaltung und anschließende Aggregation kennzeichnen die meisten neurodegenerativen Erkrankungen und werden mit einer gestörten Proteinhomöostase (Proteostase) in Verbindung gebracht. Als bedeutende Komponenten des Proteostasenetzwerks wurden molekulare Chaperone als Modulatoren der Proteinaggregation identifiziert. Ein Verständnis ihrer Wirkmechanismen ist Voraussetzung, um sie als therapeutische Zielmoleküle gegen neurodegenerative Erkrankungen zu etablieren.

Chorea Huntington ist eine vererbbare neurodegenerative Erkrankung, die durch eine abnormale Expansion von CAG-Wiederholungen im ersten Exon des Huntingtin-Proteins verursacht wird. Es wird spekuliert, dass die Aggregation des pathogenen HTTExon1 die Hauptursache für die Neurodegeneration ist.

In Vorarbeiten konnte gezeigt werden, dass ein trimerer Chaperonkomplex bestehend aus Hsc70, DNAJB1 und Apg2 die pathogene HTTExon1-Aggregation unterdrücken und auch HTTExon1 Fibrillen disaggregieren kann. Als Mitglied der J-Domänen-Proteinfamilie (JDP) und Co-Chaperon von Hsc70 ist DNAJB1 dafür bekannt, Proteinsubstrate zu erkennen, sie auf Hsc70 zu übertragen und die ATPase-Aktivität von Hsc70 zu stimulieren. Kürzlich wurde die Interaktionsstelle zwischen DNAJB1 und HTT identifiziert. Diese Arbeit hat zur Charakterisierung dieser Bindungsstelle und Aufklärung der Funktion für die Suppressions- und Disaggregationsaktivitäten des trimeren Chaperonkomplexes beigetragen. *In vitro* Analysen haben gezeigt, dass diese Bindungsstelle die Spezifität zur Substraterkennung von DNAJB1 vermittelt und entscheidend für die Funktionalität des Chaperonkomplex zur Modulierung von HTTExon1 ist.

Darüber hinaus wurde die Assoziation zwischen den Chaperonen und HTTExon1 entlang des HTTExon1-Aggregationsweges untersucht. Die Daten zeigten, dass DNAJB1 und Hsc70 nur in Gegenwart des jeweils anderen Partners und eines intakten ATPase-Zyklus mit aggregierendem HTTExon1 assoziieren, was auf eine kooperative Assoziation dieser Chaperone mit HTTExon1 während der Aggregation hindeutet. Diese Assoziation erwies sich bei der Behandlung mit Detergenzien als stabil, was darauf hindeutet, dass die irreversible Sequestrierung von Chaperonen in HTTExon1-

Aggregaten mit dem letztendlichen Versagen der Unterdrückung der HTTExon1 Aggregation durch den Chaperonkomplex einhergeht.

1. Authorship Disclaimer

For this dissertation, the work presented was done under the supervision of Prof. Dr. Janine Kirstein in her research group at the University of Bremen. Contributions of my colleagues and MSc and BSc students of the University of Bremen that I supervised, are indicated in the results section and are listed below. These data were essential to include in the dissertation since they contribute to the overall experiments I performed.

Dr. Yasmin Richter performed FRET-based suppression of aggregation assays for the DNAJB1^{H32Q}, DNAJB1$^{H32Q\text{-}H244A}$ and DNAJB1^{H244Q} mutations.

Mohamed Elbediwi has performed the disaggregation assays in Section 3.3. during his lab rotation under my supervision.

Kunal Gharat has performed the initial experiments with binding of DNAJB1^{H32Q} mutant to HTTExon1 fibrils in FRET/Filter retardation binding assay during his lab rotation under my supervision.

Kaatje Knüwer performed the disaggregation assays of fibrils grown at different temperatures during her PM4 module and bachelor thesis under my supervision.

Georg Bossenz worked with me to establish the FRET/Filter retardation binding assay and performed experiments for the association of DNAJB1/Hsc70 to HTTExon1 in the presence of AMP-PNP. He also performed initial analysis of chaperone binding at different stages on the aggregation pathway during his Master´s thesis under my supervision.

2. Introduction

Proteins are essential components of living organisms and are involved in a variety of intracellular functions. Upon translation by the ribosome as a linear chain of amino acids, proteins need to fold into a three-dimensional structure to be biologically active. However, proteins can misfold or fail to maintain their native functional state for several different reasons within the cell. This could be due to the intracellular crowding, environmental stress, or inherent mutations in the protein itself.

Misfolded proteins accumulate in neurons, and failure to clear the aggregates leaves neurons vulnerable to dysfunction or even cell death. Protein misfolding is one of the most pronounced factors underlying neurodegenerative diseases. Alzheimer's, Parkinson's, Amyotrophic Lateral Sclerosis (ALS) and Huntington's are among the most prominent neurodegenerative diseases. Despite significant research efforts, the extreme complexity underlying the neuronal damage caused by protein misfolding has resulted in a lack of effective treatments for these devastating diseases.

2.1 Huntington´s Disease

Huntington's disease (HD), is an autosomal-dominant, inherited neurodegenerative disease that progressively affects the nervous system, resulting in severe motor, cognitive, and mental dysfunction. Historically, the disease was perceived as demonic because the symptoms of chorea were seen as jerky dance movements that led to the social ostracism of those affected with the disease (Vale and Cardoso, 2015). George Huntington, after whom the disease was named, provided the first scientific and medical description of the disease in 1872 (Bhattacharya, 2016). He described it as a neurological disorder, which is inherited, and emphasized that it tends to develop at a late stage (Huntington, 1872). The global estimated prevalence of the disease is within the range of 2.7 to 4.88 per 100,0000 people (Medina *et al*., 2022). The onset of the disease is usually between the ages of 30 and 50 years, with rare juvenile cases occurring before the age of 20 years (Bates *et al.*, 2015; Roos *et al.,* 2010). Patients with HD have an average life expectancy of 15-18 years after the onset of the disease (Caron *et al.,* 1993). Although clinical trials are underway, there is still no cure that can prevent or reverse the effects of this devastating disease.

2.1.1 Genetics and Mechanism of Pathogenesis in HD

The genetic features of the pathogenic Huntingtin were first published in 1993 by The Huntington´s Disease Collaborative Research Group. The gene that encodes Huntingtin protein (HTT) is located at chromosome 4 (4.16) and consists of CAG (Cytosine-Adenosine-Guanine) trinucleotide repeats in the first exon (MacDonald *et al.,* 1993). Aberrant expansion of CAG repeats is known to be the primary cause of the disease, with individuals affected by HD found to have CAG repeat expansions of more than 35 repeats, strongly linking the disease to this expansion (Kremer *et al*., 1994; Mangiarini *et al.,* 1996). An inverse correlation between CAG repeat length and age of onset has been demonstrated, with CAG repeats >75 associated with the rare juvenile form of HD (Lee *et al.,* 2012).

HTT is ubiquitously expressed in all tissues, with highest expression observed in the nervous system and testes (Li *et al*., 1993; DiFiglia M. *et al.,* 1995; Schulte and Littleton, 2011). Although the striatum is most vulnerable to pathogenesis (Vonsattel *et al.,* 1985; Hodges *et al.,* 2006), high levels of neuronal degeneration extend to the cerebral cortex and hippocampus (Mann *et al.,* 1993; Montoya *et al.,* 2006; Han *et al*., 2010; Ransome *et al.,* 2012). Proteolytic cleavage of mutant HTT by caspases and calpains results in intracellular aggregation in neurons and induces pathogenesis in peripheral tissues (Gafni *et al.,* 2002; Wellington and Lunkes *et al*., 2002). Within the cell, HTT is mainly found in the cytoplasm, nuclear inclusions of mutant HTT exhibit distinct mechanisms of toxicity (Hackam and Peters *et al.,* 1999; Riguet *et al.,* 2021). Although various organelles such as the endoplasmic reticulum, Golgi apparatus and endosomes have been found to co-localize with HTT (Schulte *et al*., 2011), the cellular function of HTT is poorly understood. To date, HTT has been implicated in transcription, endosomal trafficking, vesicular trafficking, signalling, regulation of autophagy, and morphological maintenance of tissues (Saudou and Humbert, 2016). However, since the exact functions of HTT are still not understood, the mechanism of cytotoxicity remains unclear. An increase in HD phenotype in HTT knockout mouse models suggests loss-of-function mechanisms underlying the pathogenesis (Dragatsis *et al.,* 2000; Cattaneo *et al.,* 2005; Pircs *et al.,* 2018). On the other hand, dysregulation of transcription, axonal transport, autophagy and endoplasmic reticulum activities by the cleavage fragments and inclusions of HTT raises the prospect of toxic gain of function (Steffan *et al.,* 2000;

Piccioni *et al.,* 2002; Martin and El-Daher *et al*., 2015). Furthermore, components of intracellular protein quality control network are thought to be compromised by getting sequestered into amyloid inclusions, leading to increased protein misfolding and toxicity (Hay *et al.,* 2004; Park *et al.,* 2013). Therefore, several different pathological mechanisms may exist, but the exact cause of toxicity in HD remains controversial.

2.1.2 Pathogenic Huntingtin Exon1

Full-length HTT consists of 3144 amino acids and has a molecular weight of 350 kDa. Structural studies lay the foundation to unravel the aggregation mechanism of HTT. Full-length HTT protein has been expressed and purified from mammalian cells and its structure solved by cryo-EM, yet due to high flexibility, the first exon has remained unresolved (Guo *et al.,* 2018). This 3D structure has revealed that HTT is predominantly α-helical and contains multiple HEAT (**H**untingtin, **E**longation factor 3, protein phosphatase 2**A**, **T**OR1) repeats which are thought to act as a multivalent scaffold for the assembly of multiple proteins.

The aggregation-prone fragment, HTTExon1 comprises three domains: an N-terminal 17-residue-long region (N17), a polyQ domain and a C-terminal proline-rich domain (PRD), which consists of two proline stretches, P1 and P2, harbouring 11 and 10 residues respectively and interspaced by a short proline/glutamine rich segment.

The long-standing "linear lattice" model proposes that polyQ adopts a random-coil structure for both physiological and expanded polyQ in monomeric HTTExon1. (Bennett *et al.,* 2002). However, the cytotoxicity is thought to be related to the increased affinity for other proteins due to an increased number of binding epitopes that appear in the expanded polyQ in the pathogenic HTTExon1 (Legleiter *et al.,* 2009; Newcombe *et al.,* 2018).

The morphology of HTTExon1 fibrils is similar to that of other amyloids such as α-synuclein (α-syn) associated with Parkinson´s disease or amyloid-β (Aβ) associated with Alzheimer´s disease, with extended cross-beta sheets forming the stable core of the fibrils **(Fig. 2.1)**. Inside the cell, HTTExon1 forms large aggregates that are observed to be insoluble in the strong detergent SDS (Mitsui *et al.,* 2002; Busch *et al*., 2003; Kim *et al.,* 2016). *In situ* cryo-ET analysis provided detailed insight into

HTTExon1 inclusions in an intact neuron, showing that µm-sized inclusions interact with the ER membranes erroneously and cause defects in the membrane integrity (Bäuerlein *et al.,* 2017). Even though the structural details of the HTTExon1 fibrils at the atomistic level have not yet been fully elucidated, new studies are beginning to shed light on the key aspects that drive amyloid formation and ultimate cytotoxicity. Recently, residue-specific NMR analyses have shown that the expanded polyQ stretch adopts predominantly α-helical conformations and that the stability of the α-helices outweighs the number of glutamines in the defining aggregation propensity and the resulting fibrillar structure (Elena-Real *et al.,* 2023). Another detailed integrative analysis using EM, NMR and molecular dynamics simulations has revealed a structure of HTTExon1 fibrils showing that flanking domains do not interact with the polyQ domain, leaving it accessible for interaction partners (Helabad *et al*., 2023). In this study, the PRD was shown to dock to the N17 region, thereby preventing it from interacting with other proteins, but it was noted that this conformation, and the accessibility of the flanking domains, can change under different cellular conditions. Helabad *et al.* further stated that the stability of the rigid polyQ core is provided by the hydrogen bonds between the expanded glutamines, consistent with the long-standing "polar zipper" hypothesis, in which the expanded polyglutamine strand is thought to act as a polar zipper, with pleated beta strands linked by hydrogen bonds, giving the structure a zipper-like appearance (Perutz *et al.,*1994).

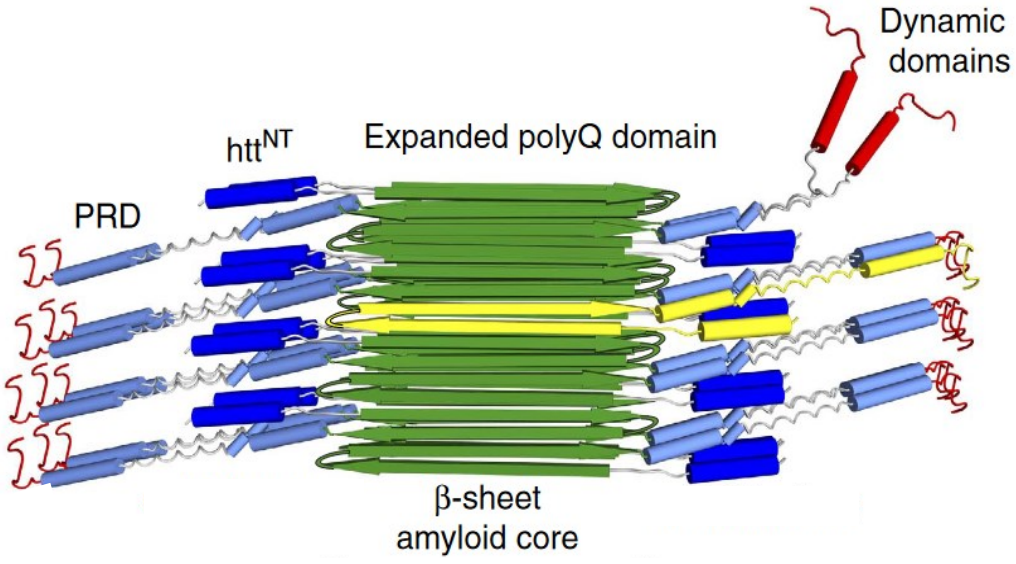

Figure 2.1: Structural model of fibrillar mutant HTTExon1.

PolyQ core (green) is flanked by the immobilized N17 (dark blue) and proline-rich domain (PRD) (light blue). The clustered, rigid polyQ core is composed of HTTEx1 monomers rich in β-hairpin-structures (yellow). The PRDs exhibit greater degree of structural flexibility (Image adapted from Lin *et al.,* 2017).

2.1.3 Aggregation Theories on HTT

The mechanism of progressive aggregation of HTTExon1 is not fully understood. However, a two-step process of primary and secondary nucleation is one of the most widely speculated aggregation mechanisms. According to this model, fibril assembly begins with the formation of nuclei, which are presumed to be unstable oligomeric entities that occur during the lag phase of fibril formation (Cohen *et al.,* 2012; Wagner *et al.,* 2018). The subsequent binding of monomers or oligomers to the nucleus gives rise to the formation of protofibrils which are short, metastable assemblies rich in β-sheets. This step is thought to be responsible for the rapid growth of the fibrils (Chiti and Dobson, 2006; Hasecke *et al.,* 2018). The time required for the formation of "nuclei" is defined as the lag phase. However, the addition of preformed fibrillar moieties, or "seeds", to an aggregation-prone protein can shorten and even eliminate the lag phase (Scherzinger et al., 1999; Cohen *et al.,* 2012; Ast *et al.* 2018). The next step is the self-assembly of protofibrils into highly ordered, mature amyloid fibrils, which may involve restructuring of the aggregates (Harper and Lansbury 1997; Poirier *et al.,* 2002). It is thought that primary nucleation is favored, and aggregation kinetics accelerated by an increased polyQ length and higher protein concentrations (Thakur *et al.,* 2009; Kar *et al.,* 2011; Chen and Wolynes, 2017; Wagner *et al.,* 2018). A proposed model for the aggregation of the pathogenic HTTExon1 involves nucleated branching following primary nucleation (Wagner *et al.,* 2018). In this model, new branches grow and adhere to preformed fibrils, and this process has been defined as "nucleated branching", a type of secondary nucleation mechanism. New branches are added in proportion to the concentration of the preformed aggregate during this self-catalyzing process. Another approach involves the transient, globular or spherical oligomers to which monomers are added over time become wider but not longer. The resulting aggregates coalesce with each other and increase in size (Duim *et al.,* 2014)

Increasing evidence suggests that intrinsically disordered proteins undergo liquid-liquid phase separation (LLPS) prior to amyloid fibril formation (Xing *et al.,* 2021; Ahmad *et al.,* 2022; Zhang *et al*., 2023). To date, amyloid peptides such as α-synuclein (Ray *et al.,* 2020), amyloid-β (Gui and Sudhakar *et al*., 2023), tau (Ambadipudi *et al.,* 2017; Kanaan *et al.,* 2020), TDP-43 (Babinchak *et al.,* 2020) and HTTExon1 (Peskett *et al*., 2018) have been shown to phase separate and subsequently form mature aggregates.

Modulation of HTTExon1 aggregation by the polyQ flanking sequences were investigated as contributing factors to aggregation kinetics. The N17 region is thought to be the driver of initial aggregation (Crick *et al.,* 2013; Arndt *et al.,* 2015; Pandey *et al.,* 2018). It has been proposed that this is caused by the self-assembly of this domain, leading to the formation of oligomers enriched in α-helices that propagate the association of polyQ domains (Williamson *et al.,* 2010). The N17 region has also been suggested to anchor HTTExon1 to the cell membrane by its amphipathicity to increase the local concentration, thereby accelerating aggregation (Côté *et al.,* 2015; Pandey *et al.,* 2018). On the other hand, deletion of the PRD in HTTExon1 was observed to cause a significant change in the morphology of polyQ aggregates and provoked toxicity in yeast models (Dehay and Bertolotti*,* 2006). Additional studies have shown that the PRD has the potential to mitigate HTTExon1 neurotoxicity by reducing the propensity for aggregation (Duennwald *et al.,* 2006; Crick *et al.,* 2013; Pigazzini *et al.,* 2021). The PRD was found to maintain a highly dynamic conformational state during fibril formation (Hoop *et al.,* 2014; Isas *et al.,* 2015; Falk *et al.,* 2020). Proline residues provide a hydrophobic surface and are susceptible to hydrogen bonding with interactors that are involved in signaling, splicing, or motility (Faber *et al.,* 1998; Macias *et al.,* 2002; Moradi *et al.,* 2011).

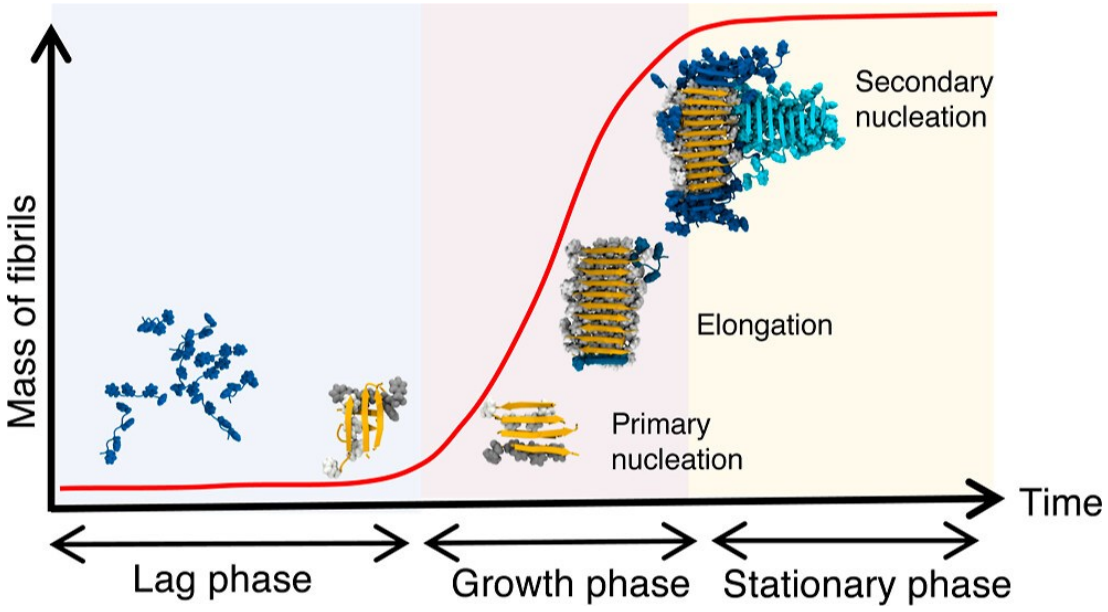

Figure 2.2: Schematic representation of the amyloidogenic aggregation mechanism based on nucleated branching.

First, monomers assemble and form the nuclei during lag phase and is followed by the growth phase, which involves the elongation of the primary nucleus. In the stationary phase, secondary nucleation takes place on the surface of a pre-assembled fibril (Image adapted from Jalali *et al.,* 2023).

2.2 Proteostasis Network

Misfolded proteins can lead to a loss of their function, or they may also acquire a toxic gain of function that can perturb cellular physiology. To counteract aberrant misfolding and subsequent aggregation, cells employ a complex network of quality control mechanisms. The regulation of the correct fold and function of proteins is called protein homeostasis or 'proteostasis'. The proteostasis network (PN) regulates protein synthesis, folding at the correct stoichiometries in multi-protein assemblies and their proteolytic turnover (Hipp *et al.,* 2019). Due to a variety of internal and external strains, even conformationally well-structured proteins are prone to misfold. To avoid harmful effects, proteins that do not maintain their functional state must be eliminated by degradation (Jayaraj *et al.,* 2020). Yet, the proteostatic capacity declines with aging and is compromised upon environmental stress. At the same time, the collapse of proteostasis network reciprocally cause aberrant protein misfolding and aggregation. Research in bacteria and yeast has provided a basic framework for PN (Kerner and Shaner *et al.,* 2005; Albanèse *et al.* 2006; Finley *et al.* 2012; Santra *et al.,* 2017), while

the composition of human PN is much more complex (Brehme *et al.,* 2014; Klaips *et al.,* 2018; Jayaraj *et al.,* 2020). This network can be viewed as three interrelated branches: *de novo* protein synthesis, maintenance of structural integrity, degradation/clearance of misfolded and toxic proteins (Hipp *et al.,* 2019).

Key proteostasis nodes include the ubiquitin-proteasome system (UPS), the autophagy-lysosome system, and molecular chaperones. The UPS is a complex intracellular degradation pathway in which short-lived proteins are targeted by ubiquitination and proteolytically processed by the proteasome (Vilchez *et al.,* 2014; Gong *et al.,* 2016). Autophagy involves the delivery of dysfunctional proteins to lysosomes via double-layered membrane spherical structures called autophagosomes, which then engage with lysosomes for subsequent degradation (Pan *et al.,* 2008; Chen *et al.,* 2010; Schneider *et al.,* 2015). The third component of the PN are molecular chaperones that modulate the cellular folding landscape and prevent or remodel the non-native misfolded products (Hartl *et al.,* 2011).

Protein folding was initially thought to be a spontaneous process, and while this may be true for short proteins (Kubelka *et al.,* 2004), larger and more complex proteins and multi-domain assemblies need molecular chaperones to help them fold into functional states (Hipp *et al.,* 2019). The cellular environment of nascent chains and conditions during co-translational folding add another layer of complexity to *in vivo* folding compared to *in vitro* folding where the role of chaperones *in vivo* is particularly crucial (Hingorani and Gierasch, 2014).

Molecular chaperones are known to be upregulated during periods of cellular stress such as heat shock, when the levels of aggregation-prone folding intermediates are elevated (Hartl *et al.,* 2011). More than 300 genes that encode molecular chaperones exist in the human genome translating into an array of chaperones varying in sequence, size, and structure (Brehme *et al.,* 2014; Arhar *et al.,* 2021). The nomenclature and classification of chaperones is historically based on their approximate molecular weight; for example, the 70-kDa heat shock protein is referred to as Hsp70 (Kampinga *et al*., 2009).

Hsp60, Hsp70, Hsp90, Hsp100 are extensively involved in *de novo* protein folding and refolding of misfolded proteins (Mayer, 2010). They usually consist of multiple

components to facilitate ATP-dependent folding, along with co-chaperones that regulate the interaction cycles with substrates (Mayer and Bukau, 2005; Hartl *et al.,* 2011). The exposure of hydrophobic regions in non-native proteins provides a common recognition site for such chaperones (Clerico *et al.,* 2015; Jores *et al.,* 2018). On the other hand, ATP-independent chaperones, such as the Hsp40s, small Hsps, Spy or SecB, either serve as co-chaperones of ATP-dependent chaperones or as passive holdases and mitigate aggregation (Mitra *et al.,* 2022).

Dysregulated proteostasis and its decline upon aging can lead to protein aggregation and toxic oligomeric species, which can contribute to a variety of diseases, particularly neurodegenerative diseases. Recently, molecular chaperones have emerged as potential therapeutic targets against neurodegenerative diseases (Kampinga and Bergink, 2016; Sharma *et al.,* 2023). Both *in vivo* and *in vitro* studies have shown that chaperone families such as Hsp70, Hsp90, TRIC counteract protein aggregation or degrade pre-existing aggregates of neurodegenerative proteins such as α-syn (Gao *et al*., 2015; Tittelmeier *et al*., 2020; Hu *et al.,* 2021), tau (Miyata *et al.,* 2011; Kundel *et al.,* 2018; Nachman *et al.,* 2020; Ryder *et al.,* 2022), Aβ (Sakono *et al.,* 2008; Huang *et al.,* 2018; Chen *et al.,* 2020; Abelein and Johannson, 2023), TDP-43 (Kitamura *et al.,* 2018; Lin *et al.,* 2021; Carrasco *et al.,* 2023), or polyQ (Gillis *et al.,* 2013; Kakkar *et al.,* 2016; Kuiper *et al*., 2017; Scior *et al.,* 2018) in various contexts.

2.2.1 Hsp70-Hsp40 Cycle

Hsp70 has been shown to play a significant role in mitigating aggregation in disease models by preventing aggregation, but also in facilitating the refolding of misfolded proteins, and assisting the degradation mechanisms to eliminate dysfunctional proteins (Rosenzweig *et al.,* 2019). Members of the Hsp40 co-chaperone family (also known as J-domain proteins) and nucleotide exchange factors (NEFs) are essential modulators of the ATP-driven chaperone cycle of Hsp70.

The structural features of Hsp70 have long been studied and are essentially described as follows: a nucleotide binding domain (NBD) at the N-terminus flanked by a substrate binding domain (SBDβ) together with a helical lid domain (SBDα) at the C-terminus. A

short, flexible interdomain linker, connects these two functional domains (Sharma and Masison, 2009).

The NBD consists of four subdomains (IA, IB, IIA, and IIB) that form two large domains sandwiched between a groove. The binding and hydrolysis of ATP to the catalytic center in this groove orchestrates the subdomains of the NBD and controls the allosteric organization. The SBD consists of two subdomains, the α-helical domain, SBDα, which acts as a lid that opens and closes on the SBDβ which is composed of eight β-strands that contain a cleft that functions as a peptide binding pocket (Rosenzweig, Mayer and Gierasch, 2019).

Substrate association/disassociation requires rapid and precise regulation by Hsp70 to avoid misfolding and aggregation and is finely tuned by the intramolecular, allosteric ATP hydrolysis cycle (Rosenzweig *et al.,* 2019). Canonical model of Hsp70 cycle is described as: In the ADP-bound state, Hsp70s have a high affinity for the substrates. In this state, the α-helical lid of SBDα docks onto the SBDβ, forming a closed conformation, resulting in low on/off rates, thus preventing release of substrate peptides. (Kityk *et al.,* 2015, 2018; Clerico and Rosenzweig *et al.,* 2019). In the ATP-bound state, a cascade of conformational rearrangements occurs in which the a-helical lid disengages and adopts an open conformation that substantially increases the on/off rates of substrates. Through ATP hydrolysis and nucleotide exchange, Hsp70 cycles between "open" and "closed" conformations, alternately binding and releasing substrates. By that, according to the theory of “kinetic partitioning”, the concentration of free substrates is kept low enough to avoid aggregation while allowing free substrates to fold properly. On the other hand, the "local unfolding" view predicts that the recurrent binding cycle causes a local unfolding of the misfolded β-sheets in the substrate and promotes the overcoming of the kinetic threshold to reach the native state (Mayer and Bukau, 2005).

Diversity in substrate targeting for Hsp70 is provided by the Hsp40 co-chaperone family. Hsp40s, also known as JDPs, are a class of multidomain proteins with a conserved N-terminal J-domain that facilitates binding to Hsp70 and induces its ATPase activity (Kelley*,* 1998; Hennessy *et al.,* 2005). Depending on the domain architecture, JDPs are categorized as class A, B, or C. Class A and B JDPs commonly contain an N-terminal J-domain followed by a flexible glycine-phenylalanine (G/F) rich linker which is adjacent

to two β-barrel C-terminal domains (CTDI and CTDII) and a dimerization domain (DD). Class A JDPs have a zinc finger-like region (ZFLR) between the G/F linker and the C-terminal domain, whereas class B JDPs lack this region. JDPs that contain the J-domain, but the other subdomains do not conform to class A or B structures, fall into the class C category (Rosenzweig *et al*., 2019; Ayala Mariscal and Kirstein, 2021).

JDPs recognize the peptide substrates and deliver them to the SBD of Hsp70 in the ATP-bound state for further processing in the canonical Hsp70 cycle. Substrate transfer and J-domain interaction with Hsp70 stimulates hydrolysis of ATP to ADP, which further leads to the closed conformation of Hsp70, trapping the substrate with a high affinity in Hsp70's binding pocket. Subsequently, either spontaneously or by nucleotide exchange factor (NEF)-assisted rebinding of ATP, the substrate dissociates from Hsp70 (Laufen *et al.,* 1999; Mayer and Gierasch., 2019; Zhang *et al.,* 2023).

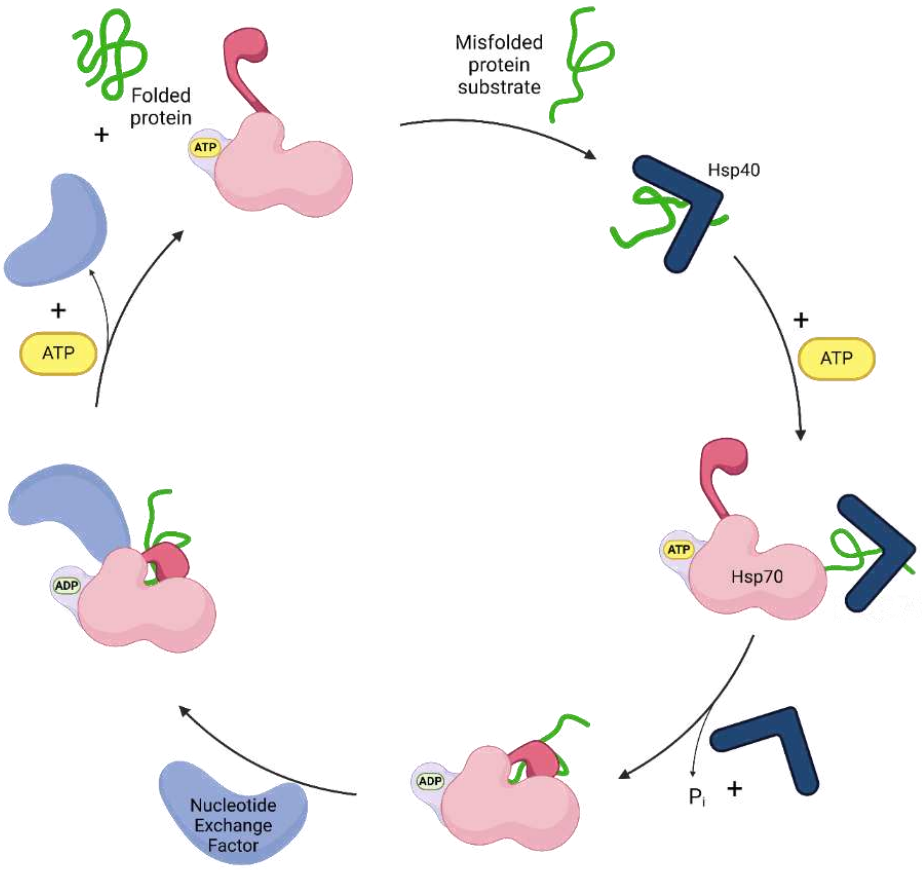

Figure 2.3 Overview of substrate binding/release cycle mediated by Hsp70/Hsp40/NEF

Initial recognition of the misfolded substrate (green) by Hsp40 (dark blue) is followed by the transfer of the substrate to the substrate binding domain (SBD) (light pink) of ATP bound Hsp70. Upon hydrolysis of ATP to ADP in the nucleotide binding domain (NBD) (purple), the lid in the SBD (dark pink) alters to closed conformation and induces the processing of the substrate. Nucleotide exchange factor (NEF) (light blue) facilitates the exchange of ADP to ATP and leads to the release of the refolded substrate.

2.2.2 Substrate Interactions of JDPs

Since the JDPs are the first to recognize and engage with the non-native client proteins, it is critical to characterize this interaction. Although the high-resolution full-length structure of JDPs has not yet been determined, important studies have shed light on the substrate interactions of this protein family.

Due to their hydrophobic nature, both CTDI and CTDII have been shown to possess peptide binding properties. Early studies have demonstrated that bacterial DNAJ recognizes an eight-residue long stretch comprising mostly hydrophobic and aromatic amino acids (Rüdiger *et al.,* 2001). On the other hand, Ydj1, the yeast ortholog of human DNAJA1, was found to bind the substrate via polar interactions with a hydrophobic patch on the CTDI but shows no preference for the aromatic residues accessible on the substrate surface (Li *et al.,* 2003). In contrast, the CTDI of the yeast homolog Sis1 (human DNAJB1) has a strong affinity for aromatic side chains, but no involvement of CTDII in substrate binding.

A recent NMR analysis of *Thermus thermophilus* type B Hsp40 (ttHsp40) has provided structural details of this protein bound to a physiological client proteins alkaline phosphatase (PhoA) and maltose binding protein (MBP). As major binding sites, grooves involving polar and hydrophobic amino acids on CTDI and CTDII were identified and found to interact with hydrophobic as well as aromatic, and large aliphatic residues of both substrates (Jiang *et al.,* 2019). This study also shows that A- and B-type Hsp40s have different preferences in binding sequences due to their different binding domain composition and that the presence or absence of the ZFLR can account for such differences and lead to the diversity in client recognition by Hsp40s.

A specific type of class B JDPs, DNAJB6 and DNAJB8, have a serine/threonine (S/T) rich motif that has been shown to provide binding interaction with the substrates including polyQ and Aβ42. Interestingly, DNAJB6 and DNAJB8 can exert an inhibitory effect on the formation of polyQ and Aβ42 aggregates, in an Hsc70-independent manner (Kakkar *et al.,* 2016; Mansson *et al.,* 2018; Österlund *et al.,* 2020).

2.2.3 Hsc70-DNAJB1-Apg2 Trimeric Chaperone Complex

The Hsp70/Hsp40 complex has long been implicated in the retardation of formation and disaggregation of amyloidogenic proteins both *in vitro* and *in vivo (*Muchowski *et al.,* 2000; Wacker *et al.,* 2004; Behrends and Evans *et al.,* 2006; Park *et al.,* 2013). More recently, Hsc70 (constitutively expressed form of Hsp70) and DNAJB1 (a class B type JDP) together with the nucleotide exchange factor Apg2, was shown to promote disaggregation of a model substrate luciferase (Rampelt *et al.,* 2012). It was also found that α-syn fibrils can be rapidly and robustly disaggregated by the same chaperone complex (Gao *et al.,* 2015; Wentink *et al.,* 2020). In addition, it has been demonstrated that tau fibrils generated *in vitro* and extracted from post-mortem Alzheimer´s patient brains can be disaggregated by this trimeric chaperone complex (Nachman *et al.,* 2020). Importantly for this study, it was shown that suppression of HTTExon1(HTT) aggregation and disaggregation of preformed fibrils could be achieved *in vitro* by this trimeric chaperone complex (Scior *et al.,* 2018; Ayala Mariscal *et al.,* 2022). However, the detailed mechanism of action of this trimeric chaperone complex and the individual interactions of each chaperone with HTTExon1 have remained elusive. Recently, an HTTExon1-specific binding site between the C-terminus of DNAJB1 and the PRD of HTTExon1 was identified by cross-linking mass spectrometry (XL-MS) and shown to be critical for the activity of the trimeric chaperone complex in suppressing HTTExon1 aggregation as well as resolubilizing preformed fibrils. However, studying interactions between chaperones and distinct HTTExon1 moieties in different aggregation states is particularly challenging due to the flexible and transient nature of these interactions, and thus mechanistic insights into chaperone activity remain limited.

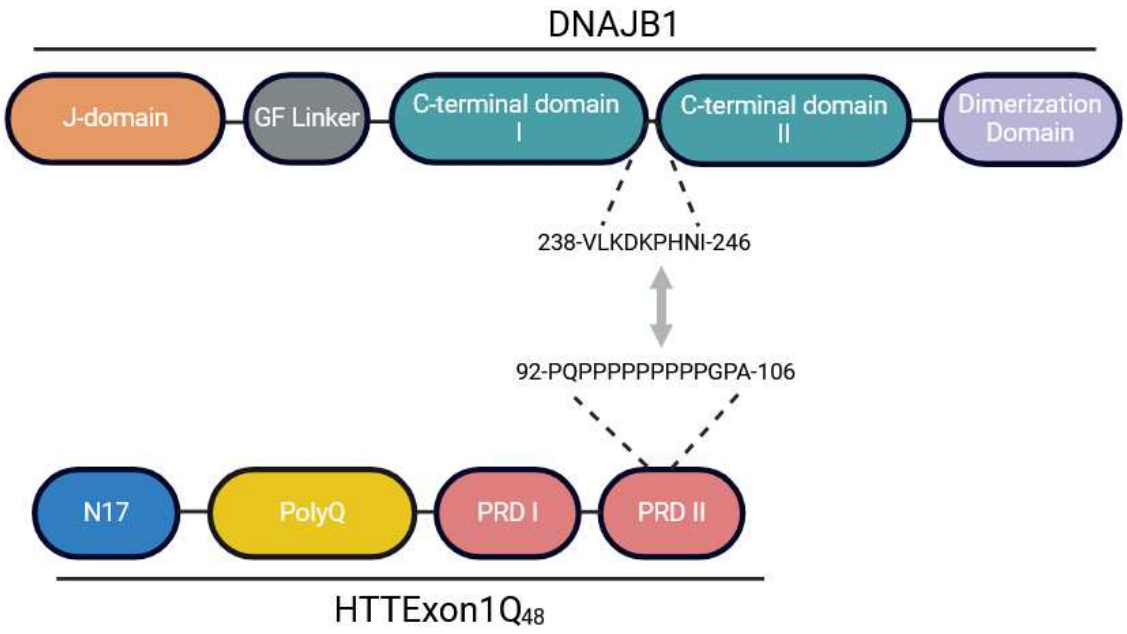

Figure 2.4 Schematic description of the binding interface between DNAJB1/HTTExon1

The nine-amino acid Huntingtin specific binding motif between the CTDI and CTDII of DNAJB1 interacts with the C-terminal PRDII region of HTTExon1Q_{48}.

2.3 Objectives of the Thesis

Although it is established that DNAJB1/Hsc70 can interact with soluble monomeric as well as mature HTT (from now on I refer to HTTExon1 as ´HTT´) fibrils, substrate recognition by the chaperones along the aggregation pathway of HTT remains enigmatic. It is not known how the different conformational entities of HTT are recognized by the trimeric chaperone complex and whether the chaperones associate with the HTT fibrils that are ultimately formed. Based on the previously identified binding site between DNAJB1 and HTT, I aimed to improve our understanding of how the trimeric chaperone complex works by addressing the following research questions:

I. Unravelling the individual mode of interactions of trimeric chaperones along the aggregation pathway of HTT.

II. Understanding the role of chaperone sequestration by HTT fibrils as a potential cause of the eventual failure of the trimeric chaperone complex in the prevention of HTT aggregation.

3. Results

3.1 DNAJB1-HTT Interaction in Suppression of HTT Aggregation

As previously reported, the trimeric chaperone complex Hsc70, DNAJB1 and Apg2 can suppress HTT aggregation as well as disaggregate preformed fibrils (Scior *et al*., 2018). However, the mechanism of action of the trimeric chaperone complex is still unclear, as the interaction between the individual chaperones and HTT has not yet been characterized in detail. Since J-domain proteins (JDPs) are known to recognize misfolded substrates and deliver them to Hsp70 (Li *et al*., 2003; Pemberton *et al*., 2011; Wentink *et al*., 2020), addressing JDP-substrate interactions is of great importance. In our lab, a binding interface between DNAJB1 and HTT was determined by utilizing cross-linking mass spectrometry. The nine-amino acid huntingtin binding motif (HBM), located between DNAJB1 C-terminal domains (CTD) I and II, was found to interact with the second proline domain (PRDII) of HTTExon1Q_{48}. Within this motif, a highly conserved, positively charged H244, emerged as the most critical residue. Mutating H244 to alanine has been shown to completely abolish the suppression of HTT aggregation by DNAJB1 together with Hsc70 and Apg2 (Ayala Mariscal *et al*., 2022).

The result of the H244A mutation raised the question of whether the positive charge at this site is essential for the interaction. Therefore, I contributed to this study by analysing the activity of a variant where the histidine residue was mutated to glutamine, which is a polar but non-charged amino acid.

To see if this mutation had disrupted the functional integrity of the protein, I first tested its ability to refold denatured luciferase. Firefly (*Photinus pyralis*) luciferase is a model substrate widely used in aggregation studies (Freeman *et al.* 1995; Thulasiraman, 1997) which catalyses the oxidation of D-Luciferin to produce bioluminescence. In the luciferase assay, luciferase was first denatured by heat and then incubated with DNAJB1 together with Hsc70 and Apg2 in the presence of ATP. Over time, the denatured luciferase was refolded by the trimeric chaperone complex, restoring its ability to oxidize luciferin, and the emitted luminescence was used as a readout of the refolding capacity of the chaperones. Compared to DNAJB1^{wt}, DNAJB1^{H244Q} showed together with Hsc70 and Apg2 the same level of luciferase refolding activity **(Fig. 3.1 1 a)**, confirming that this mutation does not deteriorate its general chaperone function.

The next step was to test the suppression of HTT aggregation by the DNAJB1^{H244Q} mutant in the presence of Hsc70 and Apg2. This was done by using a FRET-based assay where HTT was labelled with CyPet/YPet fluorophores that form a FRET pair upon aggregation of HTT, and the signal generated was used to monitor aggregation over time. The FRET signal was significantly delayed compared to the control **(Fig. 3.1 1 b, black curve)** in the presence of the trimeric chaperone complex and ATP due to their suppression of HTT aggregation activity **(Fig. 3.1 1 b, red curve)**. DNAJB1^{H244Q} together with Hsc70 and Apg2, had a reduced suppression activity and even a 2-fold excess did not improve this result **(Fig. 3.1 1 b, green and magenta curves)** (FRET assay performed by Yasmin Richter (Kirstein Lab)). Thus, I could clearly demonstrate that this binding site is specific for interaction with HTT, and that a neutral amino acid substitution of the histidine residue reduces the suppression activity.

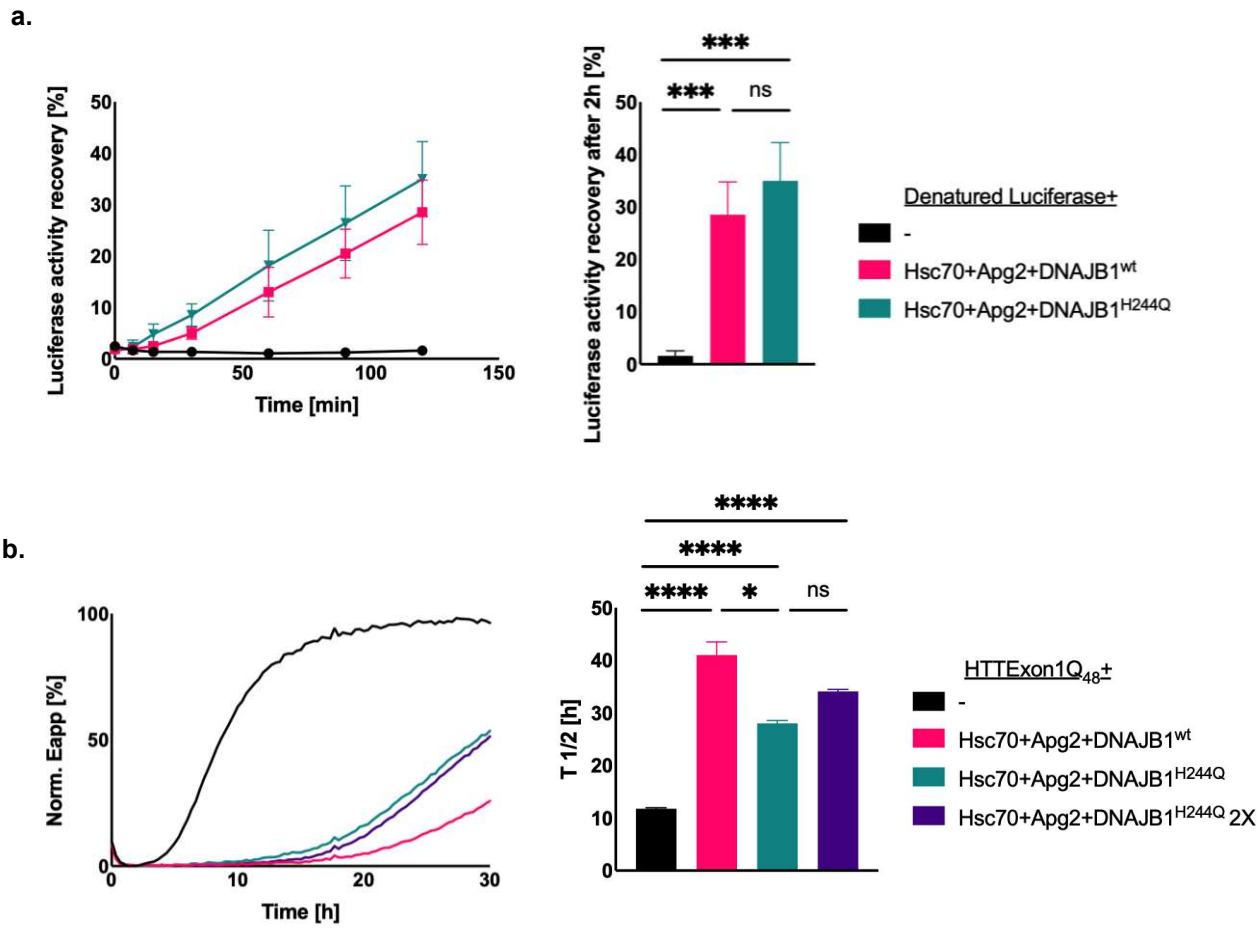

Figure 3.1 DNAJB1^{H244Q} actively refolds luciferase but is partially ineffective in suppression of HTTExon1Q$_{48}$ aggregation.

a. Refolding of heat-denatured luciferase by Hsc70, Apg2 and DNAJB1^{wt} (red) or DNAJB1^{H244Q} (green). As an indicator of refolding efficiency, luminescence emission from luciferin oxidized over time by reactivated luciferase was used. The plot on the left is representative of three independent experiments. Final recovery of luciferase activity after 2 hours is shown in the bar graph on the right. Error bars correspond to the mean SD. Statistical analysis was performed by a one-way ANOVA. ***p ≤0.001; ns not significant.

b. FRET measurements over 30 h of the fibrilization of HTTExon1Q$_{48}$ in the presence of Hsc70, Apg2 and DNAJB1^{wt} (red), or DNAJB1^{H244Q} (green) or DNAJB1^{H244Q} 2X (purple) and in the absence of chaperones (black). The bar graph on the right depicts the half-time ($T_{1/2}$) of HTTExon1Q$_{48}$ aggregation and represents the mean of three independent experiments. Error bars correspond to the mean SD. Statistical analysis was performed by a one-way ANOVA. *p≤ 0.05; ****p≤ 0.0001; ns not significant

3.2 The role of ATPase cycle for DNAJB1-HTT interaction

Previous studies have shown that the ATPase activity of Hsc70 is stimulated through an interaction with the HPD motif located in the J-domain of DNAJB1 (Wall *et al*., 1994; Chamberlain *et al*., 1997) **(Fig. 3.2 1).** Given that the presence of ATP was essential for suppressing HTT aggregation (Scior *et al.,* 2018), it was important to determine the role of an intact ATPase cycle on suppression activity. Furthermore, Scior *et al.* showed that neither DNAJB1 nor Hsc70 were able to suppress HTT aggregation individually. Therefore, my hypothesis was that a disruption of the interaction between DNAJB1 and Hsc70 would abolish the suppression of HTT aggregation activity. However, it would be interesting to see how a mutation of the HPD motif such as H32Q would affect the suppression of HTT aggregation relative to H244 mutation of the binding site between DNAJB1 and HTT. At the same time, a double mutation of these two residues needed to be assessed as well. Therefore, I set out to analyse the variants, DNAJB1^{H32Q} and DNAJB1$^{H32Q\text{-}H244A}$ in terms of ATPase, luciferase refolding, and suppression of HTT aggregation activities.

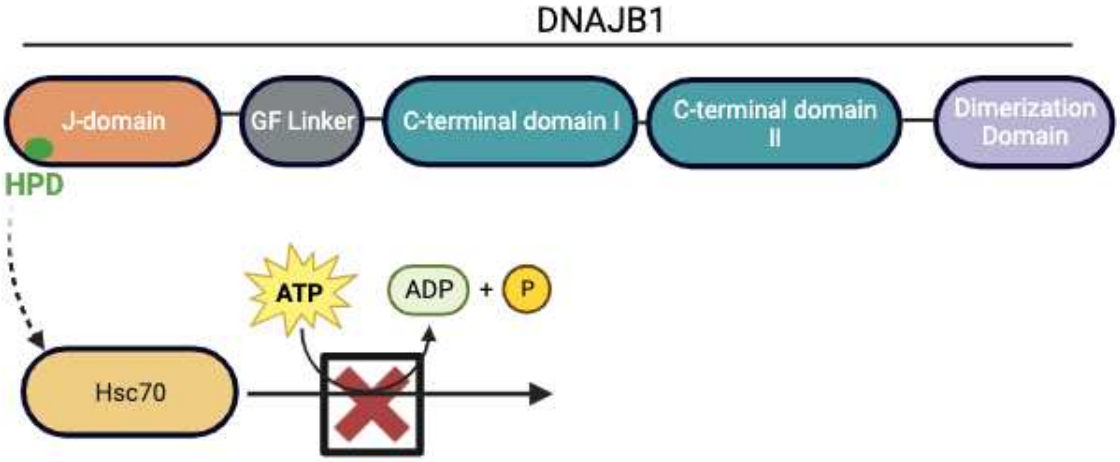

Figure 3.2 1 Schematic representation of the ATPase cycle

HPD motif depicted in green is located in the N-terminal J-domain of DNAJB1. The ATPase activity of Hsc70 is stimulated through J-domain interaction as represented by the dashed arrow and impaired by the mutation of the histidine residue.

First, the ability to induce the Hsc70 ATPase activity by DNAJB1^{H32Q} and DNAJB1$^{H32Q-H244A}$ was tested. The *in vitro* ATPase assay measures the ATP hydrolysis to ADP by Hsc70. A malachite green based colorimetric method was used to determine the free inorganic phosphate levels that are released upon hydrolysis of ATP. The ATPase activity of Hsc70 induced by the DNAJB1 variants were then normalized to the basal ATPase activity of Hsc70. As expected, the DNAJB1^{H32Q} and DNAJB1$^{H32Q-H244A}$ mutants failed to induce Hsc70 ATPase activity **(Figure 3.2 2 a)**.

Next, the two DNAJB1 variants were tested in a luciferase refolding assay. As a result, both DNAJB1^{H32Q} and DNAJB1$^{H32Q-H244A}$ together with Hsc70 and Apg2, failed to refold heat-denatured luciferase **(Fig. 3.2 2 b)**. This outcome was also expected since luciferase refolding activity requires an active ATPase cycle. Although DNAJB1^{H244A} was shown to be as active as DNAJB1^{wt} in ATPase and luciferase refolding activities (Ayala Mariscal *et al*., 2022), the disruption of the DNAJB1-Hsc70 interaction by the H32Q mutation completely impaired the most essential activities of the protein.

a.

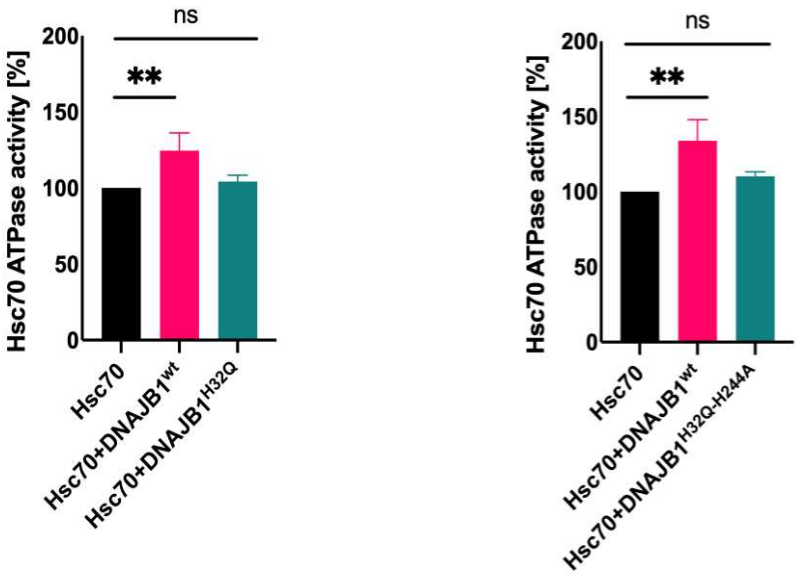
Hsc70 ATPase activity [%]
200
150
100
50
0
ns
**
Hsc70
Hsc70+DNAJB1wt
Hsc70+DNAJB1H32Q
Hsc70 ATPase activity [%]
200
150
100
50
0
ns
**
Hsc70
Hsc70+DNAJB1wt
Hsc70+DNAJB1H32Q-H244A

b.

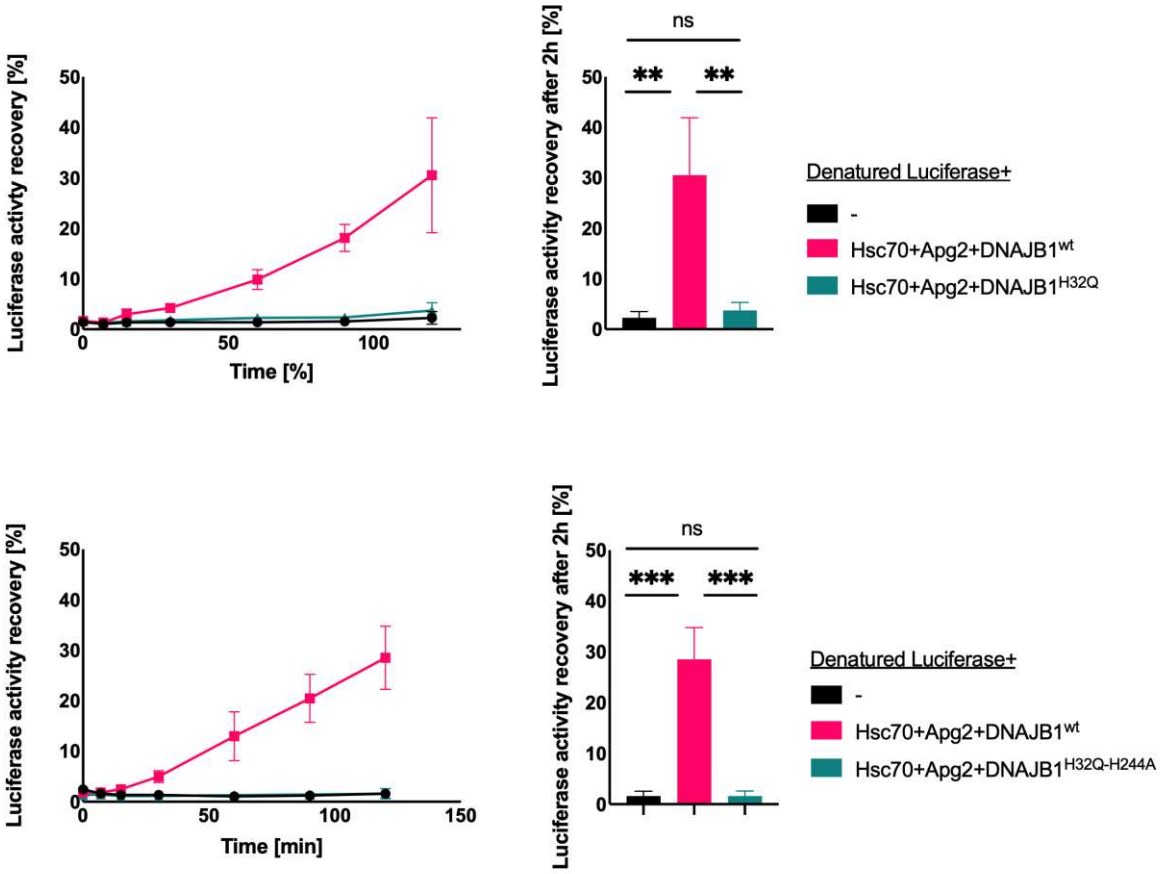
Luciferase activty recovery [%]
50
40
30
20
10
0
0
50
100
Time [%]
Luciferase activity recovery after 2h [%]
50
40
30
20
10
0
ns
**
**
Denatured Luciferase+
-
Hsc70+Apg2+DNAJB1wt
Hsc70+Apg2+DNAJB1H32Q
Luciferase activity recovery [%]
50
40
30
20
10
0
0
50
100
150
Time [min]
Luciferase activity recovery after 2h [%]
50
40
30
20
10
0
ns
***
***
Denatured Luciferase+
-
Hsc70+Apg2+DNAJB1wt
Hsc70+Apg2+DNAJB1H32Q-H244A

Figure 3.2 2 DNAJB1^{H32Q} and DNAJB1$^{H32Q-H244A}$ fail to induce the ATPase activity of Hsc70 and refolding of heat-denatured luciferase.

a. ATPase activity of Hsc70 induced by DNAJB1^{H32Q} (left) or DNAJB1$^{H32Q-H244A}$ **(**right) compared to DNAJB1^{wt}. Data normalized to basal ATPase activity of Hsc70. The graph is a representative of three independent experiments. Error bars correspond to the mean SD. Statistical analysis was performed by a one-way ANOVA. **** p≤ 0.0001; ** p≤ 0.01; ns not significant.

b. Denatured luciferase refolding activities of DNAJB1^{H32Q} (top) or DNAJB1$^{H32Q-H244A}$ (bottom) compared to DNAJB1^{wt} together with Hsc70 and Apg2. Luminescence emission was used as a readout to determine the refolding efficiency. The graph is a representative of three independent experiments. Final recovery of luciferase activity after 2 hours is shown in the bar graph on the right. Error bars correspond to the mean SD. Statistical analysis was performed by a one-way ANOVA. ** p≤0.01; ***p ≤ 0.001; ns not significant.

Subsequently, to test whether DNAJB1^{H32Q} and DNAJB1$^{H32Q-H244A}$ mutants can suppress HTT aggregation together with Hsc70 and Apg2, a FRET assay was performed. In the presence of Hsc70, Apg2 and ATP, DNAJB1^{H32Q} showed no inhibitory activity and even a 2-fold excess did not improve the ability to suppress HTT aggregation (FRET assays performed by Yasmin Richter (Kirstein Lab)) **(Fig. 3.2 3 a).** Likewise, DNAJB1$^{H32Q-H244A}$ was also completely inactive in suppression of HTT aggregation together with Hsc70 and Apg2 **(Fig. 3.2 3 b).**

Both results were expected since these DNAJB1 point mutations abolished the ability to induce Hsc70 ATPase and confirmed that an active interaction between DNAJB1 and Hsc70, in which the ATPase cycle is kept intact, is required for the suppression of HTT aggregation. An effective interaction between DNJAB1 and HTT is essential for active remodelling by the trimeric chaperone complex; however, when the interaction between DNAJB1 and Hsc70 is disrupted, the essential functionality of the trimeric chaperone complex cannot be restored.

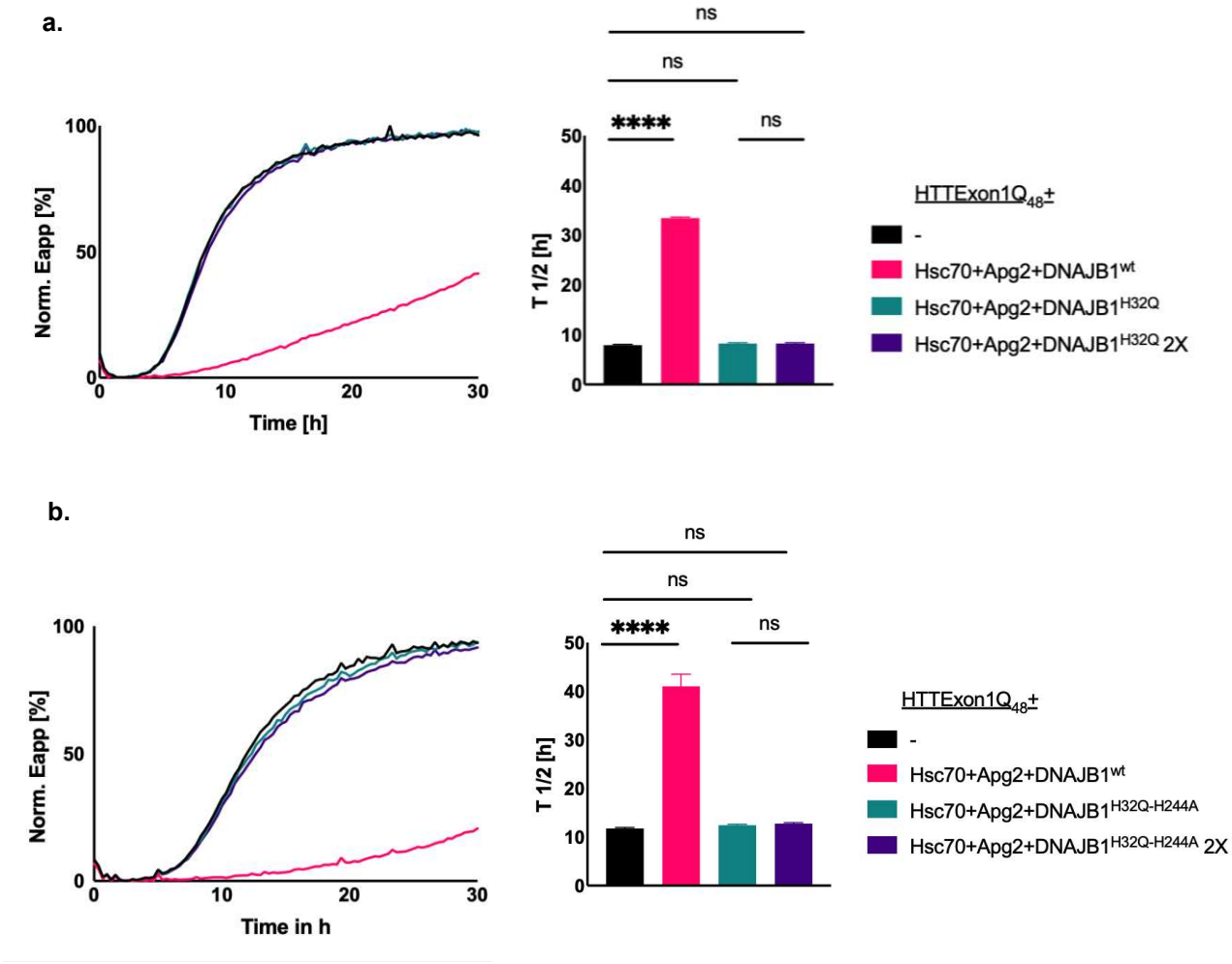

Figure 3.2 3: DNAJB1^{H32Q} and DNAJB1$^{H32Q-H244A}$ are inactive in the suppression of HTTExon1Q$_{48}$ aggregation.

a. FRET measurements over 60 h of the fibrilization of HTTExon1Q$_{48}$ in the presence of Hsc70, Apg2 and DNAJB1^{wt} (red), Hsc70, Apg2 and DNAJB1^{H32Q} (green) or DNAJB1^{H32Q} 2X (purple) and in the absence of chaperones (black). The bar graph on the right depicts the half-time ($T_{1/2}$) of HTTExon1Q$_{48}$ aggregation and represents the mean of three independent experiments. Statistical analysis was performed by a one-way ANOVA. ****p ≤ 0.0001; ns not significant.

b. FRET measurements over 30 h of the fibrilization of HTTExon1Q$_{48}$ in the presence of Hsc70, Apg2 and DNAJB1^{wt} (red), Hsc70, Apg2 and DNAJB1$^{H32Q-H244A}$ (green) or DNAJB1$^{H32Q-H244A}$ 2X (purple) and in the absence of chaperones (black). The bar graph on the right depicts the half-life ($T_{1/2}$) of HTTExon1Q$_{48}$ aggregation and represents the mean of three independent experiments. Statistical analysis was performed by a one-way ANOVA. ****p ≤ 0.0001; ns not significant.

3.3 DNAJB1-HTT Interaction in Disaggregation Activity

3.3.1 The effect of mutations in the binding interface of DNAJB1-HTT

It was previously demonstrated that the trimeric chaperone complex not only suppresses the formation of HTT aggregates, but also disaggregates preassembled HTT fibrils in the presence of ATP (Scior *et al*., 2018). As described in the previous chapter, once the DNAJB1-HTT binding site had been identified, several DNAJB1 variants were tested to determine the effect of single point mutations within this binding motif on suppression of HTT aggregation (Ayala Mariscal *et al*., 2022). Since molecular chaperones have recently been shown to interact differently with oligomeric or fibrillar moieties compared to monomeric amyloidogenic proteins (Cohen *et al*., 2015; Österlund and Wentink *et al*., 2020), it is possible that mutations in DNAJB1 affect disaggregation activity differently than the suppression activity. Therefore, in this part of the thesis, the impact of these DNAJB1 mutations on disaggregation activity together with Hsc70 and Apg2 was investigated.

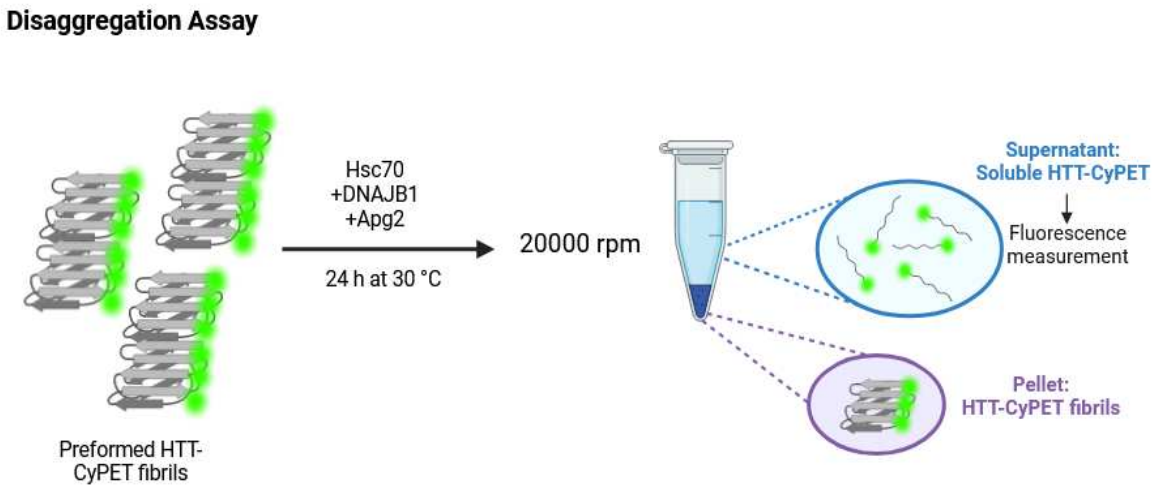

Figure 3.3.1 1 Schematic representation of the disaggregation assay

HTTExon1Q_{48}-CyPet fibrils were incubated with the trimeric chaperone complex and ATP for 24 h at 30°C. The disaggregated soluble fraction was separated from the pellet by ultracentrifugation, and the fluorescence of the supernatant was used as a readout of the resolubilized HTTExon1Q_{48}. (Image adapted from Ayala Mariscal *et al.*, 2022)

As described above with a schematic in **Fig. 3.3.1 1**, 2 µM HTT was first aggregated at 20°C for 4.5 hours. The fibrils were then incubated with the trimeric chaperone complex for 24 h to allow the disaggregation reaction. The mixture was then ultracentrifuged, and the fluorescence of the supernatant was analysed to determine the degree of resolubilization.

In the first set of the disaggregation assay, I tested the DNAJB1^{H244A} mutation that is the key residue in the DNAJB1/HTT binding interface. This mutant was found to completely abolish the suppression activity by the trimeric chaperone complex (Ayala Mariscal *et al.*, 2022). Therefore, it was important to evaluate the disaggregation activity of this mutant to see if this residue was also critical in targeting HTTExon1Q$_{48}$ in the fibrillar state. As a result, the disaggregation activity of this mutant was severely, but not completely, impaired **(Fig. 3.3.1 2)**, suggesting that new binding sites may emerge when HTT adopts a fibrillar state.

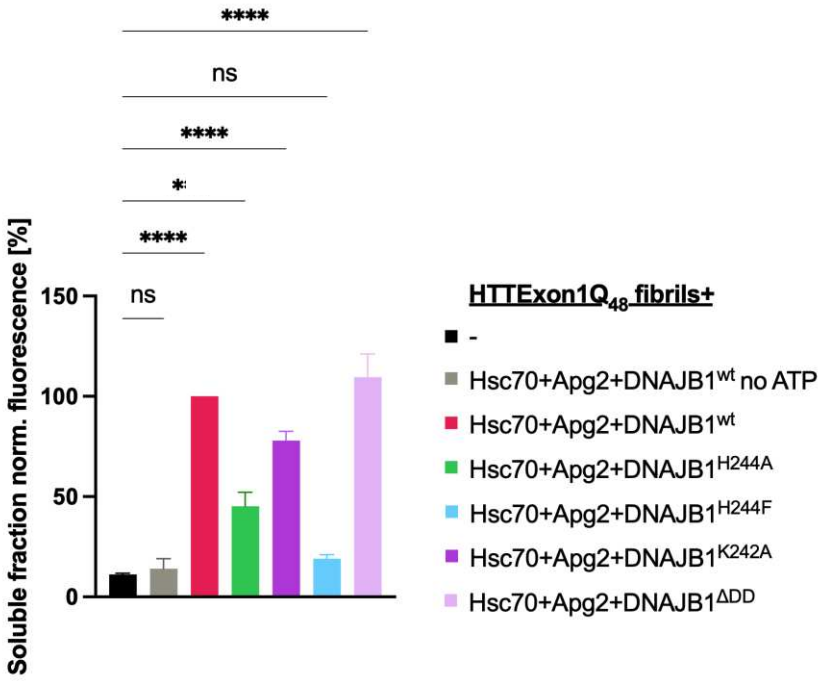

Figure 3.3.1 2 H244 is a key residue for disaggregation of HTT fibrils.

Fluorescence levels of resolubilized HTTExon1Q$_{48}$ by Hsc70, Apg2 and DNAJB1^{wt} or variants DNAJB1^{H244A}, DNAJB1^{K242A}, DNAJB1^{H244F}, DNAJB1$^{\Delta DD}$. The fluorescence intensities of each sample were normalized to the sample containing DNAJB1^{wt} in the presence of ATP. Bars represent the mean values of three independent experiments and error bars correspond to the mean SD. The significance was determined via one-way ANOVA analysis. Ns not significant; *p≤ 0.05; ****p ≤ 0.0001

Previously in our lab, the H244 residue was substituted by phenylalanine to test whether a non-polar but bulkier amino acid might affect the suppression activity, and it was shown that this mutation had no rescue effect on suppression, although it has actively refolded the heat-denatured luciferase (Ayala Mariscal *et al*., 2022). When tested in the disaggregation assay, the result was also consistent with the suppression assay, showing that H244F together with Hsc70 and Apg2 was completely inactive and in fact had a lower activity than H244A **(Fig. 3.3.1 2)**.

Then, for further insight into the importance of positively charged residues in this binding motif, K242 was mutated into alanine. This mutation has resulted in only a partial reduction in the suppression efficiency of the trimeric chaperone complex (Ayala Mariscal *et al*., 2022). In parallel, DNAJB1^{K242A} together with Hsc70 and Apg2 was partially active in disaggregating HTT fibrils, showing that this residue is also important, carrying a positive charge, but not as critical as H244 **(Fig. 3.3.1 2)**.

Next, the contribution of the dimerization domain of DNAJB1 to the disaggregation activity was evaluated. Since it was demonstrated that a class B JDP, DNAJB6 can form large oligomers which dissociate upon interaction with substrate proteins (Söderberg *et al*., 2018; Karamanos *et al*., 2019; Österlund *et al*., 2020), the question was what effect the dimeric state of DNAJB1 would have on its function as part of the disaggregase complex resolubilising HTT fibrils. By size exclusion chromatography, DNAJB1 was shown to adopt a dimeric form, and deletion of the dimerization domain significantly improved the ability of the trimeric chaperones to suppress HTT aggregation (Ayala Mariscal *et al*., 2022). However, in the disaggregation assay, monomeric DNAJB1 (DNAJB1$^{\Delta DD}$) did not differ from DNAJB1^{wt} **(Fig. 3.3.1 2)**. This result suggests that dimerization of DNAJB1 plays a different role when targeting soluble states of HTT in suppression of aggregation than for targeting fibrillar moieties for disaggregation by the trimeric chaperones.

In addition, the second proline stretch in the PRD of HTT was identified as a site of interaction with DNAJB1, and deletion of this region completely abolished the inhibitory effect of the trimeric chaperone complex (Ayala Mariscal *et al*., 2022).

Furthermore, structural and molecular dynamics studies have shown that the PRD region undergoes a conformational transition during aggregation, extending outwards from the fibrillar core and allowing chaperone access (Isas *et al*., 2015; Lin *et al*., 2017; Falk *et al*., 2020). Therefore, the effect of the P2 within HTTExon1Q_{48} in the context of disaggregation by the trimeric chaperones was then examined. As shown in **Fig. 3.3.1 3**, the trimeric chaperone complex was unable to disaggregate the HTTExon1Q_{48}ΔP2 variant. This indicates that the presence of this domain is required for chaperone interaction at both the soluble and fibrillar stages, and that although other binding sites might become accessible at later stages during the remodelling process, they would not be sufficient to restore disaggregation activity.

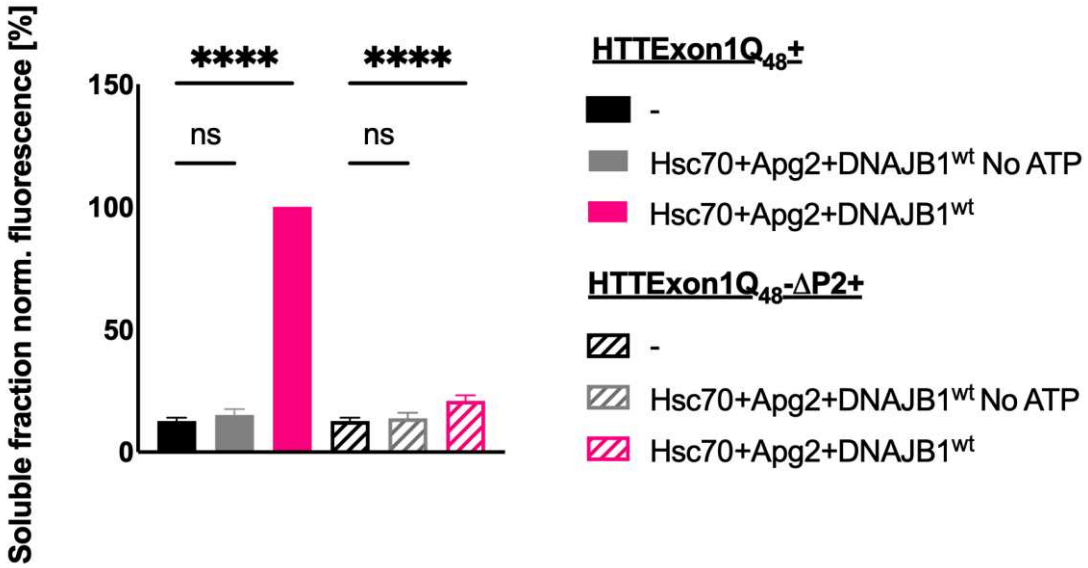

Figure 3.3.1 3 Deletion of second proline region on HTTExon1Q_{48} impairs disaggregation by the trimeric chaperone complex.

Fluorescence measurements of resolubilized HTTExon1Q_{48} or HTTExon1Q_{48}ΔP2 by Hsc70, Apg2 and DNAJB1^{wt}. The fluorescence intensities of each sample were normalized to the sample containing HTTExon1Q_{48}. Bars represent the mean values of three independent experiments and error bars correspond to the mean SD. The significance was determined via one-way ANOVA analysis. Ns; not significant; ****p ≤ 0.0001

3.3.2 The effect of the H244A mutation on the binding of DNAJB1 to HTTExon1Q$_{48}$ fibrils.

Since DNAJB1^{H244A} showed a marked reduction in HTT fibril disaggregation together with Hsc70 and Apg2, the question arose if this defect is due to a reduced affinity between preformed HTT fibrils and the mutated DNAJB1. The binding interaction between DNAJB1 and HTT fibrils is an important step in elucidating the disaggregation mechanism, as JDPs are known to recognize misfolded substrates and deliver them to Hsp70s.

Therefore, I have established a binding assay to compare the binding affinities of DNAJB1^{wt} and DNAJB1^{H244A}. Previously, it was demonstrated by immunostaining and TEM that DNAJB1 is able to bind preformed HTT fibrils (Scior *et al*., 2018). For this purpose, I incubated both DNAJB1^{wt} and DNAJB1^{H244A} with HTT fibrils for 1 h as described in **Fig. 3.3.2 1**, and then sedimented the chaperone-bound fibrils, resolubilized the fibrillar pellet fraction, and analysed the bound DNAJB1 in this fraction by Western blotting.

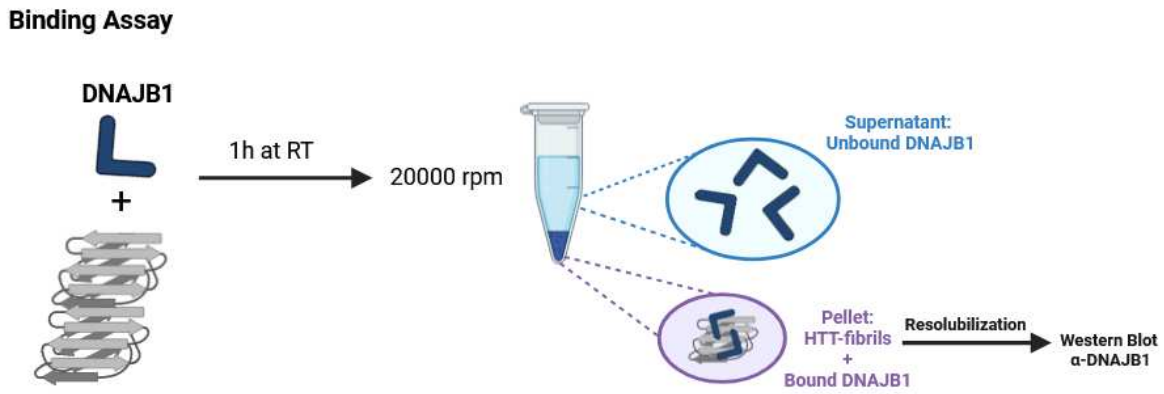

Fig. 3.3.2 1 Schematic representation of the DNAJB1-HTT fibril binding assay.

DNAJB1^{wt} or DNAJB1^{H244A} was incubated with preformed HTTExon1Q$_{48}$ fibrils for 1 hour, and fibril bound DNAJB1 was separated from soluble DNAJB1 by ultracentrifugation, followed by resolubilization and Western blot analysis (Image adapted from Ayala Mariscal *et al.*, 2022).

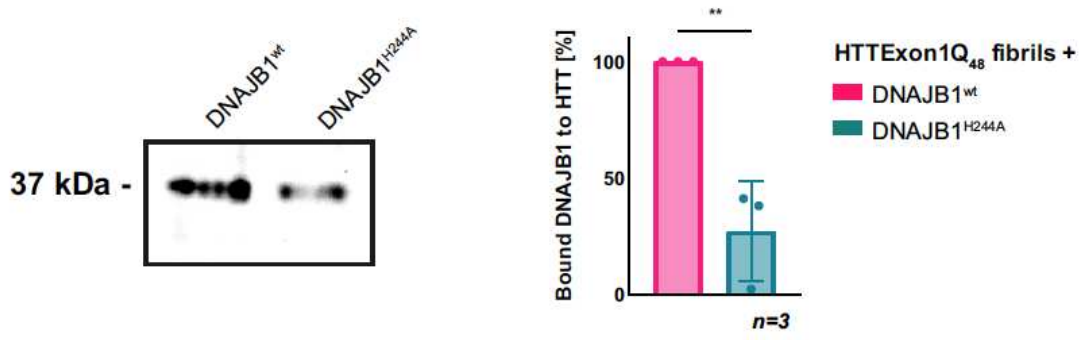

Fig. 3.3.2 2 The H244A mutant significantly impairs DNAJB1 binding to preformed HTT fibrils.

Sedimented DNAJB1^{wt} and DNAJB1^{H244A} bound to HTTExon1Q$_{48}$ fibrils were analyzed by Western blotting. Bars represent the mean values of three independent experiments and error bars correspond to the mean SD. The significance was determined via one-way ANOVA analysis. **p ≤ 0.01.

In comparison to DNAJB1^{wt}, the signal of HTT fibril-bound DNAJB1^{H244A} was almost 70% lower, demonstrating severely reduced affinity of DNAJB1^{H244A} to HTT fibrils **(Fig. 3.3.2 2)**. It is noteworthy, however, that the binding was also not completely abolished, which may explain why DNAJB1^{H244A} together with Hsc70 and Apg2 is still partially active in disaggregation of HTT **(Fig. 3.1.1 2)**.

3.3.3 The effect of the G/F Linker in providing functional specificity to DNAJB1 in disaggregation activity.

In the previous section, the key residues in the HBM of DNAJB1 were investigated how they affect disaggregation of HTT fibrils by the trimeric chaperone complex. Notably, this motif is also conserved, in a class A JDP, DNAJA1. However, DNAJA1 together with Hsc70 and Apg2 has failed to suppress HTT aggregation (Ayala Mariscal *et al.,* 2022).

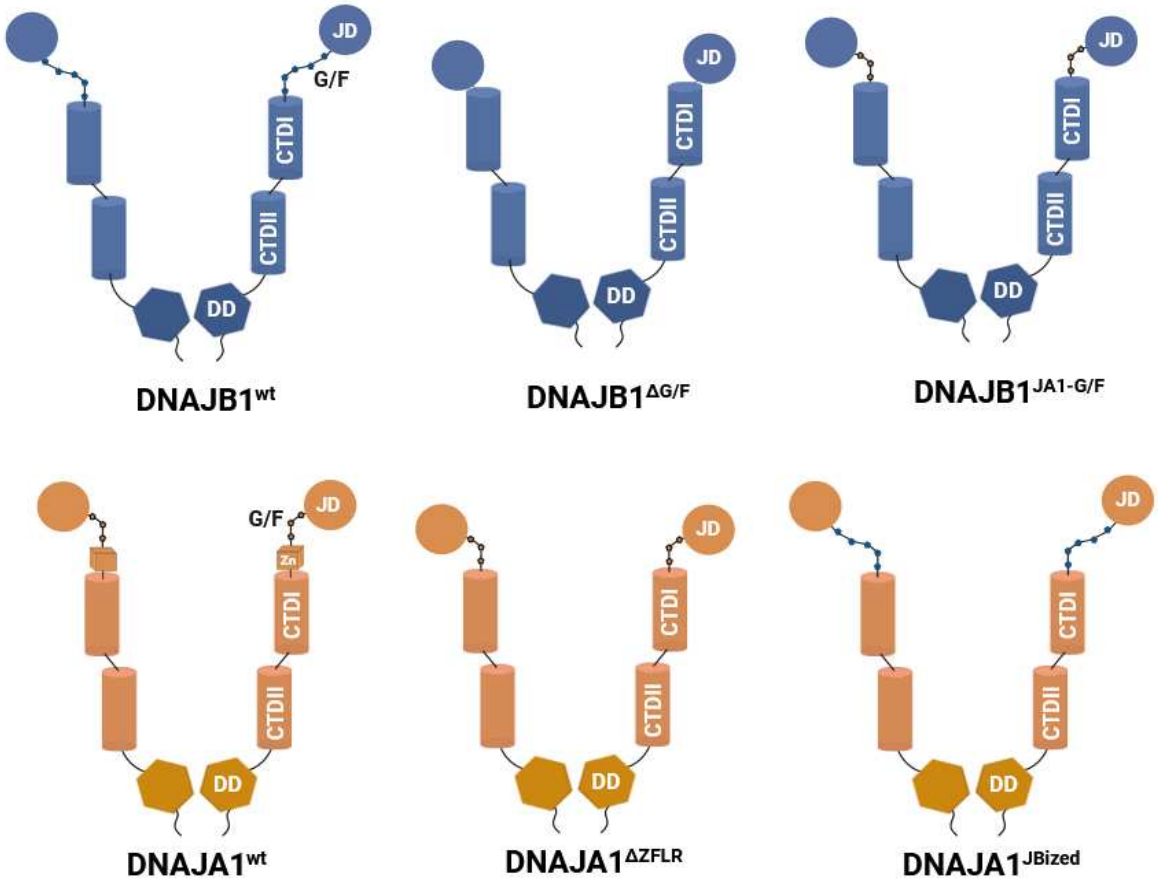

Figure 3.3.3 1 Schematic representation of the DNAJB1 and DNAJA1 variants and their domains. DNAJB1^{wt} (green), DNAJA1^{wt} (orange). In DNAJB1$^{JA1\text{-}G/F}$, the G/F linker region of DNAJB1 was substituted with a shorter G/F linker region of DNAJB1. In DNAJA1^{JB1ized}, ZFLR of DNAJA1 was deleted and the G/F region was replaced by the longer G/F linker of DNAJB1. (Image adapted from Ayala Mariscal *et al.,* 2022)

This suggests that the domains that differ between DNAJB1 and DNAJA1 **(Fig. 3.3.3 1)** must confer specificity to DNAJB1 function in the suppression of HTT aggregation. Therefore, in this chapter, the contribution of different features of DNAJB1 to the disaggregation of HTT fibrils by the trimeric chaperone complex was analysed. First, DNAJA1^{wt} in the presence of Hsc70 and Apg2 was tested in the disaggregation assay and shown to have a significantly lower activity in resolubilizing HTT aggregates **(Fig. 3.3.3 2)**. One of the major differences between DNAJA1 and DNAJB1 is that the flexible G/F-rich region connecting the J-domain to the C-terminus is shorter in DNAJA1. Thus, the G/F-rich linker of DNAJB1 was shortened to make it similar to that of DNAJA1. This variant is referred to as DNAB1$^{JA1\text{-}G/F}$. The disaggregation activity of DNAB1$^{JA1\text{-}G/F}$ was shown to be completely abolished **(Fig. 3.3.3 2)**, suggesting that the G/F-rich linker of DNAJB1 is a key modulator for the disaggregation of HTT fibrils together with Hsc70 and Apg2.

Furthermore, a deletion of the G/F-rich region completely abolished the suppression of HTT aggregation by DNAJB1 with Hsc70 and Apg2, and at the same time abrogated the activity of refolding luciferase and ATPase activities (Ayala Mariscal *et al*., 2022). Thus, expectedly, this mutant was completely inactive in disaggregation of HTT fibrils **(Fig. 3.3.3 2)**. This clearly shows that the G/F-rich region of DNAJB1 is a central element of the protein to be functional.

A second feature of DNAJA1 that distinguishes it from DNAJB1 is a zinc finger-like region (ZFLR) between its G/F region and the CTDI. This ZFLR domain was deleted and replaced with a longer G/F linker of DNAJB1, to study the effect of this region, and named this chimeric protein DNAJA1^{JB1ized}. This variant was able to achieve both the hydrolysis of ATP to ADP and the refolding of luciferase in the presence of Hsc70 and thus validating its general function. It was further tested in a FRET assay and observed that DNAJA1^{JB1ized} could partially suppress HTT aggregation, although not as effectively as DNAJB1^{wt} (Ayala Mariscal *et al*. 2022). Next, I tested DNAJA1^{JB1ized} in the disaggregation assay and similar to the suppression activity it showed a partial activity of up to 50% of the activity of DNAJB1^{wt} **(Fig. 3.3.3 2)**.

Then, the ZFLR region of DNAJA1 was deleted so that DNAJA1 resembled DNAJB1, and the role of this region was further investigated. However, deletion of ZFLR has resulted in the abolition of luciferase refolding activity and suppression of HTT

aggregation (Ayala Mariscal *et al*. 2022). As predicted, DNAJA1$^{\Delta ZFLR}$ together with Hsc70 and Apg2 did not exhibit significant disaggregation activity **(Fig. 3.3.3 2)**.

In conclusion, the data suggest that structural integrity of the G/F-rich linker is an important factor besides the HBM motif that enables DNAJB1 together with Hsc70 and Apg2 to suppress HTT aggregation and to resolubilize pre-formed HTT fibrils.

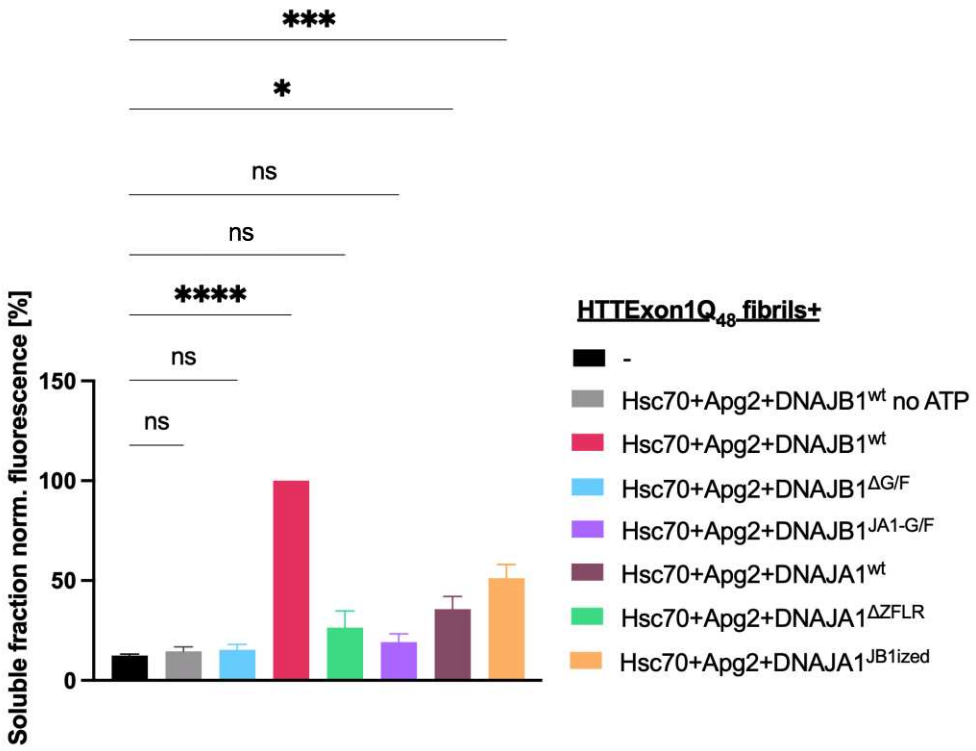

Figure 3.3.3 2 G/F-rich linker of DNAJB1 is a key modulator in disaggregation of HTT fibrils.

Fluorescence measurements of resolubilized HTTExon1Q$_{48}$ by Hsc70, Apg2 and DNAJB1^{wt} or variants. The fluorescence intensities of each sample were normalized to the sample containing HTTExon1Q$_{48}$. Bars represent the mean values of three independent experiments and error bars correspond to the mean SD. The significance was determined via one-way ANOVA analysis. **p ≤ 0.01; ****p ≤ 0.0001; ns not significant.

3.4 Association of DNAJB1/Hsc70 with HTTExon1Q$_{48}$ during fibril growth

As discussed in the previous chapters, the trimeric chaperone complex Hsc70, DNAJB1, and Apg2 has been shown to suppress HTTExon1Q$_{48}$(HTT) fibril formation for a certain period and to disaggregate preformed fibrils. Although DNAJB1 and Hsc70 have been shown to interact with both soluble monomeric and mature HTT fibrils (Scior *et al*., 2018; Ayala Mariscal *et al*., 2022), substrate recognition by the chaperones along the aggregation pathway remains unknown, as chaperone-client interactions are often particularly difficult to characterise due to their dynamic and transient nature. The main open questions are: Can the chaperones interact with different folding entities of HTT as it progresses along the off-folding pathway and forms amyloid fibrils, and do the chaperones remain associated with HTT or is their interaction of only transient nature? Based on these questions, I set out to investigate the individual modes of action of each chaperone, to gain a deeper mechanistic understanding of this machinery.

3.4.1 DNAJB1/Hsc70 target HTT aggregation at early stages.

First, the suppression ability of the trimeric chaperone complex when added at different time points during the aggregation process of HTT was investigated as outlined in **Fig. 3.4 1**. For this purpose, I prepared a number of HTT samples by incubating them for different periods of time, as indicated by the green arrows in **Fig. 3.4 2 a.** The reduction in soluble HTT at these time points was confirmed by a sedimentation analysis **(Fig. 3.4 2 b)**. Next, the three chaperones with an ATP regeneration system were added to these nine different HTT samples and the FRET signals were monitored. As expected, the suppression by the trimeric chaperone complex was compromised as the soluble fraction in these HTT samples was diminished over time **(Fig. 3.4 2 c)**. This was also supported by a sedimentation analysis where all samples were collected at t=20 h and the percentage of soluble HTT was determined. In agreement with the FRET analysis, when the chaperones were added at t=0 h, HTT can be kept completely soluble until t=20 h by the chaperones and was reduced when the chaperones were added at later time points. When aggregation of HTT already started, less HTT could be kept in the soluble state **(Fig. 3.4 2 d)**. This clearly demonstrates that the trimeric chaperone complex was only capable of inhibiting HTT aggregation before a critical aggregate

concentration has been reached, and thereafter the suppression activity has gradually decreased. This finding raised the question whether the chaperones interact with different HTT conformational moieties with different affinities.

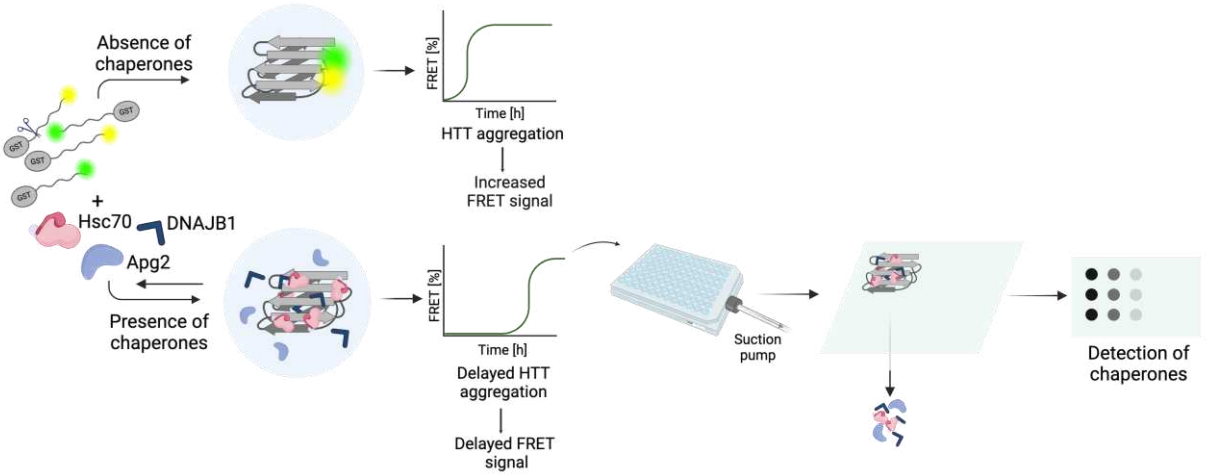

Figure 3.4 1 Schematic representation of the chaperone-HTT binding analysis by FRET assay followed by a filter retardation analysis.

At the end of the FRET assay (60 h time point), HTTExon1Q$_{48}$ (HTT) samples were analyzed by filter retardation and the membrane was stained with antibodies against DNAJB1/Hsc70 to detect HTT fibril-bound chaperones.

To address this question, I have developed a chaperone-HTT binding assay based on filter retardation analysis, as described in **Fig. 3.4 1**. Basically, the rationale of this experiment is that chaperones are added upon initiation of the aggregation process to allow them to suppress HTT aggregation. When suppression of HTT aggregation eventually fails, HTT fibrils can form which can be detected as increase in FRET signal that can reach a plateau. Samples are then collected and subjected to filter retardation. The SDS-insoluble HTT fibrils are retained on the membrane and can be detected by fluorescence imaging. Bound chaperones can be detected by immunostaining.

I collected the samples shown in **Fig. 3.4 2 a** at t=60 h, mixed them with 1% SDS and filtered them through a cellulose acetate membrane. As depicted in **Fig. 3.4 2 e and f**, remarkably, both DNAJB1 and Hsc70 interacted with HTT fibrils the strongest when they have been added at the beginning of the HTT aggregation process. The third member of the trimeric chaperone complex, Apg2, was not detected on the membranes at all, suggesting that Apg2 does not bind to HTT fibrils. For DNAJB1 and Hsc70, the

binding was progressively reduced when they were added at later stages of HTT aggregation. This observation is in agreement with the decreased suppression of HTT aggregation. This suggests a clear correlation between the chaperone association with HTT fibrils and the degree of suppression of HTT aggregation.

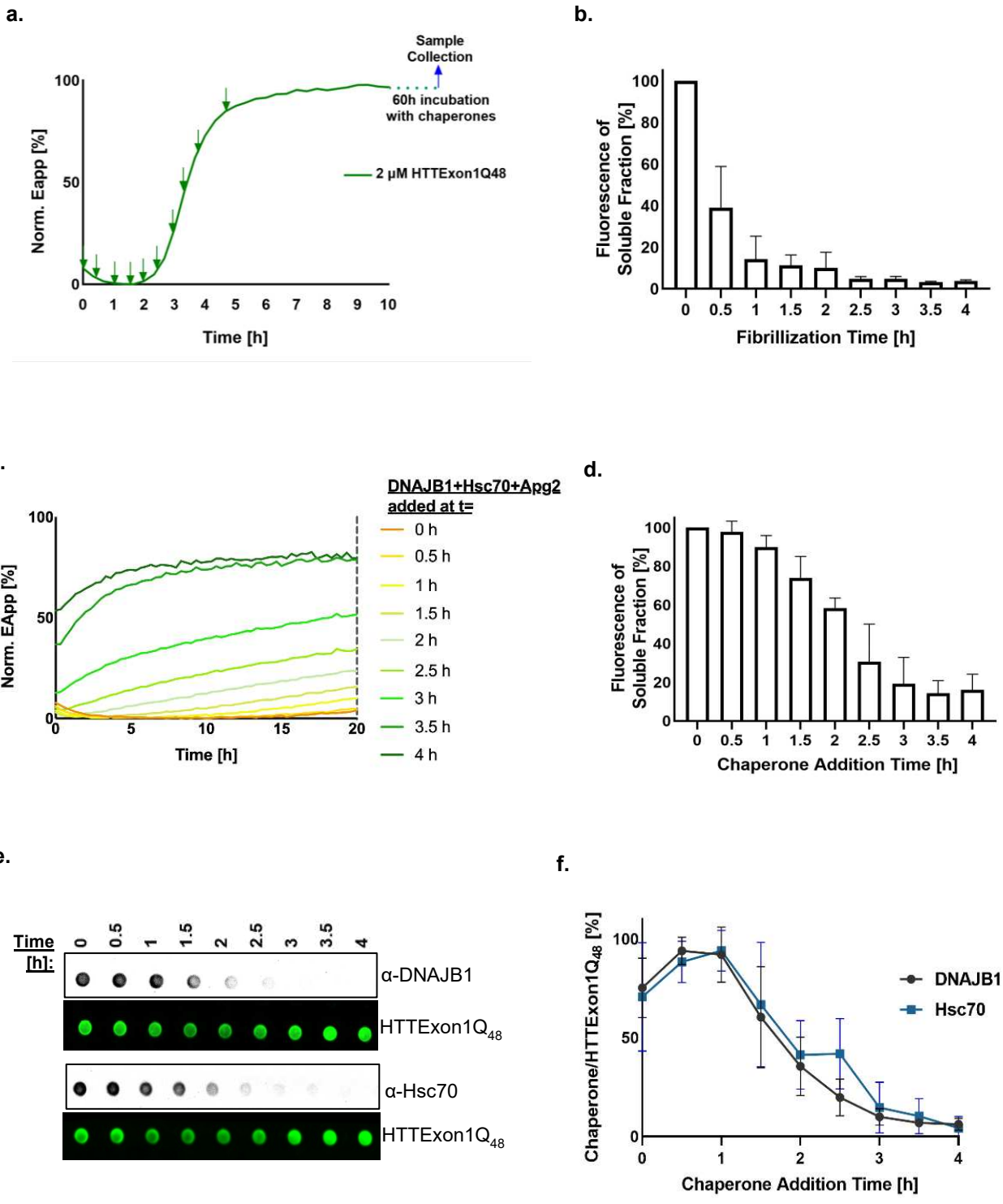

Figure 3.4 2 DNAJB1/Hsc70 preferentially bind HTT at the early stages of aggregation process.

a. FRET measurement of the fibrillization of HTTExon1Q_{48} over 10 h. An increase in FRET indicates an increase in HTT aggregation. The total concentration of HTTExon1Q_{48} is 2 µM with 1 µM each of HTTExon1Q_{48}-CyPet and HTTEQ_{48}-YPet. Green arrows depict the time points when the chaperones were added along the HTT aggregation pathway for the analyses shown in **c, d,** and **e**. All samples were collected at the t=60 h (indicated with blue arrow) and subjected to filter retardation analysis (**e**).

b. The graph depicts the soluble 2 µM HTTExon1Q_{48} levels for the first 4 hours after initiating the aggregation. At each time point, the samples were subjected to ultracentrifugation to separate soluble from aggregated HTTExon1Q_{48} and the fluorescence of the supernatant (= soluble fraction) was quantified and normalized to the signal at t = 0 h. Bars represent the mean values of three independent experiments and error bars correspond to the mean SD.

c. FRET measurements of 0.75 µM HTTExon1Q_{48} fibrilization in the presence of Hsc70+DNAJB1+Apg2 + ATP. Chaperones were added at different time points along the aggregation pathway of HTTExon1Q_{48} as depicted in **a**. All samples were collected at the 20 h time point (indicated by dashed line) for solubility analysis shown in **d**.

d. The graph depicts the solubility of HTT Exon1Q_{48} levels of samples collected in **c**. Bars represent the mean values of three independent experiments and error bars correspond to the mean SD.

e. Filter retardation analyses of the binding of Hsc70 and DNAJB1 to HTTExon1Q_{48} aggregates. The time points represent the time when the chaperones were added after initiation of HTTExon1Q_{48} aggregation as depicted by the green arrows in **a**. The binding of the chaperones was assessed at the 60-h time point as outlined in **a** and analyzed by antibody staining of the filter retardation membrane. Top rows depict the signals of the bound chaperones and bottom rows show the signals of HTT Exon1Q_{48} aggregates where the YPet fluorescence intensities of HTTExon1Q_{48}-YPet were used as readout. The depicted blots are representatives of three independent experiments.

f. The graph shows the quantification of the densitometric analyses of the filter retardation assays depicted in **e**. The ratio of DNAJB1 and Hsc70 to HTTExon1Q_{48} signal at each time point was normalized to the ratio at the time point with the highest ratio. The plot shows the mean ratios of three independent experiments at each time point. Error bars correspond to the mean SD.

3.4.2 DNAJB1/Hsc70 bind to HTT in a co-dependent manner.

In the data set shown above, I could detect binding of Hsc70 and DNAJB1, but not Apg2 to HTT fibrils when Hsc70 and DNAJB1 were added at early stages of the HTT aggregation process. The interaction pattern of both Hsc70 and DNAJB1 to HTT fibrils appears identical, raising the question if both chaperones bind together to HTT. Thus, I studied the binding of both DNAJB1 and Hsc70 to HTT aggregates in more detail. As previously published, J-domain proteins (JDPs) can bind substrate proteins independently of Hsp70s and ATP (Langer *et al*., 1992; Han *et al*., 2003; Lotz *et al*., 2010; Scior *et al*., 2018). Therefore, I wanted to test different conditions necessary for the interaction of both chaperones to HTT aggregates.

The chaperones were added at the beginning of the HTT aggregation process, and all samples were collected at t=60 h when HTT aggregation reached an equilibrium as reflected by the plateau of the FRET measurements. DNAJB1 and Hsc70 were first added to HTTExon1Q_{48} individually and as shown previously by Scior *et al*. no suppression activity was observed **(Fig. 3.4 3 a, magenta and brown curves)**. A partial suppression activity was observed when Hsc70 was added together with DNAJB1 which was further enhanced by the addition of Apg2 **(Fig. 3.4 3 a, green and red curves)**. When all three chaperones were present, but ATP and ATP regeneration system were omitted, suppression of HTT aggregation was completely abrogated as reported earlier **(Fig. 3.4 3 a, cyan curve)**. The control sample containing only HTTExon1Q_{48}, represented by the black curve in **Fig. 3.4 3 a**, produced a fluorescence signal of HTTExon1Q_{48}-YPet on the filter retardation membrane, but as expected, no immunostaining signal of the chaperone specific antibodies **(Fig. 3.4 3 b)**. The next controls were samples of DNAJB1 or Hsc70 without HTT, which also did not produce an antibody signal as soluble DNAJB1 and Hsc70 were completely denatured by 1% SDS and passed through the membrane. These controls were especially important because in the absence of SDS, even without any HTT fibrils, chaperones can stick to the membrane.

The next samples analyzed by filter retardation were HTTExon1Q_{48} + DNAJB1 and HTTExon1Q_{48} + Hsc70 which were represented by magenta and brown curves in the FRET assay, respectively **(Fig. 3.4 3 a)**. These samples did not show any signals on the membrane with chaperone-specific antibodies indicating that there is no association

of the individual chaperones with HTT fibrils. It was particularly surprising that DNAJB1 did not bind to HTT aggregates when added at the beginning of the HTT aggregation process. Our lab could previously show that DNAJB1 can bind to mature fibrils (Scior *et al*., 2018, Ayala Mariscal *et al*., 2022), suggesting that the interaction with HTT along its aggregation pathway is either too weak to detect or does not occur independently of Hsc70. However, both DNAJB1 and Hsc70 were detected to bind to aggregating HTT in the presence of each other and ATP **(Fig. 3.4 3 b).** Upon addition of Apg2, both, DNAJB1 and Hsc70 were detected to associate with HTT aggregates as expected. By densitometric analysis, the effect of Apg2 was investigated by comparing the chaperone to fibril signal ratios. However, no significant effect was observed for both, Hsc70 and DNAJB1 **(Fig. 3.4 3 c)**. Either Apg2 does not affect the binding of Hsc70 and DNAJB1 to HTT or the effect is too subtle to be detected by filter retardation analysis that. At this point, I cannot distinguish between these possibilities due to a lack of a more sensitive method. Finally, as expected, the samples consisting of trimeric chaperones that lacked ATP did not produce immunostaining signals for the chaperones **(Fig. 3.4 3 b)**, demonstrating that chaperone binding to HTT requires ATP. Taken together, these experiments show that Hsc70 and DNAJB1 require each other's presence to interact with HTT along the HTT aggregation pathway in an ATP dependent manner.

To confirm the ATP dependence of chaperone binding to HTT fibrils, I used confocal microscopy to visualise the binding of the chaperones to HTT aggregates. DNAJB1 was chemically labelled with the Alexa-647 fluorophore and incubated with HTT-CyPet/YPet in the presence of Hsc70 and Apg2, with or without ATP, for 96 hours to allow the fibrils to form. The samples were then treated with 1% SDS in the same way as I had carried out the filter retardation assays. This was followed by centrifugation and complete removal of the soluble fraction from the pellet fraction. This step was critical, as any SDS left in the solution could cause the particles to float on the microscope slide. The samples were thoroughly resuspended with resuspension buffer containing no SDS and pipetted directly onto the slides **(Fig. 3.4 4)**.

a.

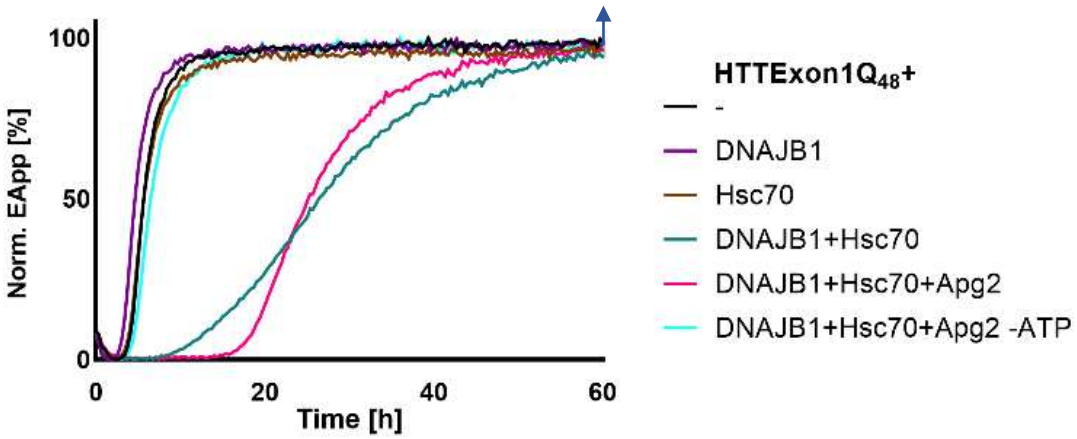
Norm. EApp [%]
100
50
0
0
20
40
60
Time [h]
HTTExon1Q48+
-
DNAJB1
Hsc70
DNAJB1+Hsc70
DNAJB1+Hsc70+Apg2
DNAJB1+Hsc70+Apg2 -ATP

b.

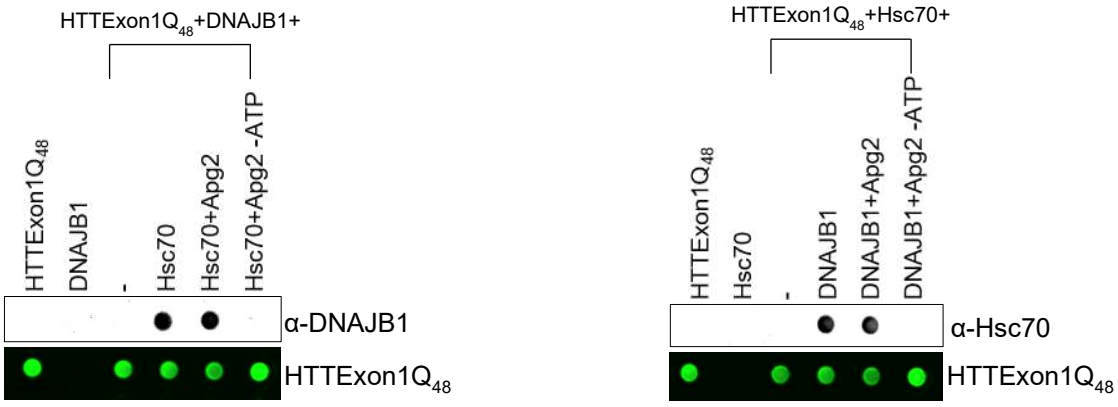
HTTExon1Q48+DNAJB1+
HTTExon1Q48
DNAJB1
-
Hsc70
Hsc70+Apg2
Hsc70+Apg2 -ATP
α-DNAJB1
HTTExon1Q48
HTTExon1Q48+Hsc70+
HTTExon1Q48
Hsc70
-
DNAJB1
DNAJB1+Apg2
DNAJB1+Apg2 -ATP
α-Hsc70
HTTExon1Q48

c.

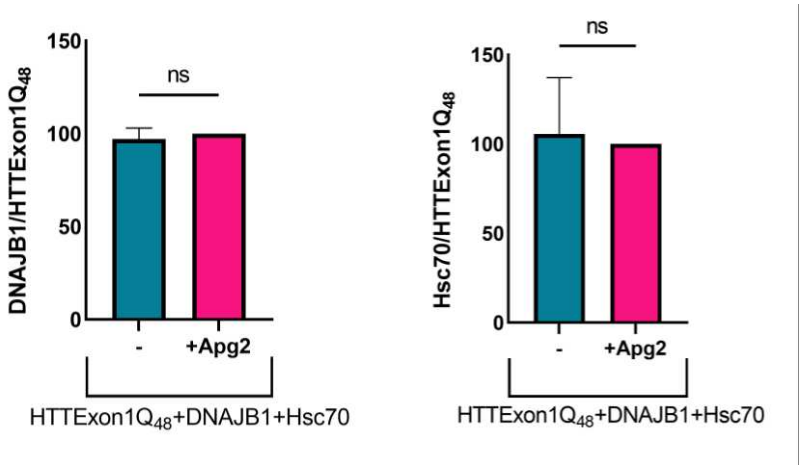
DNAJB1/HTTExon1Q48
150
100
50
0
ns
-
+Apg2
HTTExon1Q48+DNAJB1+Hsc70
Hsc70/HTTExon1Q48
150
100
50
0
ns
-
+Apg2
HTTExon1Q48+DNAJB1+Hsc70

Figure 3.4 3 DNAJB1/Hsc70 require the presence of each other and ATP to bind HTT

a. FRET measurements of the fibrillization of 0.75 µM HTTExon1Q_{48} in the absence and presence of Hsc70 and/or DNAJB1. Hsc70 + DNAJB1 (green), Hsc70 + DNAJB1 + Apg2 (red) all with the additional presence of an ATP regenerating system, and in parallel in the presence of Hsc70, DNAJB1 + Apg2, but lacking ATP and the regenerating system (blue). The chaperones were added at t = 0 h together with HTTExon1Q_{48}. At the 60h time point, all samples were collected for the subsequent filter retardation analyses depicted in **b**.

b. Filter retardation analysis of the samples as depicted in **a**. Chaperones and ATP were added at t = 0 h of the HTTExon1Q_{48} aggregation as indicated above. The membrane was analyzed with antibodies against DNAJB1 (left), and Hsc70 (right) in top rows and the fluorescent signals report on the presence of HTTExon1Q_{48} aggregates. The depicted blots are representatives of three independent experiments.

c. The graphs show the quantification of densitometric analyses of Hsc70 (right) and DNAJB1 (left) binding to HTTExon1Q_{48} aggregates in the presence and absence of Apg2. The ratio of Hsc70 and DNAJB1 to HTTExon1Q_{48} signal intensities of each sample (as shown in **b**) were normalized to the ratio of the Apg2-containing samples. The graphs depict the mean ratios of three independent experiments and the data were analyzed by an unpaired t-test. Error bars correspond to the mean SD. Ns; not significant.

The HTT fibrils appeared to be quite heterogeneous, with a range of 0.5 µm to 2.5 µm with the majority of fibrils around 1 µm sizes and different morphologies. In the presence of ATP and all three chaperones, I observed co-localisation of DNAJB1 with HTT fibrils, and when I zoomed in on a single HTT aggregate, DNAJB1 appeared to co-localise on the entire fibrillar surface **(Fig.3.4 4, top).** However, consistent with the filter retardation assay, no co-localisation of DNAJB1 with HTT fibrils was observed in the absence of ATP **(Fig. 3.4 4, bottom).** On the other hand, it should be noted that confocal microscopy can only provide a limited degree of resolution for such small and complex particles. Therefore, to obtain a more detailed view of how the chaperones are located on the fibrils, techniques such as cryo-electron microscopy must be used to achieve higher resolution. Nevertheless, these images provide a first glimpse on the interaction of DNAJB1 with HTT fibrils.

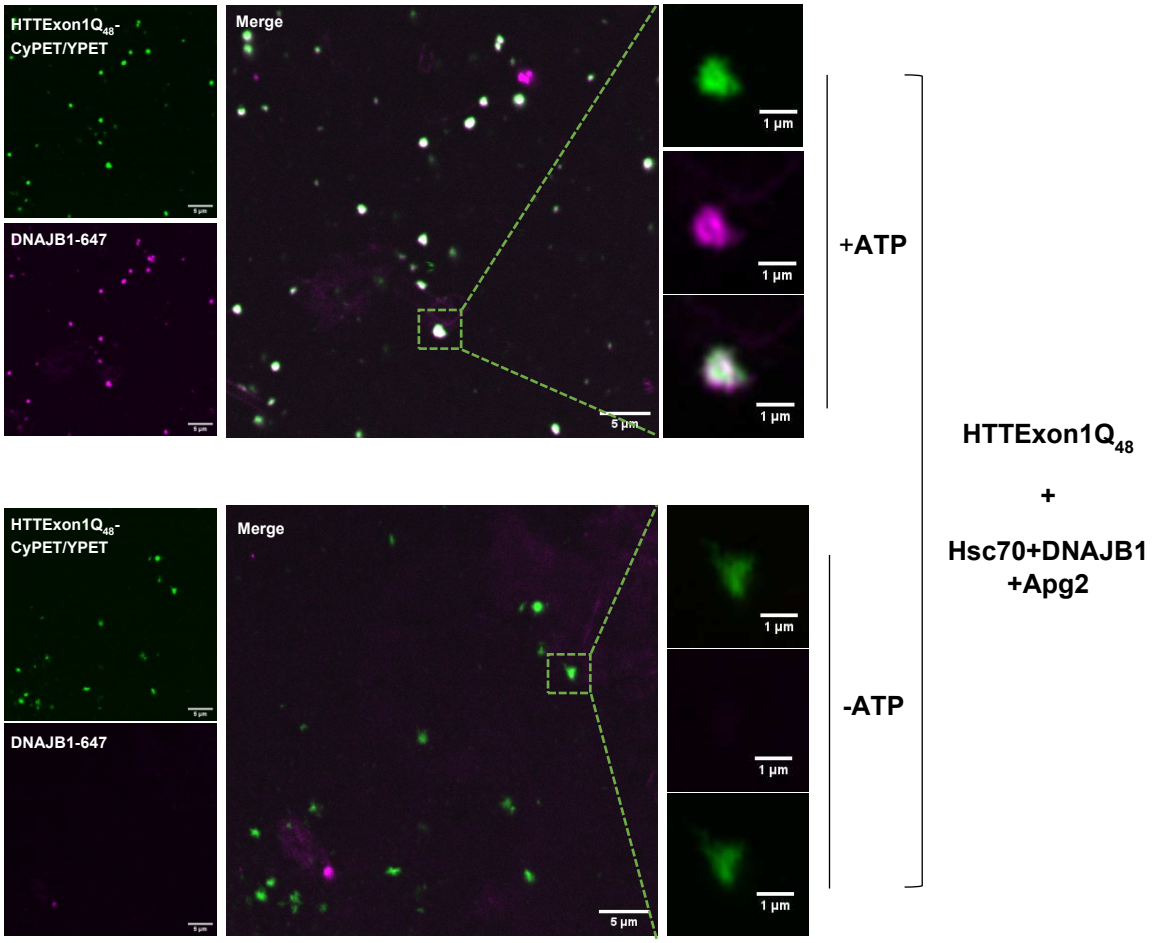

Figure 3.4 4 ATP dependence of DNAJB1 binding to HTT is confirmed by confocal microscopy.

Confocal laser scanning microscopy images of HTTExon1Q_{48}-CyPet/YPet aggregates bound by DNAJB1-Alexa647 in the presence of Hsc70 and Apg2 with (top) and without (bottom) ATP included in the mixtures. Scale bar is 1 µm.

3.4.3 Chaperone binding to HTTExon1Q_{48} requires an intact ATPase cycle.

The observation that the chaperone-fibril association requires the presence of ATP raises the question of whether it is only the binding of ATP to Hsc70 or a constant ATPase cycle that enables binding. The observation that both chaperones depend on each other to bind HTT aggregates suggests the latter as DNAJB1 activates the ATPase activity of Hsc70. JDP-mediated ATP-hydrolysis leads to dramatic conformational changes of Hsc70 (Liberek *et al*.,1991; Zuiderweg *et al*., 2013; Kityk *et al*., 2018). However, it is not clear how these structural changes affect the interaction between the Hsp70-JDP complexes and the substrate proteins. To investigate the effect of ATP hydrolysis on HTT binding, I substituted ATP with a non-hydrolysable analogue, AMP-PNP, that can also bind to the nucleotide binding domain of Hsc70 and induce allosteric changes in the structure of Hsc70 (Bhattacharya *et al*., 2009; Zhuravleva *et al*., 2012). As previously reported, AMP-PNP stabilizes Hsc70 in the ATP-bound state, inducing conformational changes in the residues in the nucleotide-binding domain, but no further changes as it does not hydrolyze (Bhattacharya *et al*., 2009). Therefore, the whole ATPase cycle is compromised and the suppression of HTT aggregation activity is completely impaired (Scior *et al*., 2018). I repeated and thereby validated the FRET assay comparing the suppression of HTT aggregation by the trimeric chaperone complex in the presence of ATP or AMP-PNP. I confirmed that there was no suppression of HTT aggregation when AMP-PNP is used as nucleotide and consequently no binding of DNAJB1 and Hsc70 was detected on the membranes in the subsequent filter retardation assay **(Fig. 3.4 5 a and b)**.

I used an additional approach by mutating the HPD motif of DNAJB1, DNAJB1^{H32Q}, to impair the ability of DNAJB1 interact with and to stimulate Hsc70´s ATPase activity (as presented earlier in section 3.2) **(Fig. 3.4 5 a)**. As depicted in **Fig. 3.4 5 b** substituting DNAJB1 by DNAJB1^{H32Q} leads to a failure of Hsc70 and DNAJB1^{H32Q} binding to HTT aggregates even in the presence of ATP. Thus, both DNAJB1 and Hsc70 binding clearly requires an intact ATPase cycle of Hsc70 to effectively bind to aggregating HTT. These results suggest that chaperone association with fibrils does not occur in a single step, but they continuously associate (and maybe also dissociate) to and from HTT along the aggregation pathway.

a.

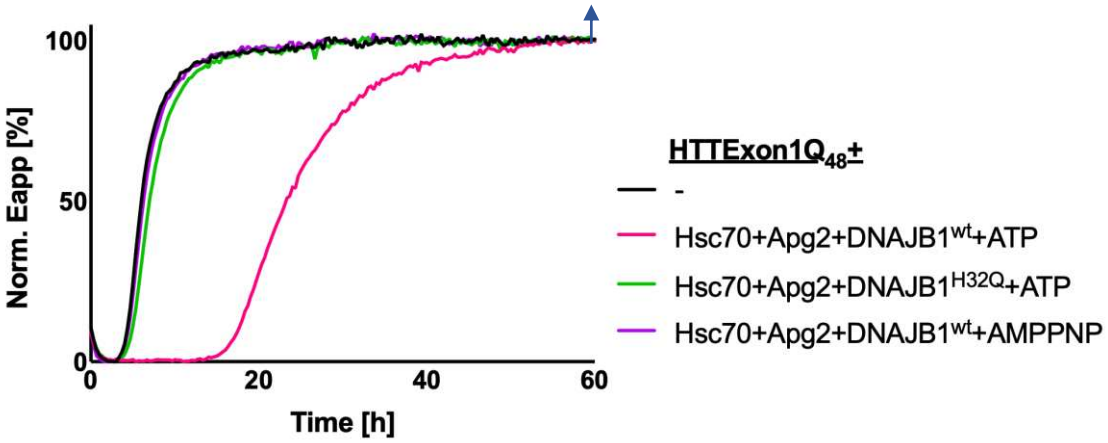

b.

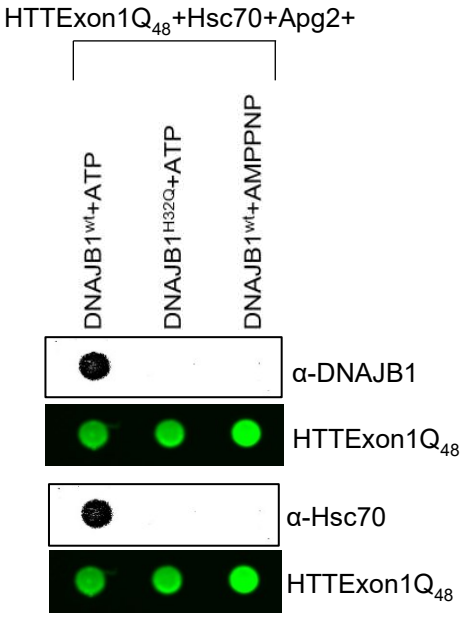

Figure 3.4 5 Disruptions in ATPase cycle impairs chaperone/fibril binding.

a. FRET measurements over 60 h of the fibrillization of HTTExon1Q_{48} in the presence of Hsc70 + Apg2 and either DNAJB1^{wt} (red), DNAJB1^{H32Q} (green) and the ATP regenerating system or DNAJB1^{wt} and the non-hydrolysable ATP analogue AMP-PNP (magenta).

b. Filter retardation assay of the samples that were collected at the 60 h time point of the FRET assay depicted in **b**. The membranes were stained with antibodies against DNAJB1 (top blot) and Hsc70 (bottom blot) and the signal intensities of the YPet fluorescence that reports on the presence of HTTExon1Q_{48}-YPet aggregates are shown below.

3.4.4 Time dependent analysis of chaperone binding

As shown in the previous experiments, Hsc70 and DNAJB1 bind preferentially to HTT in the early stages of HTT aggregation and then stay bound to HTT fibrils. To gain more mechanistic insight into the interaction of DNAJB1/Hsc70/Apg2 with HTT, the trimeric chaperone complex was added at the beginning of the aggregation, and the samples for the binding analysis were collected at specific time points as indicated by dashed lines in **Fig. 3.4 6 a**. First, HTTExon1Q_{48} in the absence of chaperones as control was analysed by the filter retardation assay **(Fig. 3.4 6 b)**. As depicted by a densitometric analysis, while the FRET curve reached a plateau at about t=10 h, the fluorescence intensity increases further until the last sample point, indicating that fibrillar growth continues beyond the point of reaching the FRET plateau **(Fig. 3.4 6 c)**. This suggests that the FRET signal becomes saturated at some point and further maturation of the fibrils must be monitored by filter retardation for a better assessment of aggregation, particularly at later stages.

The next analysis was carried out to study the binding of DNAJB1+Hsc70 with HTT in the absence or presence of Apg2. As performed in the previous sections, samples were subjected to filter retardation analysis and chaperone binding was determined by immunostaining. For this experiment, I used fluorescently labelled secondary antibodies for the analysis of chaperone binding. Filter retardation analysis for HTTExon1Q_{48} + DNAJB1 + Hsc70 and HTTExon1Q_{48} + DNAJB1 + Hsc70 + Apg2 samples showed increasing signals for HTT and DNAJB1/Hsc70 over time (**Fig. 3.4 6 d and e)**. However, it was striking that the ratio of bound DNAJB1 per HTT was at its maximum when the logarithmic phase of HTT aggregation started at t=15h and this ratio progressively decreased over time **(Fig. 3.4 6 f)**. The analysis for Hsc70 binding yielded the same result where the Hsc70/HTT ratio declined with the progression of fibrillization, too **(Fig. 3.4 6 g)**. In addition, a common outcome for both DNAJB1 and Hsc70 binding was that at t=15 h, in the presence of Apg2, chaperone/fibril ratios were slightly higher than in the absence of Apg2. However, they eventually reach the same level at subsequent time points. A possible explanation for this difference could be that in the absence of Apg2, HTT aggregation starts around t=8h, which should be the time point when this sample has its maximum level of chaperone/HTT ratio. By t=15h, the ratio might already decline as HTT starts to aggregate and escape the suppression in the presence of all three chaperones.

Lastly, it can be argued that the antibody may not reach the chaperones when they could become buried in fibrils which may account for the reduction of chaperone/fibril ratio. To eliminate this possibility, I have used fluorescently labelled DNAJB1. For this, I conjugated Alexa-647 maleimide fluorophore to DNAJB1 through free cysteines by the principles of click chemistry. The activity of $DNAJB1^{Alexa647}$ was analysed in a suppression of HTT aggregation assay by FRET and is depicted in **Fig. 3.4 7 a.** $DNAJB1^{Alexa647}$ was as active as $DNAJB1^{wt}$ if not slightly more which could be due to the extra purification steps during the labelling process in suppressing $HTTExon1Q_{48}$ together with Hsc70 and Apg2. The samples were collected for filter retardation analysis at the time points indicated in **Fig. 3.4 7 a.** The densitometric analysis showed again a decline in chaperone to fibril ratio, which supported the previous results performed by immunostaining **(Fig. 3 4 7 b and c)**.

Consequently, the decrease in the ratio of bound chaperones to HTT fibrils needs to be carefully evaluated, considering the correlation between the binding and suppressive activity of chaperones. Even though both the fibril and chaperone signals increased individually over the time course of HTT aggregation, the decreasing chaperone/HTT fibril ratio might be difficult to comprehend. The trimeric chaperone complex can only achieve suppression for a certain period, after which it starts to fail and eventually aggregation occurs. It is not known why the chaperones fail at a certain stage, and this result may indicate that, during the suppression phase, DNAJB1/Hsc70 begin to become saturated with the bound HTT. With time, more HTT aggregates accumulate and may trap DNAJB1 and Hsc70 and prevent them from suppressing HTT aggregation. This suggests that while chaperone binding to HTT is a requirement for suppression, their irreversible association with fibrils appear as the consequence of the inevitable failure of this chaperone complex.

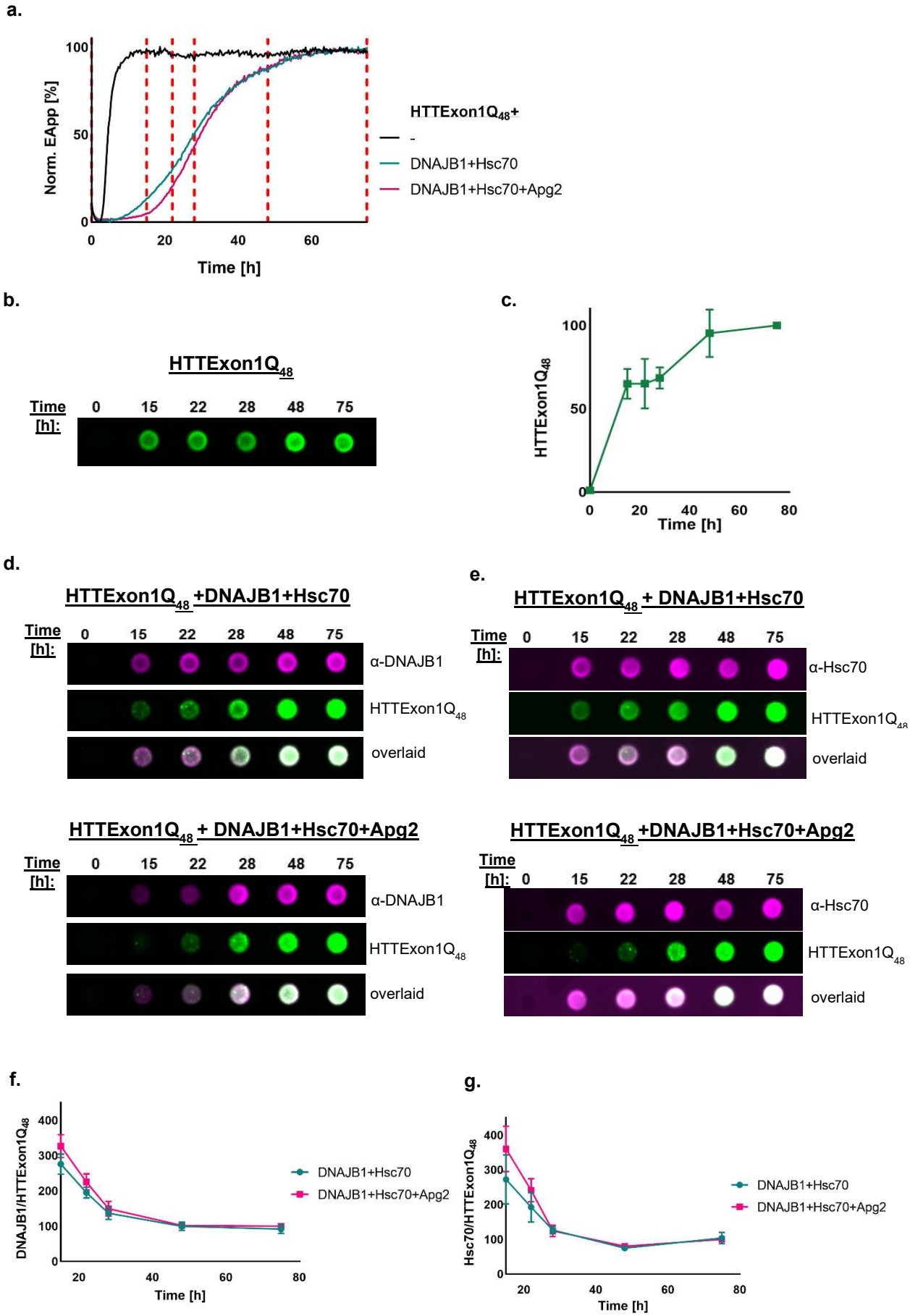
a.
Norm. EApp [%]
Time [h]
HTTExon1Q48+
-
DNAJB1+Hsc70
DNAJB1+Hsc70+Apg2
b.
HTTExon1Q48
Time [h]:
0 15 22 28 48 75
c.
HTTExon1Q48
Time [h]
d.
HTTExon1Q48 +DNAJB1+Hsc70
α-DNAJB1
HTTExon1Q48
overlaid
HTTExon1Q48 + DNAJB1+Hsc70+Apg2
e.
HTTExon1Q48 + DNAJB1+Hsc70
α-Hsc70
HTTExon1Q48 +DNAJB1+Hsc70+Apg2
f.
DNAJB1/HTTExon1Q48
g.
Hsc70/HTTExon1Q48

Figure 3.4 6 Time bound chaperone-binding assay

a. FRET measurements over 75 h of the fibrilization of HTTExon1Q_{48} in the presence of Hsc70 and DNAJB1 (green), Hsc70, DNAJB1, Apg2 (red) both supplemented with an ATP regenerating system or in the absence of chaperones and ATP (black). The dashed lines indicate the time points when the samples were collected for the subsequent filter retardation assay.

b. Filter retardation analysis of HTTExon1Q_{48}-CyPet/YPet aggregation throughout the time course of 75 h by fluorescent YPet imaging for the control sample depicted as the black curve in **a**.

c. The graph shows a densitometric analysis of the signals of the filter retardation analysis depicted in **b**. HTTExon1Q_{48} signal at each time point was normalized to the intensity at t=75 h.

d. Filter retardation analysis of the HTTExon1Q_{48} + Hsc70 + DNAJB1 (top) and HTTExon1Q_{48} + Hsc70 + DNAJB1 + Apg2 sample (bottom) and time course analysis of the binding of DNAJB1 to the HTTExon1Q_{48} aggregates. DNAJB1 binding was analysed by immunostaining and a secondary antibody labelled with Alexa-647 (magenta). HTTExon1Q_{48} was detected by the YPet fluorescence (green). A merge of both fluorescence intensities is depicted below. The depicted filter retardation analyses are representatives of three independent experiments.

e. As in **d**, but analysis of the binding of Hsc70 to HTTExon1Q_{48} aggregates. Hsc70 was also analysed by immunostaining and a secondary antibody labelled with Alexa-6478 (magenta). HTTExon1Q_{48} was detected by the YPet fluorescence (green). A merge of both fluorescence intensities is depicted below. The depicted filter retardation analyses are representatives of three independent experiments.

f. The graphs show a densitometric analysis of the signals of the filter retardation analyses depicted in **d**. The ratio of DNAJB1 to HTTExon1Q_{48} signal at each time point was normalized to the ratio at t=75 h. The DNAJB1/HTTExon1Q_{48} ratios in the presence of Hsc70, DNAJB1 and Apg2 are depicted in red and in the absence of Apg2 in green. The plots indicate the mean ratios at each time point and error bars correspond to the mean SD.

g. The graphs show a densitometric analysis of the signals of the filter retardation analyses depicted in **e**. The ratio of Hsc70 to HTTExon1Q_{48} signal at each time point was normalized to the ratio at t=75 h. The Hsc70/HTTExon1Q_{48} ratios in the presence of Hsc70, DNAJB1 and Apg2 are depicted in red and in the absence of Apg2 in green. The plots indicate the mean ratios at each time point and error bars correspond to the mean SD.

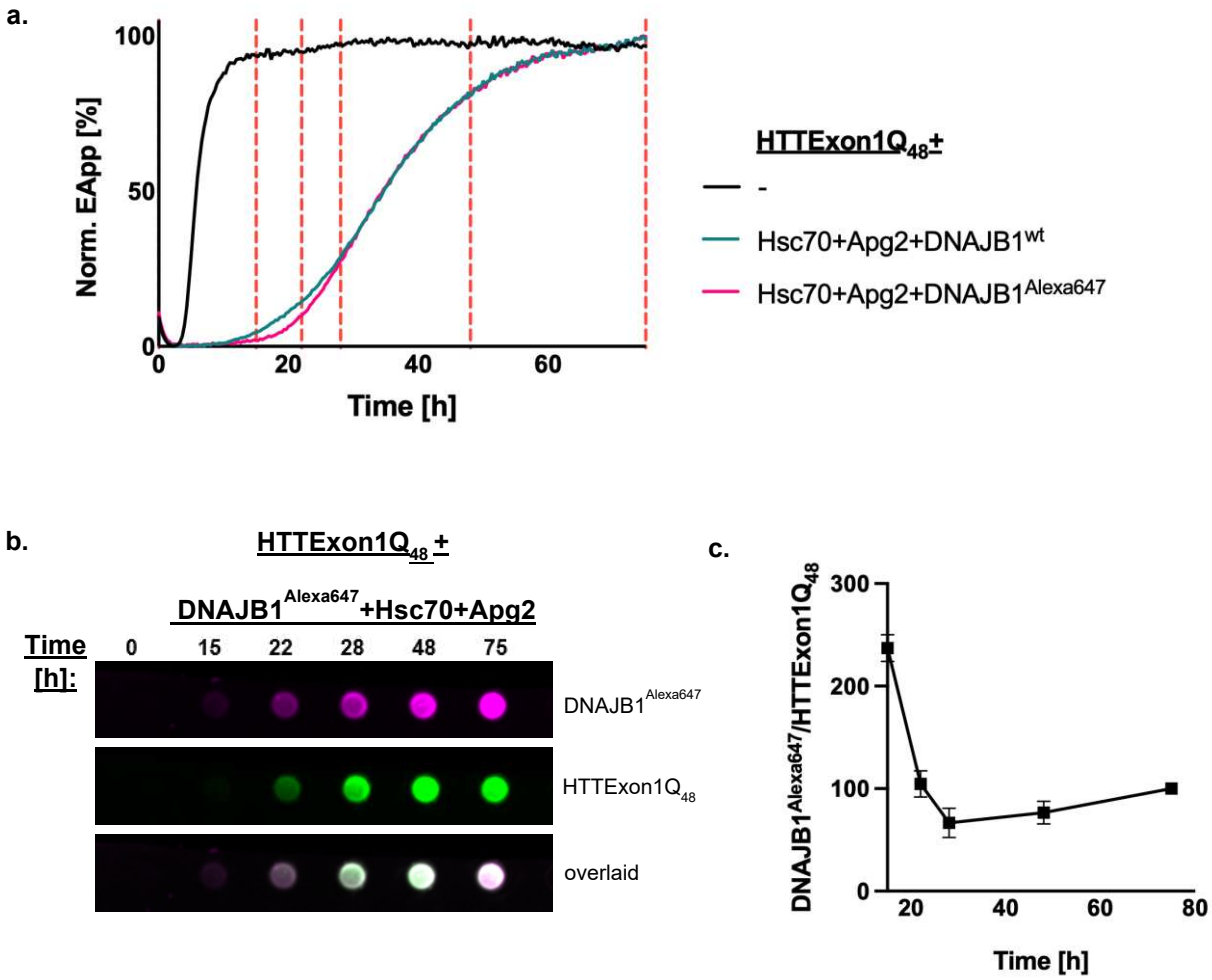

Figure 3.4 7 Time bound binding assay with fluorescently tagged DNAJB1.

a. FRET measurements over 75 h of the fibrilization of HTTExon1Q_{48} in the presence of Hsc70, Apg2 and DNAJB1^{wt} (green) or DNAJB1^{Alexa647} (red) or in the absence of chaperones (black). The dashed lines indicate the time points when samples were collected for the subsequent filter retardation assay depicted in **b**.

b. Filter retardation assay of the samples collected at the indicated time points of the FRET assay depicted in **a**. The signals of DNAJB1 were obtained by fluorescent imaging of DNAJB1^{Alexa647} (magenta) and the fluorescent signals in the second row report on the presence of HTTExon1Q_{48}-YPet (green) aggregates. A merge of DNAJB1 and HTTExon1Q_{48} signal is shown in the third row. The depicted filter retardation analyses are representatives of three independent experiments.

c. The graph shows a densitometric analysis of the signals of the filter retardation analyses depicted in **b**. The ratio of DNAJB1 to HTTExon1Q_{48} signal at each time point was normalized to the ratio at t=75 h. The plots indicate the mean ratios at each time point and error bars correspond to the mean SD.

3.4.5 Mutation of the HBM/PRD binding interface of DNAJB1 and HTT disrupts association of DNAJB1/Hsc70 with HTT fibrils.

The binding interface between HTT and DNAJB1 was previously identified by our lab (Ayala Mariscal *et al.,* 2022). DNAJB1 binds with the hinge region between C-terminal domain I and II to the polyQ-adjacent proline rich domain of HTT. H244 of DNAJB1 was identified as key amino acid in the ability of DNAJB1 to suppress HTT aggregation together with Hsc70 and Apg2 (Ayala Mariscal *et al.,* 2022). As shown previously, mutation of residue H244 in the C-terminus of DNAJB1 to alanine, completely abolished the suppression by the trimeric chaperone complex and severely impaired the disaggregation activity (Ayala Mariscal *et al*., 2022). In Section 3.3.2, a sedimentation-based binding assay performed with pre-formed HTT fibrils in the absence of SDS showed that the H244A mutant of DNAJB1 showed a significant reduction in its ability to bind HTT fibrils. Next, the SDS-stable binding of the H244A mutant along the aggregation pathway was studied. As in the previous experiments, I performed a FRET assay with this mutant **(Fig. 3.4 8 a)**, followed by a filter retardation analysis. Chaperone-HTT fibril ratios were compared between wild-type and H244A mutant of DNAJB1, and it was observed that only small fractions of DNAJB1^{H244A} were bound to the fibrils **(Fig. 3.4 8 b top row and c)**. This result is similar to the binding assay in Section 3.3.2, where DNAJB1^{H244A} was bound to the fibrils at later stages of fibrillization, but the binding was not sufficient to achieve suppression together with Hsc70 and Apg2. Interestingly, disruption of the DNAJB1-HTT interaction by the H244 mutation also abrogated the Hsc70-HTT binding interaction **(Fig. 3.4 8 b third row and c)**, consistent with previous literature suggesting that substrates are first captured by J-domain proteins and then handed over to Hsc70 for remodelling (Laufen *et al*., 1999; Wittung-Stafshede *et al*., 2003; Silberg *et al*., 2004; Kityk *et al*., 2018).

Second, the effect of the second proline region of HTT, with which DNAJB1 interact, on the binding of chaperones was investigated (Ayala Mariscal *et al*., 2022). For that, as demonstrated in Ayala Mariscal *et al*., I performed a FRET assay with HTTExon1Q$_{48}$ and HTTExon1Q$_{48}$ΔP2 in the presence of the trimeric chaperone complex and confirmed that the chaperones were unable to suppress HTTExon1Q$_{48}$ΔP2 **(Fig. 3.4 8 d)**. The filter retardation analysis clearly indicated that neither DNAJB1 nor Hsc70 bound to HTTExon1Q$_{48}$ΔP2 **(Fig. 3.4 8 e)**. In summary, the SDS-stable association of

chaperones with HTT fibrils along the aggregation pathway is highly dependent on the binding interface between the HBM of DNAJB1 and the second proline stretch of the PRD of HTT.

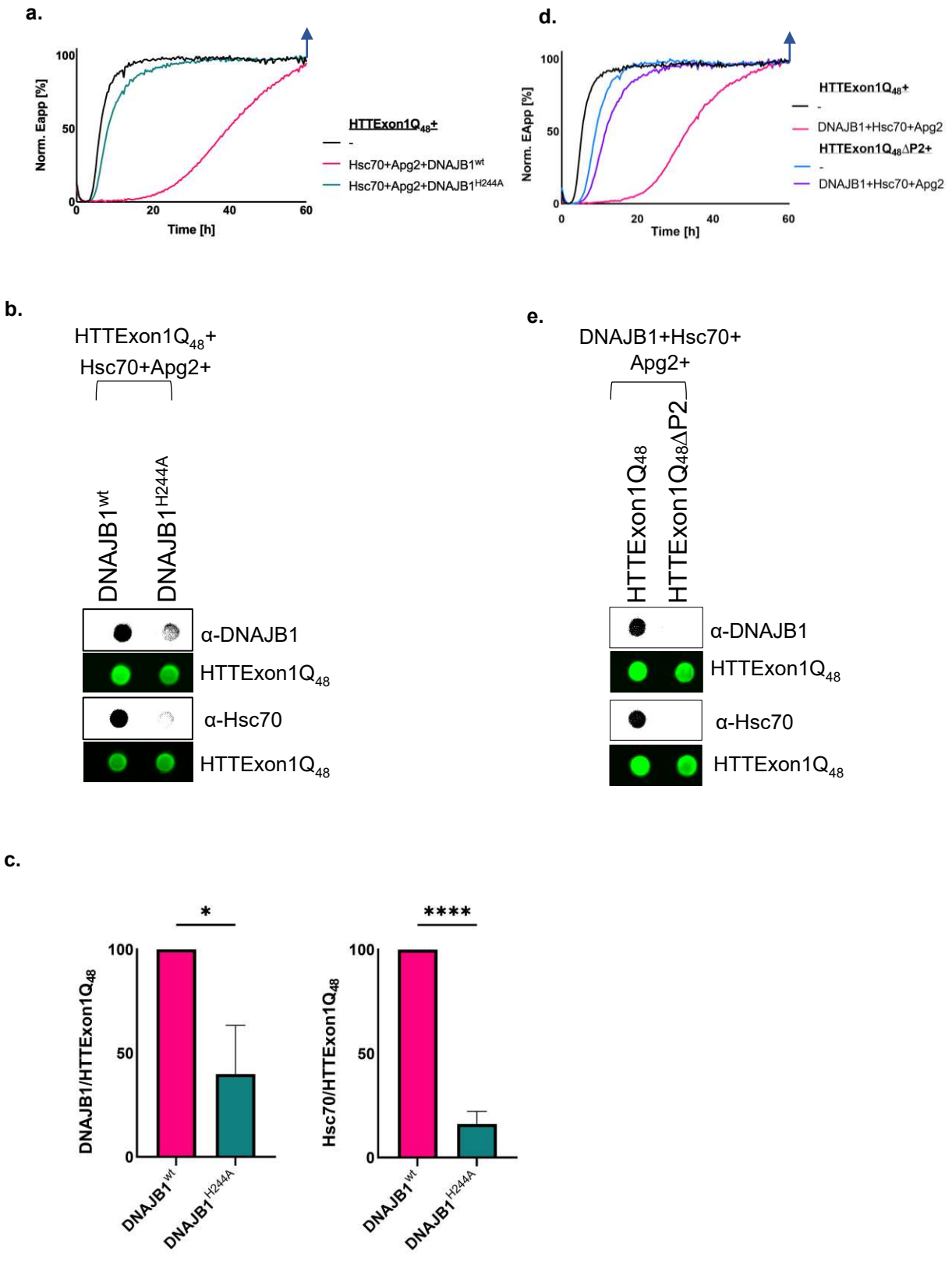

Figure 3.4 8 Mutating H244 of DNAJB1 abrogates the ability of DNAJB1 to bind to HTTExon1Q_{48} aggregates.

a. FRET measurements over 60 h of the fibrilization of HTTExon1Q_{48} in the presence of Hsc70, Apg2 and DNAJB1^{wt} (red), Hsc70, Apg2 and DNAJB1^{H244A} (green) and in the absence of chaperones (black). The arrow depicts the time point of sample collection for the subsequent filter retardation analysis.

b. Filter retardation analysis of the samples collected at t = 60 h of the FRET assay depicted in **b**. The membranes were analyzed with antibodies against DNAJB1 (top row), and Hsc70 (third row) and the fluorescent signals report on the presence of HTTExon1Q_{48} aggregates (second and fourth row). The depicted blots are representatives of three independent experiments.

c. The graphs show the quantification of densitometric analyses of Hsc70 (right) and DNAJB1 (left) binding to HTTExon1Q_{48} aggregates in the presence of DNAJB1^{WT} (red) and DNAJB1^{H244A} (green). The ratio of Hsc70 and DNAJB1 to HTTExon1Q_{48} signal intensities of each sample (as shown in b) were normalized to ratio of the DNAJB1^{WT}-containing samples. The values show the mean ratios for each sample and the data were analysed by a t-test. Error bars correspond to the mean SD.

d. FRET measurements over 60 h of the fibrilization of HTTExon1Q_{48} (black) and HTTExon1Q_{48}-ΔP2 (blue) and in the presence of Hsc70, Apg2 and DNAJB1^{wt} (red and purple, respectively).

e. Filter retardation analysis of the samples collected at t = 60 h of the FRET assay depicted in **e**. The membranes were analyzed with antibodies against DNAJB1 (top row), and Hsc70 (third row) and the fluorescent signals in the second and fourth row report on the presence of HTTExon1Q_{48} and HTTExon1Q_{48}-ΔP2 aggregates, respectively. The depicted blots are representatives of three independent experiments.

3.4.6 Deletion of the G/F linker of DNAJB1 also impairs binding to HTT.

The G/F-rich flexible linker is located between the J-domain and the C-terminus of DNAJB1 (Minami and Karzai *et al*., 1996; Yan *et al*.,1999). As mentioned earlier in Section 3.3.3, this region is a crucial determinant not only for the suppression of HTT fibrilization, but also for the disaggregation of pre-formed HTT fibrils by the trimeric chaperone complex (Ayala Mariscal *et al*., 2022). I set out to test if DNAJB1$^{\Delta G/F}$ could bind to HTT along the aggregation pathway. First, using a FRET assay, I compared DNAJB1$^{\Delta G/F}$ with DNAJB1^{wt} in their ability to suppress HTT aggregation **(Fig. 3.4 9 a)** followed by a filter retardation analysis. Notably, no binding of DNAJB1$^{\Delta G/F}$ to HTT was observed **(Fig. 3.4 9 b)**. Thus, the interaction between HTT and the DNAJB1/Hsc70 complex requires an intact G/F linker region of DNAJB1.

a.

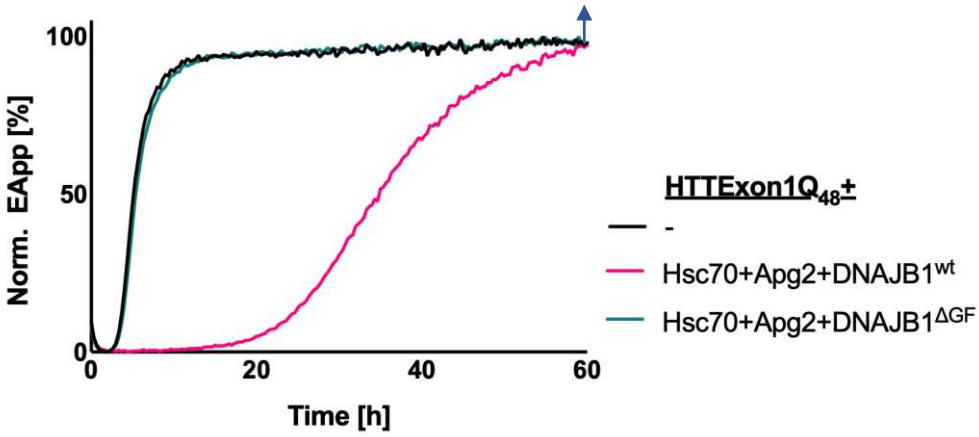

b.

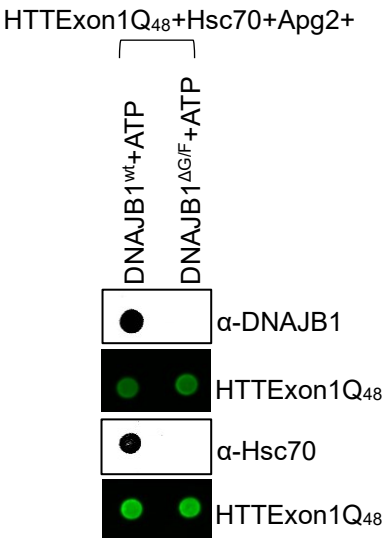

Figure 3.4 9 Deletion of G/F linker abolishes chaperone/HTT binding completely.

a. FRET measurements over 60 h of the fibrilization of HTTExon1Q_{48} in the presence of Hsc70, Apg2 and DNAJB1^{wt} (red) or DNAJB1$^{\Delta GF}$ (green) or in the absence of chaperones (black). The arrow indicates the time point of sample collection for the subsequent filter retardation analysis depicted in **b**.

b. Filter retardation assay of the samples collected at the t = 60 h time point of the FRET assay depicted in **a**. The membranes were analyzed with antibodies against DNAJB1 (top row), and Hsc70 (third row) and the fluorescent signals in the second and fourth row report on the presence of HTTExon1Q_{48} aggregates. The depicted blots are representatives of three independent experiments.

3.4.7 Deletion of Helix V in the hinge region reduces the suppression effect and binding.

An autoinhibitory mechanism in DNAJB1 via the G/F-rich linker region has been proposed in a recent study (Faust *et al*., 2020). The authors have shown that the 5-amino acid long region, Helix V, located in the G/F-rich linker region was closed onto the J-domain of DNAJB1 where the functional interaction with Hsc70 occurs. The C-terminal EEVD tail of Hsc70 interacts with the C-terminus of DNAJB1 and stimulates the release of the autoinhibition **(Fig. 3.4 10)**. This allows DNAJB1 to interact with Hsc70 through its J-domain and perform its function, whereas when the EEVD motif is deleted, the autoinhibition cannot be lifted and DNAJB1 with Hsc70 and Apg2 would be unable to refold denatured luciferase, as the authors demonstrated. In addition, Faust *et al.* showed that the autoinhibitory mechanism was essential for the disaggregation of α-synuclein fibrils.

In our lab, Mohamed ElBediwi has shown in his Master´s thesis that the disaggregation of HTT fibrils by DNAJB1$^{\Delta H5}$ together with Hsc70 and Apg2 was reduced by 25%. Therefore, I aimed to investigate how this mutation affects the suppression of HTT aggregation by the trimeric chaperone complex and the chaperone binding along the HTT aggregation pathway.

First, I tested the ability of DNAJB1$^{\Delta H5}$ mutant to suppress aggregation of HTT together with Hsc70 and Apg2**.** In parallel with the disaggregation activity, this mutant was only partially active in suppressing aggregation but not as effective as the DNAJB1^{wt} **(Fig. 3.4 11 a)**.

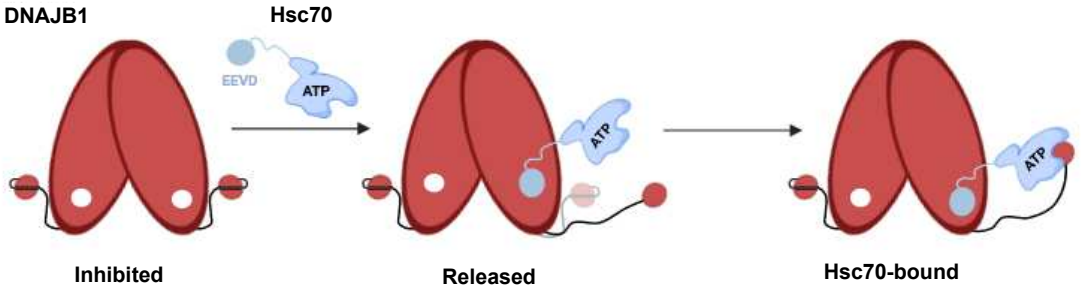

Figure 3.4 10 Schematic representation of autoinhibitory mechanism of DNAJB1.

The autoinhibition on DNAJB1(red) is lifted by the interaction of the EEVD domain of the Hsc70 (blue) with the C-terminus of DNAJB1 (Image adapted from Faust *et al.,* 2020).

Next, the chaperone association with HTT fibrils was investigated by filter retardation analysis. Both DNAJB1$^{\Delta H5}$ and Hsc70 appeared to bind HTT at the end of suppression reaction **(Fig. 3.4 11 b)**. Since there was a reduction in the suppression activity of the trimeric chaperone complex by the ΔH5 mutation, I would expect a similar reduction in the binding level as well. However, when compared to DNAJB1^{wt}, there was no significant difference in chaperone binding with HTT fibrils **(Fig. 3.4 11 c)**. Therefore, I added additional control samples with trimeric chaperones added with HTT but in the absence of ATP. These samples, as expected did not show any suppression effect **(Fig. 3.4 11 a)**, yet DNAJB1$^{\Delta H5}$ even in the absence of ATP gave an immunostaining signal with DNAJB1 antibody on the filter retardation membrane which might be indicative of binding with fibrils. However, this observation needs to be carefully evaluated, as the DNAJB1$^{\Delta H5}$ mutant itself might be highly prone to precipitate and stick to the membrane, even though it does not associate with fibrils. To exclude this effect, I reanalysed the immunostaining result of DNAJB1 by subtracting the "-ATP" control from the "+ATP" samples and the DNAJB1/HTTExon1Q$_{48}$ ratio of DNAJB1$^{\Delta H5}$ did not significantly differ from DNAJB1^{wt} **(Fig. 3.4 11 d)**.

Furthermore, Hsc70 in the presence of DNAJB1$^{\Delta H5}$ but absence of ATP, did not give any immunostaining signal **(Fig. 3.4 11 b)**. Besides, the results of the previous experiments indicated a strong correlation between suppression activity and chaperone-fibril association. Thus, if DNAJB1$^{\Delta H5}$ does indeed bind to HTT fibrils in the absence of ATP, then I would expect DNAJB1$^{\Delta H5}$ together with Hsc70 and Apg2 to suppress aggregation even without ATP and to observe that Hsc70 also binds to fibrils

as well. Therefore, the stability of DNAJB1$^{\Delta H5}$ needs to be tested with additional methods, or adding this variant without HTT fibrils and checking if it sticks to the filter retardation membrane on its own might be a good option to further investigate this result.

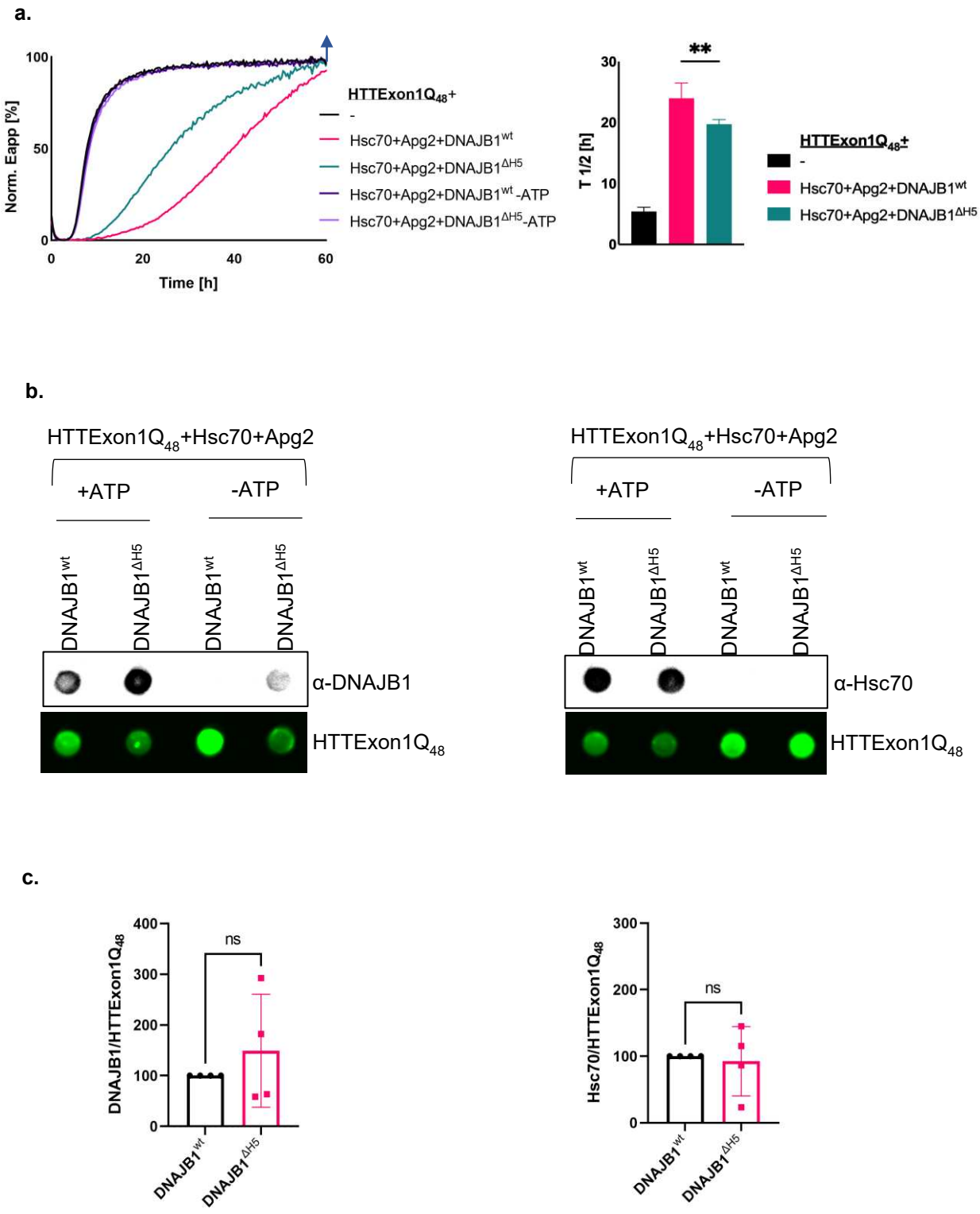

d.

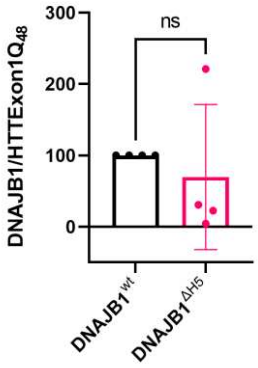

Figure 3.4 11 Effect of deletion of auto-inhibitory Helix V on DNAJB1.

a. FRET measurements over 60 h of the fibrilization of 0.75 µM HTTExon1Q_{48} in the presence of Hsc70, Apg2 and DNAJB1^{wt} (red) or DNAJB1$^{\Delta H5}$ (green) or in the absence of chaperones (black) all with the additional presence of an ATP regenerating system, and in parallel in the presence of Hsc70+Apg2 and DNAJB1^{wt}/DNAJB1$^{\Delta H5}$, but lacking ATP and the regenerating system (dark purple and light purple respectively). The arrow indicates the time point of sample collection for the subsequent filter retardation analysis depicted in **b**. The bar graph on the right depicts the half-time ($T_{1/2}$) of HTTExon1Q_{48} aggregation and represents the mean of three independent experiments. Error bars correspond to the mean SD. Statistical analysis was performed by a one-way ANOVA. **p≤ 0.01.

b. Filter retardation assay of the samples collected at the t = 60 h time point of the FRET assay depicted in **a**. The membranes were analyzed with antibodies against DNAJB1 (left), and Hsc70 (right) and the fluorescent signals in bottom rows report on the presence of HTTExon1Q_{48} aggregates. The depicted blots are representatives of three independent experiments.

c. The graphs show the quantification of densitometric analyses of blots depicted in **b** showing Hsc70 (right) and DNAJB1 (left) binding to HTTExon1Q_{48} aggregates in the presence of DNAJB1^{wt} (black) and DNAJB1$^{\Delta H5}$ (red). The ratio of Hsc70 and DNAJB1 to HTTExon1Q_{48} signal intensities of each sample were normalized to ratio of the DNAJB1^{wt}-containing samples. The depicted blots are representatives of three independent experiments. The values show the mean ratios for each sample and the data were analysed by a t-test. Error bars correspond to the mean SD. Ns; not significant.

d. The graph shows the quantification of densitometric analysis DNAJB1 binding to HTTExon1Q_{48} aggregates in the presence of DNAJB1^{wt} (black) and DNAJB1$^{\Delta H5}$ (red) where DNAJB1 immunostaining signals of -ATP samples were subtracted from the +ATP signals in the left blot depicted in **b**. The values show the mean ratios for each sample and the data were analysed by a t-test. Error bars correspond to the mean SD. Ns; not significant.

3.4.8 Disaggregation activity of chaperones on young vs. mature fibrils

It was recently demonstrated that HTT forms fibrils with different stabilities and toxicities when grown at different temperatures such as 4°C or 37°C (Nekooki-Machida, Y. *et al.,* 2009; Isas *et al*., 2021). Structural analyses revealed that the fibrils grown at 37°C had a more rigid polyQ core containing extra beta-sheets, and 4°C fibrils had more loops and coils which kept HTT fibrils more mobile (Isas *et al*., 2021). Isas *et al*. further elaborated that, at 37°C the proline-rich domain (PRD) of HTTEx1 was less mobile and formed highly entangled fibrils whereas 4°C fibrils had a more flexible PRD region with a lower fibrillar coalescence that was previously seen as the cause for elevated toxicity (Nekooki-Machida, Y. *et al.,* 2009). However, circular dichroism and solid-state NMR analysis showed that after two weeks incubation, 4°C fibrils, described as toxic fibrils, conformationally converted into non-toxic 37°C fibrils (Isas *et al*., 2021). Thus, since I have demonstrated in Section 3.4.1, that the suppression by the trimeric chaperone complex is achieved only when added with the early conformers, the question arises whether the disaggregation activity also differs between young and mature fibrils. Therefore, I first monitored HTT aggregation kinetics at different temperatures by FRET **(Fig. 3.4 12 a)**. Strikingly, the aggregation occurred with a significantly slower speed at 4°C, whereas it was quite rapid at 37°C. I then used these curves to determine the time points when the FRET signal reached a plateau. When incubated at 37°C, this time point was 3 h and at 4°C it was 20 h. Therefore, these incubation times were used to generate young fibrils, and 2 weeks of incubation time was used to obtain mature fibrils at both temperatures as indicated by down arrows in **Fig. 3.4 12 a**. Then, the trimeric chaperone complex supplemented with the ATP regeneration system was added at these time points and allowed to disaggregate the fibrils for 24 h. Subsequently, the resolubilization was analysed by ultracentrifugation and the disaggregation activities were compared between young and mature fibrils **(Fig. 3.4 12 b)**. Clearly, at both temperatures, disaggregation occurs for the younger fibrils but not for those grown for 2 weeks. Thus, although the structures differ at 4°C and 37°C, the chaperones could disaggregate both, when added early during the aggregation process.

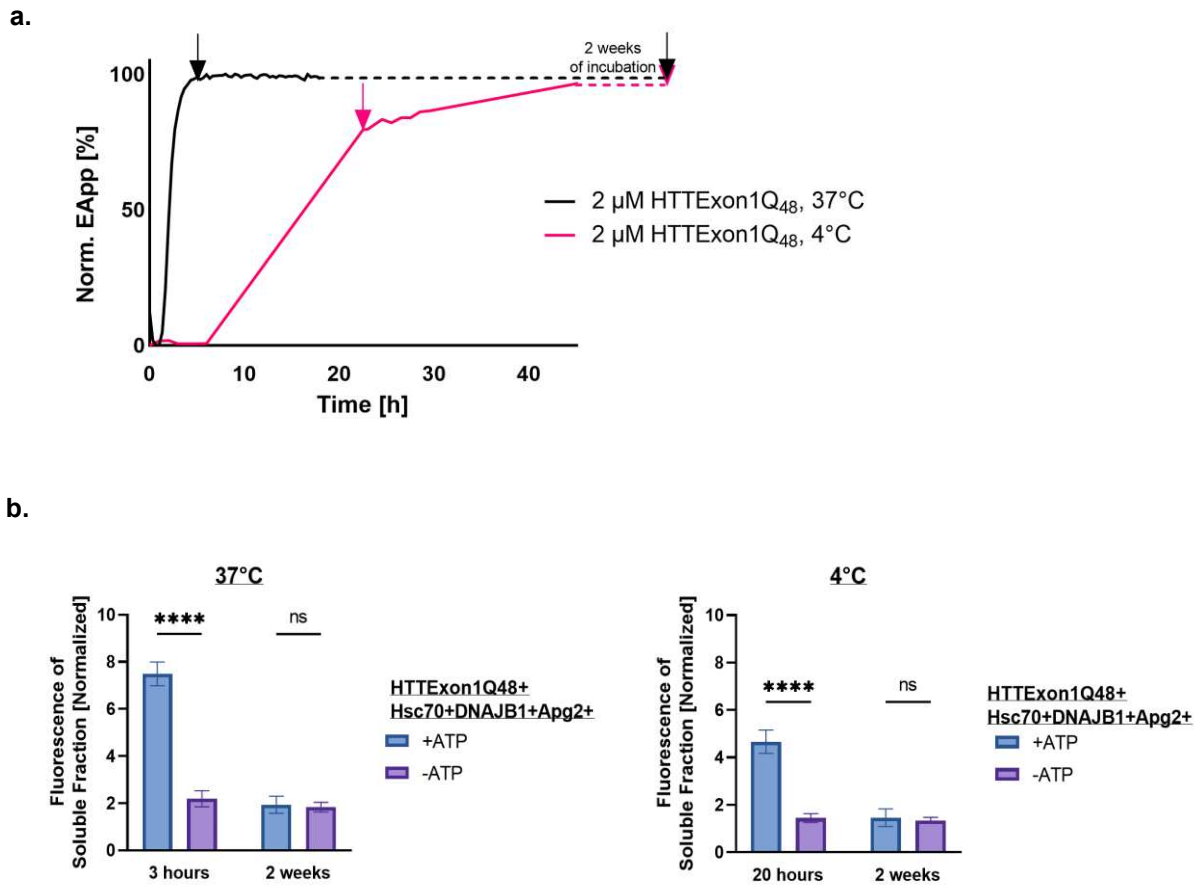

Figure 3.4 12 Hsc70, DNAJB1 and Apg2 fail to disaggregate mature HTTExon1Q$_{48}$ fibrils.

a. FRET analysis over 45 h of the aggregation of 2 µM HTTExon1Q$_{48}$ at 4°C (red) and 37°C (black). The arrows indicate the time points (entry into plateau phase) that were used for the disaggregation assay (**b**).

b. Disaggregation assays for fibrils grown at 37°C (left) for either 3 hours or 2 weeks and 4°C (right) for either 20 hours or 2 weeks. The graphs depict the fluorescence levels of soluble HTTExon1Q$_{48}$-YPet resulting from the disaggregation reaction (blue). The fluorescence intensities were quantified and normalized to the controls that contained no chaperones (purple). Bars represent the mean values of three independent experiments and error bars correspond to the mean SD. The significance was determined by a two-way ANOVA analysis. Ns; not significant, ****; p <0.0001

4. Discussion

4.1 DNAJB1-HTT interaction and an intact ATPase cycle are key to suppress aggregation.

Molecular chaperones play an important role in combating protein misfolding. Numerous chaperones and chaperone complexes have been identified to prevent or reverse the aggregation of misfolded proteins that are associated with neurodegenerative diseases (Kampinga *et al.,* 2010; Hartl *et al*., 2011; Balchin *et al.,* 2016; Wentink *et al*., 2019; Tittelmeier *et al*., 2020). Therefore, an in-depth understanding of their mechanism of action is important to pursue chaperones as therapeutic targets against neurodegenerative diseases.

Although inhibition of HTT aggregation and disaggregation of preformed HTT aggregates by a trimeric chaperone complex, consisting of Hsc70, DNAJB1, and Apg2 was previously shown (Scior *et al*., 2018), chaperone interactions with HTT along its off-folding pathway have not yet been characterized. In our lab, a distinct binding site on the C-terminal domain of DNAJB1 and the second proline-rich domain of HTT has been identified. Several single point mutations within this binding motif on DNAJB1 were generated and tested for their effect on suppressing HTT aggregation together with Hsc70 and Apg2. The highly conserved, positively charged residue H244 appeared to be a key player in this interaction, as its mutation to alanine completely abolished the suppression activity together with Hsc70 and Apg2 (Ayala Mariscal *et al*., 2022). I contributed to this study by testing the substitution of H244 for glutamine and found that this mutation partially restored the suppression of HTT aggregation as part of the trimeric chaperone complex but was not as effective as DNAJB1^{wt}. Molecular dynamics and docking analysis between HTT and DNAJB1 suggested that hydrogen bonding at position 244 appears to be essential for this interaction (Ayala Mariscal *et al.,* 2022*)*. Glutamine is a polar but uncharged amino acid that has the capacity to form hydrogen bonds which may account for its partial activity in suppression of HTT aggregation.

DNAJB1 stimulates the ATPase activity of Hsc70 via the HPD motif in the J-domain; disruption of this interaction was shown to abolish the ATPase activity (Wall *et al.,* 1994), which was confirmed by my results. I have observed that with a mutation on the HPD motif, the trimeric chaperone complex was no longer able to suppress the

aggregation of HTT. This observation clearly demonstrates that the suppression of aggregation requires an uninterrupted interaction between DNAJB1 and Hsc70 as well as an intact ATP/ADP cycle. It may be worthwhile for future studies to explore in detail how the allosteric conformational changes in DNAJB1 and Hsc70 induced by ATP/ADP exchange relate to their interaction with the aggregation-prone HTT through its off-folding pathway.

4.2 Interaction of DNAJB1 with HTT: commonalities and differences between soluble and fibrillar HTT

Our lab could previously show that the trimeric chaperone complex is also able to disaggregate preformed HTT fibrils (Scior *et al*., 2018), although the details of the mechanism remained unclear. Elucidating the intricate cycle of chaperone actions is often hampered by the complexity of chaperone-substrate interactions during the aggregation pathway. Previous studies suggest that molecular chaperones and amyloidogenic proteins at different stages of aggregation can differ (Perales-Calvo *et al*., 2010; Baaklini and Wentink *et al*., 2020; Marzano *et al*., 2022). Thus, the suppression and disaggregation of HTT fibrils can be regulated differently by the same chaperone complex e.g. Hsc70, DNAJB1 and Apg2. This is particularly relevant for DNAJB1 that initiates the binding with HTT. Therefore, the question arose whether the mutations in the characterized binding sites between DNAJB1 and soluble HTT are the same contact sites as those between DNAJB1 and HTT fibrils.

I observed that the key point mutant within the HTT-binding motif (HBM), DNAJB1^{H244A}, could partially maintain the disaggregation activity of the trimeric chaperone complex while it was shown that the suppression activity was completely abolished (Ayala Mariscal *et al.,* 2022). This may be because additional binding sites become accessible or are used with different conformational structures that are formed during the off-folding pathway of HTT (Ko *et al*., 2001; LeGleiter *et al*., 2009; Lin *et al.,* 2017). As DNAJB1 has been shown to bind preformed HTT fibrils previously (Scior *et al*., 2018), I performed a binding analysis and demonstrated that compared to DNAJB1^{wt}, binding of DNAJB1^{H244A} to preformed HTT fibrils was significantly reduced, but still present, which may explain why the disaggregation activity was still preserved for DNAJB1^{H244A}

with Hsc70 and Apg2 albeit with a reduced activity. In this regard, a recent study on the interaction between DNAJB1 and α-synuclein (α-syn), an amyloidogenic protein linked to Parkinson's disease, is noteworthy (Wentink *et al*., 2020). Using fluorescence anisotropy and microscale thermophoresis techniques, they measured the binding affinities of DNAJB1 to soluble and fibrillar α-syn. DNAJB1 was observed to bind fibrillar α-syn with a binding affinity 300-fold higher than soluble α-syn. Therefore, a similar difference in monomer/fibril interactions of DNAJB1 may account for the difference in the effect of the H244A mutation on suppression and disaggregation activities. So far, it is unclear how DNAJB1 interacts with monomeric, oligomeric or fibrillar HTT. To understand the mechanistic differences between chaperone-mediated suppression and disaggregation activities, it will be important for future studies to address the nature of DNAJB1-HTT interaction at earlier and later stages of aggregation.

One open question was how the HTT binding site affects the disaggregation activity by the trimeric chaperone complex. The PRD was shown to play a protective role in HTT aggregation (Bhattacharyya *et al*., 2006; Pigazzini *et al*., 2021). As a chaperone binding site, it was newly identified (Ayala Mariscal *et al*., 2022), whereas the N17 and polyQ regions were previously known to interact with chaperones (Tam *et al*., 2009; Choudhury and Bhattacharyya, Monsellier *et al*., 2015; Kakkar *et al*., 2016). As demonstrated in Ayala Mariscal *et al.,* upon deletion of PRDI, the trimeric chaperone complex could still suppress HTT aggregation effectively. In contrast, deletion of PRDII completely abolished the suppression activity by the trimeric chaperone complex (Ayala Mariscal *et al*., 2022). I could confirm these data for the disaggregation reaction. The trimeric chaperone complex failed to disaggregate fibrils formed by HTTExon1Q_{48}ΔP2. These results are consistent with previous modelling and structural analyses suggesting a “bottlebrush” model for HTT fibrils, in which the PRD region extends outward from the rigid polyQ core, making it accessible for chaperone binding (Isas *et al*., 2015; 2021). This means that although HTT adopts different conformations in soluble and aggregated states, the second proline stretch of HTT is indispensable for the interaction with DNAJB1 and the other domains of HTTExon1Q_{48} are unable to compensate and provide another interaction site for DNAJB1. In our lab, it has recently been shown that nematodes expressing GFP-tagged DNJ-13 that is the homolog of DNAJB1 crossed with HTTExon1Q_{48} displayed significantly higher co-localization

between HTT aggregates than with HTTExon1Q_{48}ΔP (experiments conducted by Yasmin Richter), providing *in vivo* corroboration of my *in vitro* results. Thus, chaperone association during HTT aggregation occurred primarily between the HBM of the JDP and the second proline stretch of HTT. Additional sites within the JDP and likely also HTT could contribute to the interaction, which may also change along the off-folding pathway of HTT and the suppression, association and disaggregation process. I could for instance show that the G/F-rich linker of DNAJB1 is important for the association with and remodelling of HTT.

DNAJA1, a class A JDP, was found to be inactive in suppressing HTT aggregation together with Hsc70 and Apg2 (Ayala Mariscal *et al*., 2022), and it was also ineffective in disaggregating HTT fibrils even though it also contains the HBM. However, the DNAJA1^{JB1ized} mutant, in which the longer G/F-rich linker region of DNAJB1 replaced the one of DNAJA1, showed an enhanced disaggregation activity, highlighting the importance of the specific features of the G/F-rich region of DNAJB1 that confer functionality in the disaggregation reaction of the trimeric chaperone complex.

4. 3 DNAJB1 and Hsc70 associates with early HTT conformers along the aggregation pathway

As a member of the Hsp40 family, J-domain proteins (JDPs) are known to recognize non-native proteins and recruit them to Hsp70s for folding, refolding or disaggregation and thereby provide substrate specificity (Kampinga *et al*., 2010; Ahmad *et al*., 2011; Faust *et al*., 2020; Ryder *et al*., 2022). Therefore, characterization of the interactions between client proteins and JDPs is of great importance for understanding their mechanism of action. However, due to the transient or weak interactions involved in such dynamic processes, it is challenging to determine the states of misfolded substrates that are recognized by JDPs. Amyloidogenic proteins are difficult to work with due to their often intrinsically disordered structures and aggregate heterogeneity, leading to numerous technical limitations. Structural or biophysical tools may fail to unravel the mechanism of suppression and disaggregation by the molecular chaperones.

Even though the trimeric chaperone complex of DNAJB1, Hsc70 and Apg2 has been shown to suppress HTT aggregation (Scior *et al*., 2018), it is still unclear how these chaperones individually act on aggregation prone HTT and achieve suppression. In addition, the reason for their eventual failure after a period of delayed aggregation remains enigmatic. It is a matter of debate whether the chaperones are associated with the fibrils at the end of the suppression reaction, or the amyloid fibrils remain purely homomolecular at the endpoint of suppression. (Sinnige and Morimoto, 2020; Linse *et al*., 2021). These questions require mechanistic elucidation, as previous *in vitro* and *in vivo* studies point to chaperone sequestration in amyloid inclusions (Olzscha *et al.,* 2011; Park *et al*., 2013; Månsson *et al*., 2014; Yu *et al*., 2019). *In vitro* experiments are key to understand the mechanism of how the chaperones are deposited in these inclusions, as this may be one of the reasons for the failure of the proteostasis network in protein misfolding pathologies.

To address these questions, I established a tandem FRET/Filter retardation assay and observed that the trimeric chaperone complex can suppress aggregation and that DNAJB1/Hsc70 associates with fibrils at a maximal level when added at the beginning of HTT aggregation. The inhibitory effect and the association of chaperones gradually diminish when they are added later along the HTT aggregation pathway. This may be related to the widely speculated notion in the amyloid field that soluble oligomers are more toxic than mature fibrils due to their aberrant interactions with a wide variety of proteins within the cell (Fandrich, 2012; Leitman *et al*., 2013; Hipp *et al*., 2014; Kim *et al*., 2016; Bigi and Gropp *et al.,* 2022). I have also demonstrated that this chaperone-fibril association is SDS stable, indicating an irreversible sequestration of chaperones by the HTTExon1Q_{48} during the fibrillar growth.

A very similar experiment was previously performed with Aβ42, the amyloidogenic peptide associated with Alzheimer's disease, and DNAJB6, a member of type B JDPs that acts independently of Hsc70 and ATP (Månsson *et al*., 2014). In this study, Månsson and colleagues showed that DNAJB6 alone was able to suppress the formation of Aβ42 fibrils. However, when added at later stages of aggregation, the ability of DNAJB6 to suppress aggregation was progressively impaired. Even more interestingly, a filter retardation assay in the presence of 1% SDS was performed

between Aβ42 and DNAJB6 to investigate binding after the suppression phase was completed. Highly complementary to my results, they detected DNAJB6 signals simultaneously with Aβ42 on the filter retardation membrane, and this signal gradually decreased with the addition of DNAJB6 at later time points in the aggregation process. Strikingly, another study demonstrated that DNAJB6 alone also inhibited the aggregation of polyQ and was found to bind aggregates in an SDS-stable manner at the end of the suppression reaction (Kakkar *et al*., 2016). Thus, these highly complementary results suggest that chaperone-amyloid association represents a universal mechanism for suppressing aggregation. This concept was discussed in a review article (Linse *et al*. 2021), in which co-aggregation with chaperones was suggested as the main thermodynamic mechanism to enhance the solubility of amyloid proteins. According to their hypothesis, chaperones alone have an exceptionally high chemical potential that is the amount of energy that can be absorbed or released by the addition of a new component to a system. This makes chaperones susceptible to bind other proteins in solution, and their association with amyloid proteins forms heteromolecular aggregates that significantly reduce the chemical potential of the chaperones. On the other hand, amyloid proteins gain a higher chemical potential when bound to chaperones as opposed to the formation of pure homo-molecular amyloidogenic aggregates. Consequently, this leads to a change in the equilibrium so that the amyloid proteins have an increased solubility via resolubilization of aggregates or retardation of aggregation.

Having shown that DNAJB1/Hsc70 remains associated with HTT fibrils at the end of the aggregation suppression reaction, the question remained as to when exactly this association began and how it changes during the aggregation process. I have found that chaperone binding starts at the point where fibrillization begins after the suppression reaction, and the ratio of bound chaperones per fibril gradually decreases along the aggregation pathway. The explanation for this result may be as follows and represented by a schematic in **Fig. 4.1**: During the suppression phase on the FRET curve, DNAJB1 and Hsc70 are continuously interacting with HTT in a dynamic and possibly transient manner such that they may achieve to inhibit the assembly of monomers into fibrils. However, DNAJB1/Hsc70 would become saturated and depleted from the solution after a certain period, which would correspond to the time when the

first increase in the FRET signal is observed. At this time point, the first SDS-stable chaperone-HTT fibril complexes would form and show a maximum chaperone-HTT fibril ratio according to densitometric analysis. As aggregation proceeds, as indicated by a rapid increase in FRET signal, more HTT would be deposited on the already formed HTT-DNAJB1-Hsc70 complexes. As a result, the ratio of chaperones per fibril would gradually decline. Therefore, saturation and sequestration of DNAJB1/Hsc70 appears to be one of the key reasons why this chaperone machinery collapses and fails to suppress after a certain point in time.

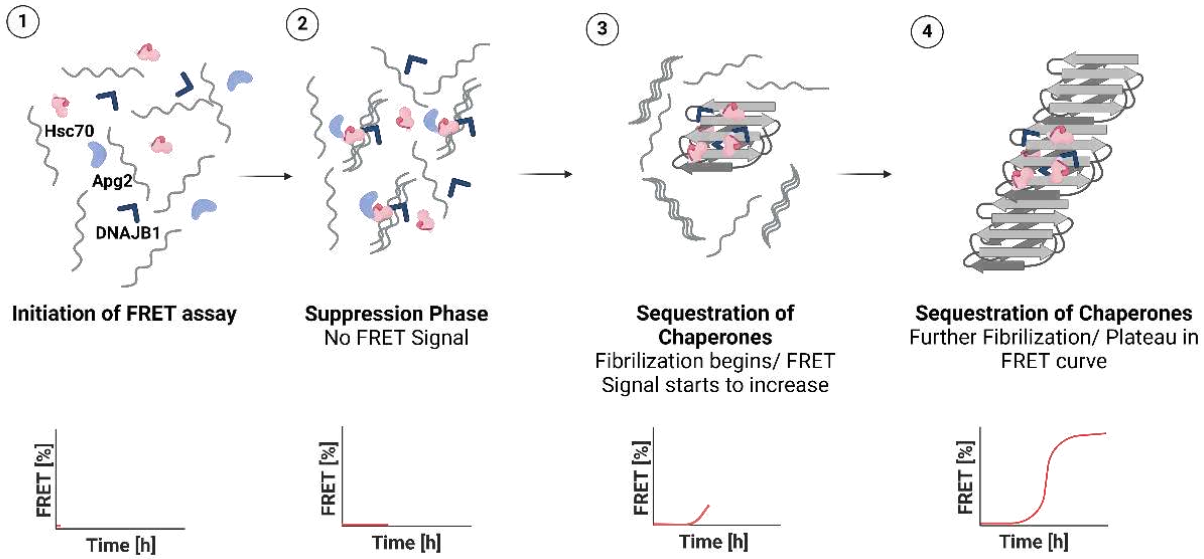

Figure 4.1. Schematic description of chaperone sequestration mechanism by HTT

Proposed model of sequestration of DNAJB1 and Hsc70 with along the aggregation pathway of HTTExon1Q_{48} in the presence of ATP. Each stage of chaperone association with fibrils is represented by the corresponding time point on the FRET curve, which depicts the suppression of aggregation by the trimeric chaperone complex.

In contrast to DNAJB6, DNAJB1 requires the presence of Hsc70 and Apg2 and an active ATPase cycle to achieve suppression of aggregation and disaggregation of misfolded substrates (Rampelt *et al.,* 2012; Nillegoda and Gao *et al*., 2015; Scior *et al*., 2018). I have clearly demonstrated that the association of DNAJB1 and Hsc70 with HTT fibrils requires not only the presence of each other but also an intact ATPase cycle, further supporting the co-dependence concept. Hence, chaperone-HTT fibril binding appears to be the result of a continuous ATPase cycle rather than a single ATP/ADP

turnover. Interestingly, a recent *in vitro* study analysing the binding between an amyloidogenic yeast prion Sup35 and yeast homologues of Ssa1(Hsc70)/Sis1(DNAJB1) have also demonstrated that the interaction of these chaperones with the substrate were co-dependent and required an intact ATPase cycle to actively associate with the substrate and achieve disaggregation (Nakagawa *et al.,* 2022). Therefore, in Hsp40/Hsp70 systems, substrate interactions during suppression or disaggregation mechanisms seem to carry a possibly conserved mechanism on different types of amyloid substrates. On the other hand, it is also possible that chaperones not only bind to fibrils but also dissociate from them simultaneously on very fast time scales. Technically, studying such a release mechanism would be a very challenging task, but time-resolved structural methods could be used to gain insight into such a highly complex and dynamic interaction. Nevertheless, my results already provide strong evidence that the conditions required for successful suppression of aggregation appear to be correlated with chaperone-fibril association.

I have also been able to support my data on ATP dependence in chaperone-fibril association by confocal microscopy and have provided images of my *in vitro* reconstituted chaperone-fibril complexes. The resolution of confocal microscopy was only sufficient to show that the chaperones were present on the entire fibrillar surface, without any localization to a specific spot. However, these chaperone-fibril complexes I have visualized could be very promising samples for high-resolution cryo-EM or integrative structural analysis in the future to see how chaperones are located on the fibrillar surface (or whether incorporated inside the fibrils), and even better, obtaining an atomistic model would provide detailed insight into the binding sites.

HTT fibrils have previously been shown to exhibit remarkable heterogeneity depending on growth conditions. For instance, fibrils produced *in vitro* and introduced into mammalian cells were found to differ in structure and toxicity depending on the temperature at which the fibrils were grown, e.g. fibrils produced at 4°C were more toxic than those grown at 37°C (Nekooki-Machida *et al*., 2009). In addition, structural analysis showed that 4°C fibrils had a highly dynamic and accessible PRD region, whereas 37°C fibrils had a more entangled PRD which would potentially reduce interaction capacity of this domain. These two different types of fibrils were found to

interconvert, with the 4°C fibrils showing similar structural features to 37°C fibrils after prolonged incubation (Isas *et al*., 2021).

This led to the question of whether disaggregation by the trimeric chaperone complex might differ for different fibril types. I compared young and mature fibrils grown at two different temperatures and found that at both temperatures, only the younger fibrils were disaggregated whereas the mature fibrils remained unaffected by the trimeric chaperone complex. Therefore, just as the addition of chaperones earlier and later affects inhibitory activity, the addition of chaperones to young and mature fibrils affects disaggregation. In this case, the terms "earlier" and "later" and "young" and "mature" may be confusing when referring to HTT samples in different experimental settings. When chaperones were added at the beginning of the FRET plateau, I refer to the fibrils as "young" and when added 2 weeks later, I refer to those fibrils as "mature" in the disaggregation assay. The time points between the initiation of aggregation and obtaining the FRET plateau is referred to as “earlier” and “later” in suppression and binding assays **(Fig. 4.2)**. The observation that there was no SDS-stable binding at this “young fibril” time point is an indication that the chaperones have different binding modes for suppression and disaggregation. As demonstrated by immunostaining and TEM, DNAJB1 and Hsc70 were able to bind to mature fibrils (Scior *et al*., 2018). I have also shown that DNAJB1^{wt} is able to bind to preformed fibrils **(Fig 3.3.2 2**). However, it should be noted that in such binding experiments, the samples were not treated with SDS. This means that even in the absence of soluble HTT, chaperones can still bind to fibrils, but not in an SDS-stable manner, which may indicate a more dynamic or reversible binding rather than sequestration of chaperones. This observation may explain how disaggregation can occur at this point of aggregation, where HTT is completely insoluble. If the chaperones were irreversibly bound to the fibrils at that stage, they would not be able to pull apart and break down the aggregates. However, in my work, chaperone binding from the disaggregation angle has been studied more qualitatively, so this aspect needs to be further explored with more sensitive and

quantitative biophysical methods to have a more profound understanding of the mechanism.

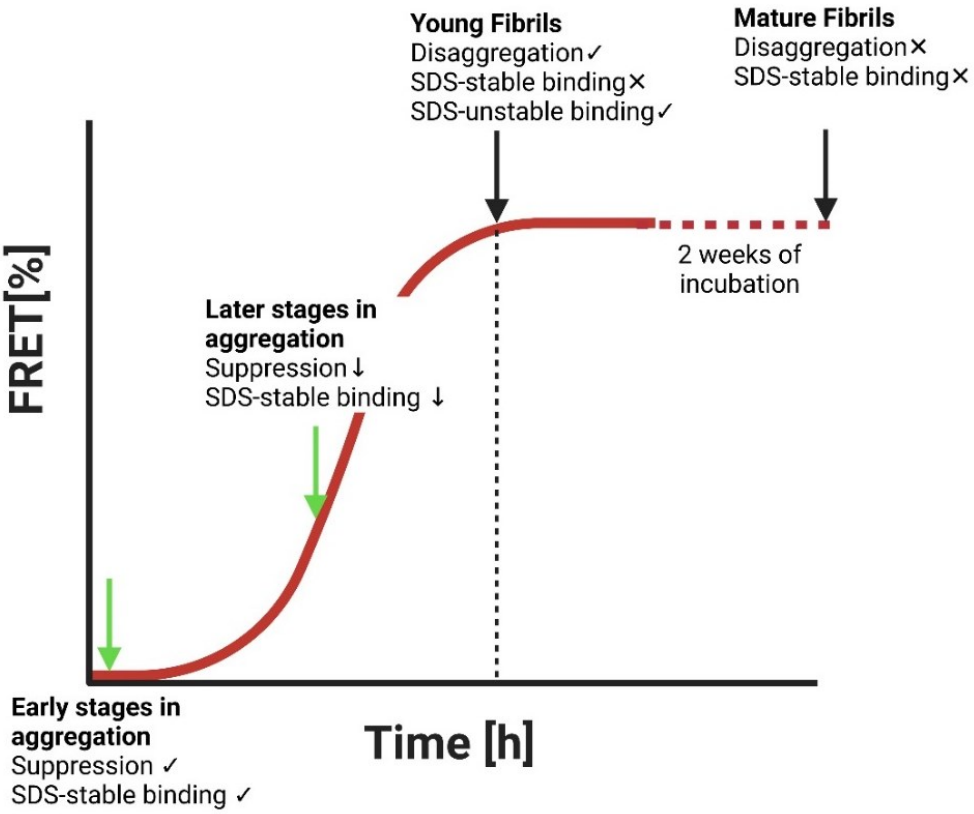

Figure 4.2 Schematic summary of the binding behaviour in suppression and disaggregation activities

Green arrows indicate the time points at which chaperones were added to HTT for the suppression and binding assays in section 3.3.2, which were performed up to the time point indicated by the dashed line. Black arrows indicate the time points where chaperones were added to preformed HTT fibrils to analyse their effect on disaggregation in section 3.4.8.

The impairment of proteostasis upon sequestration of chaperones has also been investigated *in vivo* and the results appear to correlate with the *in vitro* framework of my thesis. DNAJB1 has been detected in polyQ aggregates in the postmortem brains of patients with Machado-Joseph disease (also known as spinocerebellar ataxia type 3), which is caused by an abnormal expansion of polyQ of Ataxin (Chai *et al*., 1999; Seidel *et al*, 2012). Proteomic analysis revealed that the yeast homolog of DNAJB1, Sis1, was sequestered into the SDS-insoluble inclusions of HTTExon1Q_{96} which was shown to be detrimental for the proteostasis capacity (Park *et al.,* 2013). Quantitative proteomics

was then used to analyse the interactome of soluble HTT oligomers and insoluble HTT aggregates in mammalian cells (Kim *et al*., 2016). The results indicated that the soluble oligomers of HTT yield a significantly larger list of interacting partners than the mature insoluble inclusions and the authors noted that the formation of large HTT inclusions apparently results in a reduced ability to interact with other proteins within the cell. In this study, DNAJB1, along with other types of JDPs, was predominantly detected in the SDS-insoluble fractions of HTT, indicating irreversible binding, whereas Hsp70 and Hsp110 were found to interact with soluble oligomers to a lesser extent. More recently, the association of overexpressed Sis1 with the oligomeric HTTExon1Q_{97} was detected in the presence of SDS in yeast cell lysates. Strikingly, deletion of the G/F-rich linker or the CTD abolished the binding of these Sis1 mutants to HTT oligomers (Klaips *et al*., 2020), which complements the *in vitro* observations I have described for DNAJB1$^{\Delta G/F}$ and HTTExon1Q_{48}. Finally, it has been previously shown in our lab that the endogenous nematode orthologues of trimeric chaperones, DNJ-13 (DNAJB1), HSP-1 (Hsc70) and HSP-110 (Apg2) co-localize with HTT aggregates in *C. elegans*. However, it should be further investigated whether they associate with HTT in an irreversible manner (Scior *et al.*, 2018).

In summary, my work provides the first *in vitro* analysis of human chaperone sequestration along the aggregation pathway of HTT, complementing previous *in vivo* and *in vitro* experiments and contributing to our understanding of these highly complicated cascading interactions. The data I obtained provides significant mechanistic insights for chaperone sequestration as a major cause of the collapse of protein quality control systems in Huntington´s Disease. More importantly, the combination of my data with previous studies suggests that chaperone sequestration is a general concept that occurs in the same or a very similar manner for other amyloid proteins associated with neurogenerative diseases and should be further investigated.

5. Materials

5.1 Plasmid List

Plasmid Name	Source	Antibiotic Resistance
pCA528-DNAJB1-G194C	Bukau Lab	Kanamycin
pET-6His-Smt3-Apg2	Bukau Lab	Kanamycin
pET-6His-Smt3-DNAJB1	Bukau Lab	Kanamycin
pET-6His-Smt3-DNAJB1-H244A	Kirstein Lab	Kanamycin
pET-6His-Smt3-DNAJB1-H244Q	Kirstein Lab	Kanamycin
pET-6His-Smt3-DNAJB1-H32Q	Kirstein Lab	Kanamycin
pET-6His-Smt3-DNAJB1-H32Q-H244A	Kirstein Lab	Kanamycin
pET-6His-Smt3-DNAJB1-ΔDimer	Kirstein Lab	Kanamycin
pET-6His-Smt3-DNAJB1-ΔH5	Kirstein Lab	Kanamycin
pET-6His-Smt3-DNAJB1-ΔLinker	Kirstein Lab	Kanamycin
pET-6His-Smt3-DNAJB1^{K242A}	Kirstein Lab	Kanamycin
pET-6His-Smt3-DNAJB1^{H244F}	Kirstein Lab	Kanamycin
pET-6His-Smt3-DNAJB1$^{\Delta G/F}$	Kirstein Lab	Kanamycin
pET-6His-Smt3-DNAJB1$^{JA1\text{-}G/F}$	Kirstein Lab	Kanamycin
pET-6His-Smt3-DNAJA1	Kirstein Lab	Kanamycin
pET-6His-Smt3-DNAJA1$^{\Delta ZFLR}$	Kirstein Lab	Kanamycin
pET-6His-Smt3-DNAJA1^{JB1ized}	Kirstein Lab	Kanamycin
pET-6His-Smt3-Hsc70	Bukau Lab	Kanamycin

pGEX-6P1-HTTExon1Q$_{48}$-CyPET	Wanker Lab	Ampicillin
pGEX-6P1-HTTExon1Q$_{48}$-YPET	Wanker Lab	Ampicillin
pGEX-6P1-HTTExon1Q$_{48}$CyPETΔP2	Kirstein Lab	Ampicillin
pGEX-6P1-HTTExon1Q$_{48}$YPETΔP2	Kirstein Lab	Ampicillin
pGEX-6P1-HTTExon1Q$_{48}$	Kirstein Lab	Ampicillin
pGEX-6P1-PreScission	Kirstein lab	Ampicillin
pULP-1-6X His	Kirstein Lab	Kanamycin

5.2 Bacterial strains

Strain Name	**Genotype**
DH5α	*E. coli* [*dlacZ Delta M15 Delta(lacZY AargF) U169 recA1 endA1 hsdR17(rKmK+) supE44 thi-1 gyrA96 relA1*] (plasmid preparation)
BL21 (DE3) pRare	*E. coli* [*fhuA2 [lon] ompT gal (λ DE3) [dcm] ΔhsdS* pRARE (CamR) *λ DE3 = λ sBamHIo ΔEcoRI-B int::(lacI::PlacUV5::T7 gene1) i21 Δnin5*] (protein expression)

5.3 Buffers

Protein Expression

LB (Luria Broth) medium	1 % Bacto Peptone, 0.5% yeast-extract, 1 % NaCl
Isopropyl β-D-1-thiogalactopyranoside (IPTG)	Stock concentration: 1 M (stored at -20°C)
Kanamycin sulfate	Stock concentration: 25 mg/mL (stored at 20°C)
Ampicillin	Stock concentration: 100 mg/mL (stored at -20°C)

ULP-SUMO Protease Purification

Lysis Buffer	40 mM Hepes-KOH pH 7.4, 150 mM KCl, 20 mM betamercaptoethanol, complete Roche Protease (1 capsule in 50 mL), DNase I powder (1 scoop per 50 mL) PMSF 500 uL 0,1 M stock per 50 mL
Elution buffer	40 mM Hepes/KOH pH 7.4, 150 mM KCl, 250 mM imidazole, 20 mM betamercaptoethanol
Dialysis Buffer	40 mM Hepes/KOH pH 7.4, 100 mM KCl, 10 mM betamercaptoethanol

Chaperone Purification

Lysis Buffer	30 mM Hepes/KOH pH 7.4 0.5 M KCl 5 mM $MgCl_2$ 20 mM Imidazole 10% Glycerol 1 mM phenylmethylsulfonyl fluoride (PMSF) 10 µg/mL DNase I cOmplete Roche® Protease inhibitor cocktail
High Salt Buffer	30 mM Hepes/KOH pH 7.4 1 M KCl 20 mM Imidazole 10% Glycerol 1 mM β-mercaptoethanol
Low Salt buffer	30 mM Hepes/KOH pH 7.4 50 mM KCl 20 mM Imidazole 10% Glycerol 1 mM β-mercaptoethanol
Elution buffer	30 mM Hepes/KOH pH 7.4 50 mM KCl 5 mM $MgCl_2$ 300 mM Imidazole 10% Glycerol 1 mM β-mercaptoethanol
Dialysis Buffer	30 mM Hepes/KOH pH 7.4 50 mM KCl 10% Glycerol 1 mM β-mercaptoethanol

GST-HttExon1Q_{48} Purification

Buffer 1	50 mM NaH_2PO4, 5 mM Tris, 150 mM NaCl, 1 mM EDTA, pH 8.0
Lysis Buffer	Buffer 1 1 mM phenylmethylsulfonyl fluoride (PMSF) 10 µg/mL DNase I cOmplete Roche® Protease inhibitor cocktail
Wash Buffer	Buffer 1 0.1% TritonX-100
Elution Buffer	Buffer 1 20 mM reduced glutathione (GST), pH 8.6
Dialysis Buffer	50 mM Tris, 150 mM NaCl, 1 mM EDTA, 5% Glycerol pH 7.4

FRET Assay

Reaction Buffer	30 mM Hepes-KOH, pH 7.4, 150 mM KCl, 5 mM $MgCl_2$, 1 mM DTT
ATP Regeneration System	3 mM PEP, 1 µl/50 µl Pyruvate Kinase, 5 mM ATP

ATPase Assay

Malachite green hydrochloride	0,082 % (w/v) green malachite, filtered (0.2 µm), stored at 4°C
4X reaction buffer:	200 mM HEPES, pH 7.4, 400 mM KCl, 20 mM $MgCl_2$, 0.068% Triton X-100
Ammonium Molybdate	5.7 % (w/v) ammonium molybdate prepared in 6 M HCl, filtered (0.2 µm)

Luciferase Assay

Dilution Buffer	50 mM Hepes, pH 7.4, 100 mM KCl, 5 mM MgCl2, 1 mM DTT, 10 µM BSA
Assay Buffer	25 mM Glycylglycine, 100 mM KCl, 15 mM $MgCl_2$, 5 mM ATP

Disaggregation Assay

Aggregation Buffer	30 mM Hepes-KOH pH 7.4, 150 mM KCl, 5 mM $MgCl_2$, 1 mM DTT

SDS-PAGE gel

SDS-Running Buffer	1% (w/v) SDS 250 mM Tris 1.92 M Glycine
Sample loading buffer (4X)	100 mM Tris-HCl pH 6.8 4 % SDS 30 % glycerol 0.2 % bromophenol-blue 100 mM DTT
SDS PAGE staining solution	2.5 g/l Coomassie brilliant blue G-250 40% methanol 10 % acetic acid
SDS PAGE destaining solution	40% methanol 10% acetic acid
Separation Gel Buffer	1.5 M Tris-HCl, pH 8.8, 0.04% (w/v) SDS, filtered (0.2 µm)
Stacking Gel Buffer	0.5 M Tris-HCl, pH 6.8, 0.04% (w/v) SDS, filtered (0.2 µm)

Filter Retardation Assay

Activation buffer	1% SDS in 1X TBS-T
Wash buffer	0.1% SDS in 1X TBS-T
Blocking solution	5% (w/v) milk powder in 1X TBS-T

Western Blot

Transfer buffer	5X diluted with ethanol from BioRad
TBS (10X)	200 mM Tris 1.5 M NaCl
TBS-T	200 mM Tris 1.5 M NaCl 1% Tween 20

Confocal Microscopy Imaging

Resuspension Buffer	30 mM Hepes pH 7.4, 50 mM KCl 10% Glycerol

5.4 Antibodies

Primary Antibodies

Antibody Name	Host	Provider
Anti-DNAJB1 polyclonal AB	rabbit	Proteintech, USA
Anti-Hsc70 monoclonal AB	mouse	Proteintech, USA

Secondary Antibodies

Antibody Name	Host	Provider
Goat IgG anti-rabbit IgG (H+L)-HRPO	goat	DIANOVA, Germany
Goat IgG anti-mouse IgG (H+L)-HRPO	goat	DIANOVA, Germany
Goat anti-Rabbit IgG H&L (Alexa Fluor 647)	goat	Thermo Fischer Scientific, USA
Goat Anti-Mouse IgG H&L (Alexa Fluor 647)	goat	Abcam, USA

5.5 Consumables

Consumable Name	Manufacturer
384-wells Flat Bottom Black Polystyrene Assay Plate	Corning Life Sciences, USA
96-well Microplate, transparent	Sarstedt, Germany
96-wells half-area white microplate	OptiPlate, Perkin Elmer
Cellulose Acetate Membrane (0.22 µM)	Cytiva, USA
Conical flasks	Schott, Germany
Cuvettes	Eppendorf, Germany
Dialysis membrane (MWCO 6-8 kDa)	Spectrum Laboratories
Falcon tubes (15 ml, 50 mL)	Sarstedt, Germany
Filter Paper (0.22 µM)	Sartorius, Germany
Glass Microscopy Cover Slides	Carl Roth, Germany
Glass Microscopy Slides	Epredia, Germany
Glutathione sepharose beads	GE Healthcare
Graduated cylinders	Vitlab, Germany
High-Density Nickel 6BL-QNi-100	Agarose Bead Technologies, Spain
Laboratory bottles with cap	Schott, Germany
Low Binding Tubes 1.5 ml	Sarstedt, Germany
Microfuge® Tube Polyallomer 1.5 mL	Beckman Coulter,USA
Microtubes (1.5 mL, 2 mL)	Sarstedt, Germany
NALGENE® Centrifuge bottles, 500 mL	Nalgene Inc, USA
Petri dishes	Sarstedt, Germany
Pipette tips (1000 µL, 200 µL, 10 µL)	Sarstedt, Germany
Polypropylene Columns (5 mL)	QIAGEN, Germany
Serological pipettes (5, 10, 25mL)	Sarstedt, Germany
Ultracentrifugal filter units (0.5 ml, 15 ml with 10 or 30 kDa MW cut-off)	Merck Millipore, Ireland

5.6 Chemical

Chemical Name	Provider
2-Propanol	VWR Chemical, Germany
Adenosine triphosphate (ATP)	Sigma Aldrich, USA
Alexa-488 Maleimide C2	Thermo Fisher Scientific, USA
Alexa-647 Maleimide C2	Thermo Fisher Scientific, USA
Ammonium molybdate	Riedel-de Haen AG, Germany
Ammoniumperoxodisulfat (APS)	SERVA, Germany
AMP PNP	Sigma Aldrich, USA
Ampicillin	Sigma Aldrich, USA
Beta-mercaptoethanol	Sigma Aldrich, USA
Bovine Serum Albumin (BSA)	Sigma Aldrich, USA
Bromophenol Blue	Merck, Germany
cOmplete™ protease inhibitor cocktail	Roche, Germany
Coomassie G-250 Brilliant Blue	SERVA, Germany
Dithiothreitol	Carl Roth, Germany
D-Luciferin	Sigma Aldrich, USA
EDTA	Carl Roth, Germany
Ethanol	Chemsolute, Germany
Formic Acid	Sigma Aldrich, USA
Glycerol 100%	Carl Roth, Germany
Glycerol 86%	Carl Roth, Germany
Glycylglycine	AppliChem, Germany

Hepes	Carl Roth, Germany
Hydrochloric Acid	VWR, USA
Imidazole	Carl Roth, Germany
Isopropyl-β-dthiogalactopyranosid (IPTG)	Thermo Fisher Scientific, USA
Kanamycin	Carl Roth, Germany
LB agar	SERVA, Germany
LB medium	Carl Roth, Germany
L-Glutathione (reduced)	Sigma Aldrich, USA
Magnesium Chloride	Carl Roth, Germany
Malachite Green	Carl Roth, Germany
Milk Powder	Sucofin, Poland
Mono- & disodium phosphate	Carl Roth, Germany
Monosodium Citrate	Carl Roth, Germany
Phenylmethylsulfonylfluorid (PMSF)	Sigma Aldrich, USA
Phosphoenolpyruvic acid (PEP)	Sigma Aldrich, USA
Potassium Chloride	Sigma Aldrich, USA
Potassium chloride	Sigma Aldrich, USA
Potassium Hydroxide	Merck, Germany
Potassium hydroxide	Merck, Germany
Rotiphorese 30%	Carl Roth, Germany
Sodium Chloride	Carl Roth, Germany
Sodium Dodecyl Sulfate	Carl Roth, Germany
Sodium Hydroxide	Carl Roth, Germany

TCEP	Sigma Aldrich, USA
Tetramethylethylenediamine (TEMED)	Merck, Germany
Tris Base	Carl Roth, Germany
Triton X-100	Sigma Aldrich, USA
Tween 20	SERVA, Germany

5.7 Enzymes

Enzyme Name	Company
DNase I	AppliChem GmbH, Germany
DpnI	New England Biolabs, USA
Luciferase	Sigma Aldrich, USA
PreScission Protease	Kirstein lab
Pyruvate kinase	Sigma Aldrich, USA
ULP1 (SUMO protease)	Kirstein lab

5.1 Kits

Kit Name	Company
NucleoSpin Plasmid Mini	Macherey-Nagel, Germany
Trans-Blot RTA Turbo Mini 0.2 µm Nitrocellulose Transfer Kit	BioRads, USA
Pierce ECL Western Blot Substrate	Thermo Fisher Scientific, USA

5.8 Dyes

Dye Name	Company
PageRuler Plus Prestained Protein Ladder	Thermo Fisher Scientific, USA
Alexa 647 C2 Maleimide	Thermo Fisher Scientific, USA
Roti®Blue 5X concentrated	Carl Roth, Germany

5.9 Laboratory Equipment

Device Name	Manufacturer
5810 R Centrifuge	Eppendorf, Germany
***Ä*KTA Pure**	Cytiva, USA
Bio-Dot® Microfiltration Apparatus	Bio-Rad, USA
Biophotometer	Eppendorf, Germany
ChemoStar Touch ECL& Fluorescence Imager	INTAS, Germany
Digital Heatblock	VWR/Avantor, USA
Electroporator 2510	Eppendorf, Germany
Fixed-angle rotor F-34-6-39	Eppendorf, Germany
GFL Shaker 3016	Lauda, Germany
Heating Thermo Shaker MHR 11	Ditabis, Germany
Heidolph DIAX 900 Mixer	Heidolph Instruments, Germany
Heraeus Kelvitron Incubator	Thermo Fisher Scientific, USA
IKA Roller 6 digital	Carl Roth, Germany
Laser Scanning Microscope 880 with Airyscan	Zeiss, Germany
Microfluidizer LM10	Microfluidics, USA
Microscale, BP 221 S	Sartorius, Germany
MiniSpin® bench-top centrifuge	Eppendorf, Germany
Multichannel Pipettes (100uL, 200 uL)	Brand, Germany
NanoPhotometer® N60	IMPLEN, Germany
Optima™ Ultracentrifuge	Beckman Coulter, USA
Orbital shaker LLG-uniSHAKER 25	LLG®-Labware, Germany
pH Meter	Mettler Toledo, USA
Pipetteboy	Integra Bioscience, Germany
PowerPac™ Basic power supply	Bio-Rad, USA

Sorvall® EvolutionTM Rc Superspeed Centrifuge	Thermo Fisher Scientific, USA
Sorvall® SLA-3000 Fixed Angle Rotor	Thermo Fisher Scientific, USA
Tecan Infinite® 200 PRO Plate Reader	Tecan, Switzerland
TLA-55 fixed-angle Rotor	Bio-Rad, USA
Trans-Blot Turbo Transfer system	Bio-Rad, USA
Transfer Pipettes (2, 20, 100, 200, 1000 uL)	Brand, Germany
Vacuum Pump	H.Saur Laborbedarf, Germany
Vortex VF2 Mixer	Janke & Kunkel Labortechnik

5.10 Software/Online Tools

Name	Provider
BioRender web App	Science Suite, Canada
ChemoStar Touch	INTAS, Germany
i-control™ 2.0	Tecan, Switzerland
ImageJ with Fiji v2.0	ImageJ
Microsoft Excel 2019	Microsoft Corporation, USA
Microsoft Word 2019	Microsoft Corporation, USA
Prism 9.3.1	GraphPad, USA
SnapGene Viewer	SnapGene, USA
UNICORN 7.1	General Electric Company, USA
Zen 2.3 SP1	Zeiss, Germany
Zen Lite	Zeiss, Germany

6.1 Methods

6.1 Bacterial Transformation

Heat shock

Chemically competent *E. coli* BL21 (DE3) cells were mixed with 0.5-1 µL of plasmid DNA and were incubated on ice for 30 min. Next, the mixture was rapidly placed into a 42°C incubator for 1 min and then moved back on ice and incubated for 2-3 min. Then, 0.5 mL of SOC medium was added to the mix and incubated at 37°C for 1 h with shaking. Afterwards, 25-50 µL of the mixture was plated on a LB-Agar plate supplemented with the antibiotics of the interest and mixed thoroughly with sterile plastic beads. The LB-Agar plate was incubated at 37°C overnight and next the day the colonies were picked for the subsequent inoculation.

Electroporation

Electrocompetent *E. coli* BL21 (DE3) cells were mixed with 0.5-1 µL of plasmid DNA. Then, the mixture was directly pipetted into a 1-mm electroporation cuvette and placed on the cuvette holder of the electroporator. A pulse of 1800 Volts was applied for 2 seconds and immediately afterwards, 0.5 mL of SOC medium was added to the cuvette. The mixture was gently mixed up and down and transferred to a 1.5 mL microtube followed by 1 h of incubation at 37°C with shaking. The following steps of the transformation was performed as it was described above in the heat shock transformation section.

6.2 Protein Expression and Purification (Sumo Protease Ulp1)

ULP1-Sumo protease was used to cleave off the SUMO-His tag during the chaperone purifications in this study. First, pULP1-6His plasmid was transformed into *E. coli* BL21 (DE3) cells. Next, the transformants were picked and inoculated overnight in 20 mL LB medium supplemented with Kanamycin (25 µg/mL) and Chloramphenicol (100 µg/mL) at 37°C in a shaking incubator. Next morning, the pre-culture was inoculated into 2 L of LB medium supplemented with Kanamycin (25 µg/mL) and Chloramphenicol (100 µg/mL) at 30°C with shaking at 180 rpm until it reached OD_{600}=0.6. Then, the culture was moved to 20°C and after 1h of further incubation, the expression was induced with

0.5 mM IPTG. The culture was kept in the shaking incubator for protein expression overnight. Next morning the culture was centrifuged in Nalgene bottles at 8000 rpm for 30 minutes at 4 °C for harvesting. The supernatant was discarded, and the pellets were scraped off and transferred to 50 mL falcon tubes. The remaining pellets were resuspended with 10 mL of media and added onto the pellets in the falcon tubes and re-centrifuged at 16000 rpm at 4°C for 30 min. Finally, the supernatant medium was discarded, and the pellet fraction was stored until purification at -80°C.

On the purification day, the pellets were resuspended coarsely by either stirring using a glass rod or by constantly pipetting up and down. Then, the bacterial resuspensions were incubated for 30 min with the lysis buffer on a rotator for further solubilization. The lysate was then mixed with an electric mixer to dissolve any remaining clumps. Next, for homogenization, the resuspended pellet was passed through the microfluidizer for 5 rounds at 18000 PSI. Next, the lysate was spun down for 30 minutes at 16000 rpm at 4°C and the supernatant was transferred into a 50 mL falcon tube and 3 mL of Ni-NTA agarose purification beads were added and the mixture was incubated for 1 hour at 4°C on a rotator. The mixture was then transferred to a 5 mL polypropylene column and the flow through was discarded carefully by applying pressure on the lid with a glove. Afterwards, the beads were washed 5 times with 50 mL of lysis buffer and immediately afterwards, the bottom end of the column was closed with a cap and 3 mL of elution buffer was added. The top of the column was also closed with a lid to avoid leaking and was incubated on a rotator at RT for 30 min. Next, the protein was eluted by dripping and no pressure was applied at this step. After the collection of the elution fractions, a 6-8 kDa dialysis membrane was washed with ddH_2O, and equilibrated with dialysis buffer for 5 min. Later, the eluted protein was transferred to the dialysis membrane and placed in to a 2 L bucket containing dialysis buffer and kept stirring overnight at 4°C. Next morning, the protein was removed from the membrane and spun down at maximum speed in a 15 mL conical tube to separate precipitates that sedimented and the supernatant was carefully transferred to a new conical tube and the pellet was discarded. The protein was diluted 1:1 with 100% glycerol and mixed thoroughly. Finally, the purified protein was aliquoted, flash frozen in liquid nitrogen and stored at -80°C.

6.3 Protein Expression and Purification (Chaperones)

For recombinant protein expression, a single transformant colony was picked from the transformation plate and inoculated in 25 mL LB medium supplemented with 100 µg/mL Kanamycin at 37°C with shaking at 180 rpm. Next, 20 mL of pre-culture was inoculated to 2L LB medium with 100 µg/mL of Kanamycin with shaking at 180 rpm at 37°C until an OD_{600}=0.6-0.8 was achieved to add 0.5 mM IPTG to induce protein expression. The expression culture was incubated overnight at 20°C with shaking at 180 rpm. The cells were harvested as described in the above section (6.2.).

As the first step of the purification, the bacterial pellets were lysed coarsely with a glass rod in lysis buffer supplemented by a scoop of DNase I, cOmplete Roche protease inhibitor (1 tablet per 50 mL lysate) and 100 mM PMSF, followed by a thorough resuspension with an electric mixer. The lysate was then homogenized by the microfluidizer at 18000 PSI five times until the lysate became clear. Afterwards, the lysate was centrifuged for 30 min at 16000 rpm 4°C. The supernatant was then incubated with 2 mL Ni-NTA beads in a rotator for 1 h at 4°C. The mixture was poured into a Qiagen polypropylene column, and the flow-through was discarded. Next, the resin was carefully washed with 25 mL of High-Salt Buffer and then with 25 mL of Low-salt buffer. Next, 4 mL of elution buffer was added to the resin and incubated rotating at 4°C for 20 min. The elution fraction was collected and added to a 6-8 kDa cut-off dialysis membrane, which was placed in 2 L of dialysis buffer at 4°C overnight with stirring. The next day, the protein was removed from the dialysis membrane and centrifuged for 5 min at 16000 rpm to separate precipitated protein. Then, the protein sample was incubated with 1 mL of fresh Ni-NTA resin for 30 min at 4°C on the rotator to remove the cleaved SUMO-His tag and ULP1-Sumo protease. Next, the cleaved protein was collected from the resin. The protein concentration was determined by a Bradford Assay. Finally, the purified protein was aliquoted in small volumes for further use and were flash-frozen in liquid nitrogen and stored at -80°.

6.4 Protein Expression and Purification (HTTExon1Q_{48} constructs)

The expression of the HTTExon1Q_{48}-X constructs was performed similarly as described above in the chaperone expression section. Only for the expression of constructs containing the CyPet/YPet fluorophores, the overnight incubation was carried out at 18°C instead of 20°C to avoid processing of the fusion constructs.

The bacterial pellets were lysed coarsely with a glass rod in lysis buffer supplemented by DNase I and cOmplete Roche protease inhibitor (1 tablet per 50 mL lysate) and 100 mM PMSF followed by a thorough resuspension with an electric mixer. The lysate was then homogenized by the microfluidizer at 18000 PSI for five consecutive rounds. Afterwards, 1% Triton X-100 was added to the lysate and left to stir for 15 min at 4°C and then centrifuged for 30 min at 16000 rpm 4°C. The supernatant was incubated with 2 mL Sepharose glutathione beads on a rotator for 1 h at 4°C. The mixture was poured into a polypropylene column, and the flow-through was discarded. Next, the resin was carefully washed with 10 mL of washing buffer and subsequently with 10 mL of Buffer 1. Next, 4 mL of elution buffer was added to the resin and incubated on a rotator or an incubation roller at 4°C for 20 min. The elution fraction was collected and added to a 6-8 kDa dialysis membrane which was placed in 2 L dialysis buffer and stirred at 4°C overnight. The next day, the protein solution was removed from the dialysis membrane and aliquoted to small fractions. The aliquots were flash-frozen in liquid nitrogen and stored at -80°

6.5 Protein Expression and Purification-PreScission Protease

The expression and purification of PreScission protease was performed as described above since it consists of the same backbone and purification tag as the HTTExon1Q_{48} constructs.

6.6 Bradford Assay

To determine the protein concentrations in this study, a Bradford assay was performed. First, Bradford standards were prepared with a dilution series of 10 mg/mL BSA in ddH_2O. Then, 5X RotiQuant Bradford Reagent was diluted to 1X concentration with ddH_2O and was pipetted to a transparent, flat-bottomed, 96-well plate in 200 µL of volume. Then, calibration standards between 0.25 mg/mL to 6 mg/mL were pipetted and the first three wells contained only the diluted Bradford reagent for blank measurement. Each protein sample and standard were pipetted in triplicates. Immediately after, the assay plate was incubated at 37°C for 10 min. with thorough mixing of the samples with the reagent. Then, the absorbances were measured at 595 nm using a plate reader. Finally, a linear regression curve was created with the standards and the protein concentrations were determined using this curve.

6.7 Fluorescent Labelling of Chaperones

Freshly purified DNAJB1^{G194C} was incubated with 10 mM DTT for 30 min to reduce the disulfide bonds. Then, DTT was removed by centrifugation with a spin concentrator at 13000 rpm for 30 min to avoid a competition of the dye with the thiol groups present in DTT. Then, 3-4 mg/mL protein was incubated with Alexa-488/647 C2-maleimide dye in 5-fold molar excess in the presence of 500 µM TCEP at RT for 2 h with agitation. Removal of the free dye was performed by size-exclusion chromatography with a Superdex^{TM} 75 Increase 10/300 GL column. Labelling efficiencies were determined by Nanodrop, and the degree of labelling was determined to range between 70-100%.

6.8 Size-Exclusion Chromatography

For size-exclusion chromatography, the *Ä*KTA pure system was used. Superdex^{TM} 75 Increase 10/300 GL column was kept in 20% ethanol for extended storage periods. Prior to usage, the ethanol was first exchanged by double-distilled, degassed water with a flow rate of 0.300 mL/min. Then, the column was equilibrated with running buffer twice with a flow rate of 0.400 mL/min. If the running buffer contained glycerol, the flow rate was reduced to 0.200 mL/min to avoid exposing the column to high pressure. All samples were always quickly spun down on a bench-top centrifuge prior to loading onto

the column by injection. For that, the precipitates were eliminated by the centrifugation step to avoid clogging of the column. Then, depending on the volume of the sample to be injected, either 1-, 2- or 5-mL loops were used. The samples were loaded into a syringe and air bubbles in the syringe were carefully removed to avoid air entering to the columns which could cause drying of the columns. The samples were then injected into the loop and then loaded onto the column. Fractions were either collected by the fraction collector or by manual collection of the eluate directly from the outlet valve. Immediately after the run, the column was washed with ddH_2O twice at a flow rate of 0.400 mL/min and then with 20% ethanol. The analysis of the chromatograms was performed using Microsoft Excel.

6.9 SDS-PAGE

The gels used in this study were cast according to the composition indicated in Table 6.1. Protein samples were mixed with 4X loading dye and boiled at 95°C for 10 min. Then, the samples were carefully loaded onto the wells and the 12% SDS-PAGE gel was subjected to 70 V until the protein ladder started to resolve upon passing the stacking gel and then for separation a constant voltage of 140 V was applied. The gels were stained with Coomassie Blue staining solution for 20 min and destained with destaining solution overnight at RT on a shaker.

Table 6.1 SDS-PAGE gel composition for a 1.5 mM mini gel

Components	Stacking gel (4%)	Separation Gel (12%)
Acrylamide/Bisacrylamide (Rotiphorese® Gel 30)	0.67 mL	4 mL
Stacking gel buffer	1.25 mL	-
Resolving gel buffer	-	2.5 mL
ddH2O	3 mL	3.32 mL
10% (w/v) APS	50 µL	76 µL
TEMED	7 µL	20 µL

6.10 Western Blotting

SDS-PAGE gel was blotted to a nitrocellulose membrane by a semi-dry blotting system. Transfer stacks and the membrane were equilibrated in transfer buffer for 5 min. For blotting, a pre-defined standard program for 1.5 mm gels was used for 10 min. Immediately after blotting, the membrane was placed in a blocking buffer for an hour and then incubated with a primary antibody overnight at 4°C with shaking. The membrane was washed three times with wash buffer for 15 minutes at RT and incubated with secondary antibody for 2h at RT with shaking. Antibody signals were detected by using Pierce™ ECL Western Blotting substrate and imaging was performed by INTAS ECL Chemostar imaging device. Densitometric image analysis was done by ImageJ/Fiji software.

6.11 ATPase Assay

To detect the level of free phosphate released upon ATP hydrolysis during chaperone assisted nucleotide exchange activity, an ATPase assay was used. First, 1 µM Hsc70, 0.5 µM of the J-domain protein and 0.25 µM Apg2 were prepared to a total volume of 160 µL in low-binding tubes. A final concentration of 1 mM ATP was added to initiate the reaction. All the samples were incubated at 20 °C for 2.5 h. Next, 50 µl of phosphate dilution standards and samples were pipetted in triplicates to a 96-well transparent plate and mixed with 160 µl of green malachite reaction solution and immediately followed by the addition of 20 µl of 34% sodium citrate. To determine the free phosphate concentration, absorbance at 650 nm was measured in the plate reader. The concentration of the free phosphate in each sample was calculated based on the phosphate calibration curve. Lastly, the phosphate concentrations in each sample were normalized to the basal ATPase activity of Hsc70.

6.12 Luciferase Refolding Assay

First, 15 nM luciferase in 1x dilution buffer at 45 °C was denatured for 15 min. Then, a final concentration of 5 nM denatured luciferase was mixed with 2.5 µM Hsc70, 0.125 µM Apg2, and 2.5 µM J-domain protein. Next, 5 µl from each sample were pipetted in triplicates to a 96-well, white microplate containing 50 µl of assay buffer, at time points

0, 7, 15, 30, 60, 90, and 120 min. Following the addition of 50 µl of 0.25 mM luciferin to each well, luminescence was measured in the plate reader, with an integration time of 1000 ms, and settling time of 0 ms without attenuation. The data at each time point were normalized to the values measured for the native luciferase and were plotted as the recovered luciferase activity in percentage, over the time course of the experiment.

6.13 FRET assay

HTTExon1Q_{48}-CyPet, HTTExon1Q_{48}-YPet and the chaperones were ultracentrifuged at 40000 rpm for 40 min at 4°C, and about 90% of the supernatant was taken used to remove possible aggregations of these proteins prior to the assay. To monitor the HTT control aggregation without chaperones, equimolar concentrations of HTTExon1Q_{48}-CyPet (donor) and HTTExon1Q_{48}-YPet (acceptor) were pipetted in total of 0.75 µM unless stated otherwise. Samples containing chaperones consisted of 5 µM Hsc70, 0.5 µM Apg2 and 5 µM J-Protein unless stated otherwise and a total sample volume of 100 µL with the Reaction Buffer and ATP regeneration system was prepared. The formation of HTTExon1Q_{48} fibrils was initiated upon the cleavage of the GST-tag by PreScission protease. All samples were pipetted in triplicates into a 384-well plate which was then covered by a transparent foil to avoid evaporation over the time course of the measurement. The measurements were performed by the Infinite F200 PRO Tecan plate reader. The data analysis with the calculation of the fluorescence data as well as the measurement parameters are included in the Appendix.

6.14 Disaggregation Assay

Fibrils were prepared with 2 µM HTTExon1Q_{48}-CyPet in Aggregation Buffer. Fibrillization was initiated by the cleavage of GST tag upon addition of PreScission protease and incubation was done for 4.5 h at 20 °C. A final concentration of 0.75 µM fibrillar HTTExon1Q_{48}-CyPET in Aggregation Buffer was mixed with 10 µM Hsc70, 0.5 µM Apg2 and 10 µM J-domain protein. Disaggregation reaction was initiated by the addition of ATP regeneration system and incubated at 30 °C for 24h. Next, the samples were centrifuged at 20000 rpm for 30 min at 4°C and subsequently the supernatant was carefully separated from the pellet fraction. Fluorescence of the soluble fraction was measured in triplicates with Tecan F200 plate reader (Exλ: 430 nm; Emλ: 485 nm)

and the resulting data was normalized to the sample of HTTExon1Q_{48} fibrils with Hsc70, Apg2 and DNAJB1^{wt}.

6.15 Binding Assay by Co-sedimentation

First, 2 µM HTTExon1Q_{48} fibrils were prepared as described above in the Disaggregation Assay section. Next, a final concentration of 5 µM DNAJB1^{wt} and DNAJB1^{H244A} were incubated with 1 µM of HTT fibrils for 1 h at RT. Subsequently, the samples were sedimented at 20000 rpm for 30 min at 4 °C by ultracentrifugation. The supernatant fraction was carefully removed and discarded. Afterwards, the pellets containing the fibrillar fraction were resolubilized with 100% formic acid for 1 h at RT. To obtain dry pellets, overnight vacuum centrifugation of the formic acid was done. Finally, the pellets were solubilized with 20 µL of aggregation buffer and further analysis of fibril bound J-domain proteins was performed by Western Blotting.

6.16 Binding Assay by Filter Retardation

At the indicated time points, samples were collected from the FRET assay plate and diluted into 1% SDS. The cellulose acetate membrane was soaked with the activation buffer for 5 min. Next, the filter retardation apparatus was constructed with the membrane in between the top and bottom parts of the apparatus. The membrane was then washed, and each well was filled with 100 µL of wash buffer. To each well, 30 µL of sample was loaded and following the aspiration of the samples, the membrane was washed twice with 200 µL of wash buffer and aspirated for 3 min to dry the membrane. Finally, the apparatus was dismantled, and the membrane was placed in blocking solution. For the detection of chaperones, the membrane was incubated with 1:3000 anti-DNAJB1 primary antibody and 1:1000 anti-Hsc70 primary antibodies at 4°C overnight. The membranes were subsequently incubated with 1:6000 anti-rabbit-HRP for DNAJB1 and 1:3000 anti-mouse-HRP for Hsc70 secondary antibodies. The signals were developed using Pierce™ ECL (ThermoFisher) and detected on an ChemoStar Touch ECL (INTAS) imager. For the detection of the fluorescently tagged secondary antibodies and DNAJB1^{Alexa647} signals on the membrane, a pre-defined red fluorophore

channel in the software was used. Densitometric analysis was performed by ImageJ/Fiji software.

6.17 Confocal Laser Scanning Microscopy

Samples for imaging were diluted in 1% SDS and spun down at 20000 rpm, 30 min at RT. Then, the supernatant was completely discarded, the pellet fraction was resuspended with 5 µL of Resuspension Buffer and directly pipetted on the glass microscopy slide. Imaging was performed by a laser scanning confocal microscope (LSM 880, Zeiss) with an airy scan detector and a Zeiss Plan-Apochromat Neofluar 40x/1,4 oil DIC M27 objective. For HTTExon1Q_{48}CyPet/YPet, excitation wavelength of 488 nm and emission wavelength of 523 nm was used. For DNAJB1-Alexa647 excitation wavelength of 633 nm and emission wavelength of 654 nm was used. All images were taken with an image size of 512x512. Image recording was done with Zen Blue 2.3 SP1 Software, and the subsequent image analysis was performed with ImageJ/Fiji.

6.18 Statistical Analysis

Statistical analysis and the graphs were generated by Microsoft Excel and GraphPad Prism 8 and 9 software. Two-way or one-way ANOVA was used for data group comparisons. Unpaired t-test was used for the statistical significance analysis ($p < 0,05$ (*), $< 0,01$ (**), $< 0,001$ (***), $< 0,0001$ (****)), and the confidence level was set at 0.05 (95% confidence level).

6. Appendix

6.1 FRET assay measurement parameters:

Plate reader parameters:

Plate type: 384-well Flat Bottom Black Polystyrene (Corning)

Temperature: 20°C

Kinetic cycles: 1000

Interval time: 20 minutes

Mode: Fluorescence top reading

Label 1 (Donor-CyPET):

Excitation wavelength: 430 nm; Bandwidth: 20 nm

Emission wavelength: 485 nm; Bandwidth: 20 nm

Mirror (automatic): 50%

Gain:80

Label 2 (Acceptor-YPET):

Excitation wavelength: 485 nm; Bandwidth: 20 nm

Emission wavelength: 535 nm; Bandwidth: 25 nm

Mirror (automatic): dichroic 510

Gain:80

Label 3 (FRET):

Excitation wavelength: 430 nm; Bandwidth: 20 nm

Emission wavelength: 535 nm; Bandwidth: 25 nm

Mirror (automatic): dichroic 510

Gain:80

Settle time: 0 us

Integration time: 20 us

Number of flashes: 10

Lag time: 0 us

6.2 Calculation of the Apparent FRET Efficiency (E_{App}%):

1. Three empty wells were selected for blank measurement. The average of the blank wells was calculated and subtracted from values for all the samples.

2. $$Rd = \frac{Donor\ fluorescence\ in\ Label\ 3}{Donor\ fluorescence\ in\ Label\ 1}$$

$$Ra = \frac{Acceptor\ Fluorescence\ in\ Label\ 3}{Acceptor\ Fluorescence\ in\ Label\ 2}$$

3. RD and RA were averaged.

4. $FRET_{SE}$=S$ample\ fluorescence\ in$ l$abel$ 3 − ((S$ample\ fluorescence\ in\ label1*$ Rd) − (S$ample\ fluorescence\ in\ label$ 2$*$ Ra))

5. FRET efficiency (E_{app}%):

$$Eapp\% = \left(\frac{FRETSE}{Sample\ fluorescence\ in\ label\ 3}\right) * 100$$

E_{app}% of each triplicate was averaged and plotted against time.

7. References

Abelein, A. and Johansson, J. (2023) ‘Amyloid inhibition by molecular chaperones can be translated to Alzheimer’s pathology’, *RSC Medicinal Chemistry*, 14(5), pp. 848–857. Available at: https://doi.org/10.1039/D3MD00040K.

Ahmad, A. *et al.* (2011) ‘Heat shock protein 70 kDa chaperone/DnaJ cochaperone complex employs an unusual dynamic interface’, *Proceedings of the National Academy of Sciences*, 108(47), pp. 18966–18971. Available at: https://doi.org/10.1073/pnas.1111220108.

Ahmad, A., Uversky, V.N. and Khan, R.H. (2022) ‘Aberrant liquid-liquid phase separation and amyloid aggregation of proteins related to neurodegenerative diseases’, *International Journal of Biological Macromolecules*, 220, pp. 703–720. Available at: https://doi.org/10.1016/j.ijbiomac.2022.08.132.

Albanèse, V. *et al.* (2006) ‘Systems Analyses Reveal Two Chaperone Networks with Distinct Functions in Eukaryotic Cells’, *Cell*, 124(1), pp. 75–88. Available at: https://doi.org/10.1016/j.cell.2005.11.039.

Alonso, M. *et al.* (2006) ‘Brain imaging and cognitive dysfunctions in Huntington’s disease’, *Journal of Psychiatry and Neuroscience,* 31(1), pp. 21–29.

Ambadipudi, S. *et al.* (2017) ‘Liquid–liquid phase separation of the microtubule-binding repeats of the Alzheimer-related protein Tau’, *Nature Communications*, 8(1), p. 275. Available at: https://doi.org/10.1038/s41467-017-00480-0.

Arhar, T. *et al.* (2021) ‘The interactions of molecular chaperones with client proteins: why are they so weak?’, *Journal of Biological Chemistry*, 297(5), p. 101282. Available at: https://doi.org/10.1016/j.jbc.2021.101282.

Arndt, J.R., Chaibva, M. and Legleiter, J. (2015) ‘The emerging role of the first 17 amino acids of huntingtin in Huntington’s disease’, *Biomolecular Concepts*, 6(1), pp. 33–46. Available at: https://doi.org/10.1515/bmc-2015-0001.

Ast, A. *et al.* (2018) ‘mHTT Seeding Activity: A Marker of Disease Progression and Neurotoxicity in Models of Huntington’s Disease’, *Molecular Cell*, 71(5), pp. 675-688.e6. Available at: https://doi.org/10.1016/j.molcel.2018.07.032.

Ayala Mariscal, S.M. *et al.* (2022) ‘Identification of a HTT-specific binding motif in DNAJB1 essential for suppression and disaggregation of HTT’, *Nature Communications*, 13(1), p. 4692. Available at: https://doi.org/10.1038/s41467-022-32370-5.

Ayala Mariscal, S.M. and Kirstein, J. (2021) ‘J-domain proteins interaction with neurodegenerative disease-related proteins’, *Experimental Cell Research*, 399(2), p. 112491. Available at: https://doi.org/10.1016/j.yexcr.2021.112491.

Baaklini, I. *et al.* (2020) ‘Selective Binding of HSC70 and its Co-Chaperones to Structural Hotspots on CFTR’, *Scientific Reports*, 10(1), p. 4176. Available at: https://doi.org/10.1038/s41598-020-61107-x.

Babinchak, W.M. *et al.* (2020) ‘Small molecules as potent biphasic modulators of protein liquid-liquid phase separation’, *Nature Communications*, 11(1), p. 5574. Available at: https://doi.org/10.1038/s41467-020-19211-z.

Balchin, D., Hayer-Hartl, M. and Hartl, F.U. (2016) ‘In vivo aspects of protein folding and quality control’, *Science*, 353(6294). Available at: https://doi.org/10.1126/science.aac4354.

Bates, G.P. *et al.* (2015) ‘Huntington disease’, *Nature Reviews Disease Primers*, 1(1), p. 15005. Available at: https://doi.org/10.1038/nrdp.2015.5.

Bäuerlein, F.J.B. *et al.* (2017) ‘In Situ Architecture and Cellular Interactions of PolyQ Inclusions’, *Cell*, 171(1), pp. 179-187.e10. Available at: https://doi.org/10.1016/j.cell.2017.08.009.

Behrends, C. *et al.* (2006) ‘Chaperonin TRiC Promotes the Assembly of polyQ Expansion Proteins into Nontoxic Oligomers’, *Molecular Cell*, 23(6), pp. 887–897. Available at: https://doi.org/10.1016/j.molcel.2006.08.017.

Bennett, M.J. *et al.* (2002) ‘A linear lattice model for polyglutamine in CAG-expansion diseases’, *Proceedings of the National Academy of Sciences*, 99(18), pp. 11634–11639. Available at: https://doi.org/10.1073/pnas.182393899.

Bhattacharya, A. *et al.* (2009) ‘Allostery in Hsp70 Chaperones Is Transduced by Subdomain Rotations’, *Journal of Molecular Biology*, 388(3), pp. 475–490. Available at: https://doi.org/10.1016/j.jmb.2009.01.062.

Bhattacharyya, A. *et al.* (2006) ‘Oligoproline Effects on Polyglutamine Conformation and Aggregation’, *Journal of Molecular Biology*, 355(3), pp. 524–535. Available at: https://doi.org/10.1016/j.jmb.2005.10.053.

Bhattacharyya, K. (2016) ‘The story of George Huntington and his disease’, *Annals of Indian Academy of Neurology*, 19(1), p. 25. Available at: https://doi.org/10.4103/0972-2327.175425.

Bigi, A. *et al.* (2022) ‘Amyloid fibrils act as a reservoir of soluble oligomers, the main culprits in protein deposition diseases’, *BioEssays*, 44(11). Available at: https://doi.org/10.1002/bies.202200086.

Brehme, M. *et al.* (2014) ‘A Chaperome Subnetwork Safeguards Proteostasis in Aging and Neurodegenerative Disease’, *Cell Reports*, 9(3), pp. 1135–1150. Available at: https://doi.org/10.1016/j.celrep.2014.09.042.

Busch, A. *et al.* (2003) ‘Mutant Huntingtin Promotes the Fibrillogenesis of Wild-type Huntingtin’, *Journal of Biological Chemistry*, 278(42), pp. 41452–41461. Available at: https://doi.org/10.1074/jbc.M303354200.

Caron, N.S., Wright, G.E. and Hayden, M.R. (1993) *Huntington Disease*.

Carrasco, J. *et al.* (2023) ‘Metamorphism in TDP-43 prion-like domain determines chaperone recognition’, *Nature Communications*, 14(1), p. 466. Available at: https://doi.org/10.1038/s41467-023-36023-z.

Cattaneo, E., Zuccato, C. and Tartari, M. (2005) ‘Normal huntingtin function: an alternative approach to Huntington’s disease’, *Nature Reviews Neuroscience*, 6(12), pp. 919–930. Available at: https://doi.org/10.1038/nrn1806.

Chai, Y. *et al.* (1999) ‘Analysis of the Role of Heat Shock Protein (Hsp) Molecular Chaperones in Polyglutamine Disease’, *The Journal of Neuroscience*, 19(23), pp. 10338–10347. Available at: https://doi.org/10.1523/JNEUROSCI.19-23-10338.1999.

Chamberlain, L.H. and Burgoyne, R.D. (1997) ‘Activation of the ATPase activity of heat-shock proteins Hsc70/Hsp70 by cysteine-string protein’, *Biochemical Journal*, 322(3), pp. 853–858. Available at: https://doi.org/10.1042/bj3220853.

Chen, G. *et al.* (2020) ‘Augmentation of Bri2 molecular chaperone activity against amyloid-β reduces neurotoxicity in mouse hippocampus in vitro’, *Communications Biology*, 3(1), p. 32. Available at: https://doi.org/10.1038/s42003-020-0757-z.

Chen, M. and Wolynes, P.G. (2017) ‘Aggregation landscapes of Huntingtin exon 1 protein fragments and the critical repeat length for the onset of Huntington’s disease’, *Proceedings of the National Academy of Sciences*, 114(17), pp. 4406–4411. Available at: https://doi.org/10.1073/pnas.1702237114.

Chen, S. *et al.* (2010) ‘Autophagy is a therapeutic target in anticancer drug resistance’, *Biochimica et Biophysica Acta (BBA) - Reviews on Cancer*, 1806(2), pp. 220–229. Available at: https://doi.org/10.1016/j.bbcan.2010.07.003.

Chiti, F. and Dobson, C.M. (2006) ‘Protein Misfolding, Functional Amyloid, and Human Disease’, *Annual Review of Biochemistry*, 75(1), pp. 333–366. Available at: https://doi.org/10.1146/annurev.biochem.75.101304.123901.

Choudhury, K.R. and Bhattacharyya, N.P. (2015) ‘Chaperone protein HYPK interacts with the first 17 amino acid region of Huntingtin and modulates mutant HTT-mediated aggregation and cytotoxicity’, *Biochemical and Biophysical Research Communications*, 456(1), pp. 66–73. Available at: https://doi.org/10.1016/j.bbrc.2014.11.035.

Clerico, E.M. *et al.* (2015) ‘How Hsp70 Molecular Machines Interact with Their Substrates to Mediate Diverse Physiological Functions’, *Journal of Molecular Biology*, 427(7), pp. 1575–1588. Available at: https://doi.org/10.1016/j.jmb.2015.02.004.

Clerico, E.M. *et al.* (2019) ‘Hsp70 molecular chaperones: multifunctional allosteric holding and unfolding machines’, *Biochemical Journal*, 476(11), pp. 1653–1677. Available at: https://doi.org/10.1042/BCJ20170380.

Cohen, S.I.A. *et al.* (2012) ‘From Macroscopic Measurements to Microscopic Mechanisms of Protein Aggregation’, *Journal of Molecular Biology*, 421(2–3), pp. 160–171. Available at: https://doi.org/10.1016/j.jmb.2012.02.031.

Cohen, S.I.A. *et al.* (2015) ‘A molecular chaperone breaks the catalytic cycle that generates toxic Aβ oligomers’, *Nature Structural & Molecular Biology*, 22(3), pp. 207–213. Available at: https://doi.org/10.1038/nsmb.2971.

Côté, S. *et al.* (2015) ‘Probing the Huntingtin 1-17 Membrane Anchor on a Phospholipid Bilayer by Using All-Atom Simulations’, *Biophysical Journal*, 108(5), pp. 1187–1198. Available at: https://doi.org/10.1016/j.bpj.2015.02.001.

Crick, S.L. *et al.* (2013) ‘Unmasking the roles of N- and C-terminal flanking sequences from exon 1 of huntingtin as modulators of polyglutamine aggregation’, *Proceedings of the National Academy of Sciences*, 110(50), pp. 20075–20080. Available at: https://doi.org/10.1073/pnas.1320626110.

Dehay, B. and Bertolotti, A. (2006) ‘Critical Role of the Proline-rich Region in Huntingtin for Aggregation and Cytotoxicity in Yeast’, *Journal of Biological Chemistry*, 281(47), pp. 35608–35615. Available at: https://doi.org/10.1074/jbc.M605558200.

DiFiglia, M. *et al.* (1995) ‘Huntingtin is a cytoplasmic protein associated with vesicles in human and rat brain neurons’, *Neuron*, 14(5), pp. 1075–1081. Available at: https://doi.org/10.1016/0896-6273(95)90346-1.

Dragatsis, I., Levine, M.S. and Zeitlin, S. (2000) ‘Inactivation of Hdh in the brain and testis results in progressive neurodegeneration and sterility in mice’, *Nature Genetics*, 26(3), pp. 300–306. Available at: https://doi.org/10.1038/81593.

Duennwald, M.L. *et al.* (2006) ‘Flanking sequences profoundly alter polyglutamine toxicity in yeast’, *Proceedings of the National Academy of Sciences*, 103(29), pp. 11045–11050. Available at: https://doi.org/10.1073/pnas.0604547103.

Duim, W.C. *et al.* (2014) ‘Super-Resolution Fluorescence of Huntingtin Reveals Growth of Globular Species into Short Fibers and Coexistence of Distinct Aggregates’, *ACS Chemical Biology*, 9(12), pp. 2767–2778. Available at: https://doi.org/10.1021/cb500335w.

El-Daher, M. *et al.* (2015) ‘Huntingtin proteolysis releases non-polyQ fragments that cause toxicity through dynamin 1 dysregulation’, *The EMBO Journal*, 34(17), pp. 2255–2271. Available at: https://doi.org/10.15252/embj.201490808.

Elena-Real, C.A. *et al.* (2023) ‘Multi-site-specific isotopic labeling accelerates high-resolution structural investigations of pathogenic huntingtin exon-1’, *Structure*, 31(6), pp. 644-650.e5. Available at: https://doi.org/10.1016/j.str.2023.04.003.

Evans, C.G., Wisén, S. and Gestwicki, J.E. (2006) ‘Heat Shock Proteins 70 and 90 Inhibit Early Stages of Amyloid β-(1–42) Aggregation in Vitro’, *Journal of Biological Chemistry*, 281(44), pp. 33182–33191. Available at: https://doi.org/10.1074/jbc.M606192200.

Faber, P. *et al.* (1998) ‘Huntingtin interacts with a family of WW domain proteins’, *Human Molecular Genetics*, 7(9), pp. 1463–1474. Available at: https://doi.org/10.1093/hmg/7.9.1463.

Falk, A.S. *et al.* (2020) ‘Structural Model of the Proline-Rich Domain of Huntingtin Exon-1 Fibrils’, *Biophysical Journal*, 119(10), pp. 2019–2028. Available at: https://doi.org/10.1016/j.bpj.2020.10.010.

Fändrich, M. (2012) ‘Oligomeric Intermediates in Amyloid Formation: Structure Determination and Mechanisms of Toxicity’, *Journal of Molecular Biology*, 421(4–5), pp. 427–440. Available at: https://doi.org/10.1016/j.jmb.2012.01.006.

Faust, O. *et al.* (2020) ‘HSP40 proteins use class-specific regulation to drive HSP70 functional diversity’, *Nature*, 587(7834), pp. 489–494. Available at: https://doi.org/10.1038/s41586-020-2906-4.

Finley, D. *et al.* (2012) ‘The Ubiquitin–Proteasome System of *Saccharomyces cerevisiae*’, *Genetics*, 192(2), pp. 319–360. Available at: https://doi.org/10.1534/genetics.112.140467.

Freeman, B.C. *et al.* (1995) 'Identification of a regulatory motif in Hsp70 that affects ATPase activity, substrate binding and interaction with HDJ-1.', *The EMBO Journal*, 14(10), pp. 2281–2292. Available at: https://doi.org/10.1002/j.1460-2075.1995.tb07222.x.

Gafni, J. and Ellerby, L.M. (2002) 'Calpain Activation in Huntington's Disease', *The Journal of Neuroscience*, 22(12), pp. 4842–4849. Available at: https://doi.org/10.1523/JNEUROSCI.22-12-04842.2002.

Gao, X. *et al.* (2015) 'Human Hsp70 Disaggregase Reverses Parkinson's-Linked α-Synuclein Amyloid Fibrils', *Molecular Cell*, 59(5), pp. 781–793. Available at: https://doi.org/10.1016/j.molcel.2015.07.012.

Gillis, J. *et al.* (2013) 'The DNAJB6 and DNAJB8 Protein Chaperones Prevent Intracellular Aggregation of Polyglutamine Peptides', *Journal of Biological Chemistry*, 288(24), pp. 17225–17237. Available at: https://doi.org/10.1074/jbc.M112.421685.

Gong, B. *et al.* (2016) 'The Ubiquitin-Proteasome System: Potential Therapeutic Targets for Alzheimer's Disease and Spinal Cord Injury', *Frontiers in Molecular Neuroscience*, 9. Available at: https://doi.org/10.3389/fnmol.2016.00004.

Gropp, M.H.M., Klaips, C.L. and Hartl, F.U. (2022) 'Formation of toxic oligomers of polyQ-expanded Huntingtin by prion-mediated cross-seeding', *Molecular Cell*, 82(22), pp. 4290-4306.e11. Available at: https://doi.org/10.1016/j.molcel.2022.09.031.

Gui, X. *et al.* (2023) 'Liquid–liquid phase separation of amyloid-β oligomers modulates amyloid fibrils formation', *Journal of Biological Chemistry*, 299(3), p. 102926. Available at: https://doi.org/10.1016/j.jbc.2023.102926.

Guo, Q. *et al.* (2018) 'The cryo-electron microscopy structure of huntingtin', *Nature*, 555(7694), pp. 117–120. Available at: https://doi.org/10.1038/nature25502.

Hackam, A.S. *et al.* (1999) 'Evidence for both nucleus and cytoplasm as subcellular sites of pathogenesis in Huntington's disease in cell culture and in transgenic mice expressing mutant huntingtin', *Philosophical Transactions of the Royal Society of London. Series B: Biological Sciences*, 354(1386), pp. 1047–1055. Available at: https://doi.org/10.1098/rstb.1999.0457.

Han, I. *et al.* (2010) 'Differential vulnerability of neurons in Huntington's disease: the role of cell type-specific features', *Journal of Neurochemistry*, 113(5), pp. 1073–1091. Available at: https://doi.org/10.1111/j.1471-4159.2010.06672.x.

Han, W. and Christen, P. (2003) 'Mechanism of the Targeting Action of DnaJ in the DnaK Molecular Chaperone System', *Journal of Biological Chemistry*, 278(21), pp. 19038–19043. Available at: https://doi.org/10.1074/jbc.M300756200.

Harper, J.D. and Lansbury, P.T. (1997) 'MODELS OF AMYLOID SEEDING IN ALZHEIMER'S DISEASE AND SCRAPIE: Mechanistic Truths and Physiological Consequences of the Time-Dependent Solubility of Amyloid Proteins', *Annual Review of Biochemistry*, 66(1), pp. 385–407. Available at: https://doi.org/10.1146/annurev.biochem.66.1.385.

Hartl, F.U., Bracher, A. and Hayer-Hartl, M. (2011) 'Molecular chaperones in protein folding and proteostasis', *Nature*, 475(7356), pp. 324–332. Available at: https://doi.org/10.1038/nature10317.

Hasecke, F. *et al.* (2018) ‘Origin of metastable oligomers and their effects on amyloid fibril self-assembly’, *Chemical Science*, 9(27), pp. 5937–5948. Available at: https://doi.org/10.1039/C8SC01479E.

Hay, D.G., Sathasivam, K. and Tobaben, S. (2004) ‘Progressive decrease in chaperone protein levels in a mouse model of Huntington’s disease and induction of stress proteins as a therapeutic approach’, *Human Molecular Genetics*, 13(13), pp. 1389–1405. Available at: https://doi.org/10.1093/hmg/ddh144.

Helabad MB *et al.* (2023) ‘Integrative determination of the atomic structure of mutant huntingtin exon 1 fibrils from Huntington’s disease.’, *bioRxiv [Preprint]* [Preprint]. Available at: https://doi.org/doi: 10.1101/2023.07.21.549993.

Hennessy, F. *et al.* (2005) ‘Not all J domains are created equal: Implications for the specificity of Hsp40–Hsp70 interactions’, *Protein Science*, 14(7), pp. 1697–1709. Available at: https://doi.org/10.1110/ps.051406805.

Hingorani, K.S. and Gierasch, L.M. (2014) ‘Comparing protein folding in vitro and in vivo: foldability meets the fitness challenge’, *Current Opinion in Structural Biology*, 24, pp. 81–90. Available at: https://doi.org/10.1016/j.sbi.2013.11.007.

Hipp, M.S., Kasturi, P. and Hartl, F.U. (2019) ‘The proteostasis network and its decline in ageing’, *Nature Reviews Molecular Cell Biology*, 20(7), pp. 421–435. Available at: https://doi.org/10.1038/s41580-019-0101-y.

Hipp, M.S., Park, S.-H. and Hartl, F.U. (2014) ‘Proteostasis impairment in protein-misfolding and -aggregation diseases’, *Trends in Cell Biology*, 24(9), pp. 506–514. Available at: https://doi.org/10.1016/j.tcb.2014.05.003.

Hodges, A. *et al.* (2006) ‘Regional and cellular gene expression changes in human Huntington’s disease brain.’, *Human molecular genetics*, 15(6), pp. 965–77. Available at: https://doi.org/10.1093/hmg/ddl013.

Hoop, C.L. *et al.* (2014) ‘Polyglutamine Amyloid Core Boundaries and Flanking Domain Dynamics in Huntingtin Fragment Fibrils Determined by Solid-State Nuclear Magnetic Resonance’, *Biochemistry*, 53(42), pp. 6653–6666. Available at: https://doi.org/10.1021/bi501010q.

Hu, S. *et al.* (2021) ‘Molecular chaperones and Parkinson’s disease’, *Neurobiology of Disease*, 160, p. 105527. Available at: https://doi.org/10.1016/j.nbd.2021.105527.

Huang, F. *et al.* (2018) ‘Self-Assembly Molecular Chaperone to Concurrently Inhibit the Production and Aggregation of Amyloid β Peptide Associated with Alzheimer’s Disease’, *ACS Macro Letters*, 7(8), pp. 983–989. Available at: https://doi.org/10.1021/acsmacrolett.8b00495.

Huntington, G. (1872) ‘On Chorea’, *Medical and Surgical Reporter*, 26, pp. 317–321.

Isas, JM. *et al.* (2021) ‘Huntingtin fibrils with different toxicity, structure, and seeding potential can be interconverted’, *Nature Communications*, 12(1), p. 4272. Available at: https://doi.org/10.1038/s41467-021-24411-2.

Isas, J.M., Langen, R. and Siemer, A.B. (2015) ‘Solid-State Nuclear Magnetic Resonance on the Static and Dynamic Domains of Huntingtin Exon-1 Fibrils’,

Biochemistry, 54(25), pp. 3942–3949. Available at: https://doi.org/10.1021/acs.biochem.5b00281.

Jalali, S. *et al.* (2023) 'Nucleation and Growth of Amyloid Fibrils', *The Journal of Physical Chemistry B*, 127(45), pp. 9759–9770. Available at: https://doi.org/10.1021/acs.jpcb.3c05300.

Jayaraj, G.G., Hipp, M.S. and Hartl, F.U. (2020) 'Functional Modules of the Proteostasis Network', *Cold Spring Harbor Perspectives in Biology*, 12(1), p. a033951. Available at: https://doi.org/10.1101/cshperspect.a033951.

Jiang, Y., Rossi, P. and Kalodimos, C.G. (2019) 'Structural basis for client recognition and activity of Hsp40 chaperones', *Science*, 365(6459), pp. 1313–1319. Available at: https://doi.org/10.1126/science.aax1280.

Jores, T. *et al.* (2018) 'Cytosolic Hsp70 and Hsp40 chaperones enable the biogenesis of mitochondrial β-barrel proteins', *Journal of Cell Biology*, 217(9), pp. 3091–3108. Available at: https://doi.org/10.1083/jcb.201712029.

Kakkar, V. *et al.* (2016) 'The S/T-Rich Motif in the DNAJB6 Chaperone Delays Polyglutamine Aggregation and the Onset of Disease in a Mouse Model', *Molecular Cell*, 62(2), pp. 272–283. Available at: https://doi.org/10.1016/j.molcel.2016.03.017.

Kampinga, H.H. *et al.* (2009) 'Guidelines for the nomenclature of the human heat shock proteins', *Cell Stress and Chaperones*, 14(1), pp. 105–111. Available at: https://doi.org/10.1007/s12192-008-0068-7.

Kampinga, H.H. and Bergink, S. (2016) 'Heat shock proteins as potential targets for protective strategies in neurodegeneration', *The Lancet Neurology*, 15(7), pp. 748–759. Available at: https://doi.org/10.1016/S1474-4422(16)00099-5.

Kampinga, H.H. and Craig, E.A. (2010) 'The HSP70 chaperone machinery: J proteins as drivers of functional specificity', *Nature Reviews Molecular Cell Biology*, 11(8), pp. 579–592. Available at: https://doi.org/10.1038/nrm2941.

Kanaan, N.M. *et al.* (2020) 'Liquid-liquid phase separation induces pathogenic tau conformations in vitro', *Nature Communications*, 11(1), p. 2809. Available at: https://doi.org/10.1038/s41467-020-16580-3.

Kar, K. *et al.* (2011) 'Critical nucleus size for disease-related polyglutamine aggregation is repeat-length dependent', *Nature Structural & Molecular Biology*, 18(3), pp. 328–336. Available at: https://doi.org/10.1038/nsmb.1992.

Karamanos, T.K., Tugarinov, V. and Clore, G.M. (2019) 'Unraveling the structure and dynamics of the human DNAJB6b chaperone by NMR reveals insights into Hsp40-mediated proteostasis', *Proceedings of the National Academy of Sciences*, 116(43), pp. 21529–21538. Available at: https://doi.org/10.1073/pnas.1914999116.

Karzai, A.W. and McMacken, R. (1996) 'A Bipartite Signaling Mechanism Involved in DnaJ-mediated Activation of the Escherichia coli DnaK Protein', *Journal of Biological Chemistry*, 271(19), pp. 11236–11246. Available at: https://doi.org/10.1074/jbc.271.19.11236.

Kelley, W.L. (1998) ‘The J-domain family and the recruitment of chaperone power’, *Trends in Biochemical Sciences*, 23(6), pp. 222–227. Available at: https://doi.org/10.1016/S0968-0004(98)01215-8.

Kerner, M.J. *et al.* (2005) ‘Proteome-wide Analysis of Chaperonin-Dependent Protein Folding in Escherichia coli’, *Cell*, 122(2), pp. 209–220. Available at: https://doi.org/10.1016/j.cell.2005.05.028.

Kim, Y.E. *et al.* (2016) ‘Soluble Oligomers of PolyQ-Expanded Huntingtin Target a Multiplicity of Key Cellular Factors’, *Molecular Cell*, 63(6), pp. 951–964. Available at: https://doi.org/10.1016/j.molcel.2016.07.022.

Kitamura, A., Iwasaki, N. and Kinjo, M. (2018) ‘Molecular chaperone HSP70 prevents formation of inclusion bodies of the 25-kDa C-terminal fragment of TDP-43 by preventing aggregate accumulation’, *Cell Stress and Chaperones*, 23(6), pp. 1177–1183. Available at: https://doi.org/10.1007/s12192-018-0930-1.

Kityk, R. *et al.* (2015) ‘Pathways of allosteric regulation in Hsp70 chaperones’, *Nature Communications*, 6(1), p. 8308. Available at: https://doi.org/10.1038/ncomms9308.

Kityk, R., Kopp, J. and Mayer, M.P. (2018) ‘Molecular Mechanism of J-Domain-Triggered ATP Hydrolysis by Hsp70 Chaperones’, *Molecular Cell*, 69(2), pp. 227-237.e4. Available at: https://doi.org/10.1016/j.molcel.2017.12.003.

Klaips, C.L. *et al.* (2020) ‘Sis1 potentiates the stress response to protein aggregation and elevated temperature’, *Nature Communications*, 11(1), p. 6271. Available at: https://doi.org/10.1038/s41467-020-20000-x.

Klaips, C.L., Jayaraj, G.G. and Hartl, F.U. (2018) ‘Pathways of cellular proteostasis in aging and disease’, *Journal of Cell Biology*, 217(1), pp. 51–63. Available at: https://doi.org/10.1083/jcb.201709072.

Ko, J., Ou, S. and Patterson, P.H. (2001) ‘New anti-huntingtin monoclonal antibodies: implications for huntingtin conformation and its binding proteins’, *Brain Research Bulletin*, 56(3–4), pp. 319–329. Available at: https://doi.org/10.1016/S0361-9230(01)00599-8.

Kremer, B. *et al.* (1994) ‘A Worldwide Study of the Huntington’s Disease Mutation: The Sensitivity and Specificity of Measuring CAG Repeats’, *New England Journal of Medicine*, 330(20), pp. 1401–1406. Available at: https://doi.org/10.1056/NEJM199405193302001.

Kubelka, J., Hofrichter, J. and Eaton, W.A. (2004) ‘The protein folding “speed limit”’, *Current Opinion in Structural Biology*, 14(1), pp. 76–88. Available at: https://doi.org/10.1016/j.sbi.2004.01.013.

Kuiper, E.F.E. *et al.* (2017) ‘Chaperones in Polyglutamine Aggregation: Beyond the Q-Stretch’, *Frontiers in Neuroscience*, 11. Available at: https://doi.org/10.3389/fnins.2017.00145.

Kundel, F. *et al.* (2018) ‘Hsp70 Inhibits the Nucleation and Elongation of Tau and Sequesters Tau Aggregates with High Affinity’, *ACS Chemical Biology*, 13(3), pp. 636–646. Available at: https://doi.org/10.1021/acschembio.7b01039.

Langer, T. *et al.* (1992) 'Successive action of DnaK, DnaJ and GroEL along the pathway of chaperone-mediated protein folding', *Nature*, 356(6371), pp. 683–689. Available at: https://doi.org/10.1038/356683a0.

Laufen, T. *et al.* (1999) 'Mechanism of regulation of Hsp70 chaperones by DnaJ cochaperones', *Proceedings of the National Academy of Sciences*, 96(10), pp. 5452–5457. Available at: https://doi.org/10.1073/pnas.96.10.5452.

Lee, J.-M. *et al.* (2012) 'CAG repeat expansion in Huntington disease determines age at onset in a fully dominant fashion', *Neurology*, 78(10), pp. 690–695. Available at: https://doi.org/10.1212/WNL.0b013e318249f683.

Legleiter, J. *et al.* (2009) 'Monoclonal Antibodies Recognize Distinct Conformational Epitopes Formed by Polyglutamine in a Mutant Huntingtin Fragment', *Journal of Biological Chemistry*, 284(32), pp. 21647–21658. Available at: https://doi.org/10.1074/jbc.M109.016923.

Leitman, J., Ulrich Hartl, F. and Lederkremer, G.Z. (2013) 'Soluble forms of polyQ-expanded huntingtin rather than large aggregates cause endoplasmic reticulum stress', *Nature Communications*, 4(1), p. 2753. Available at: https://doi.org/10.1038/ncomms3753.

Li, J., Qian, X. and Sha, B. (2003) 'The Crystal Structure of the Yeast Hsp40 Ydj1 Complexed with Its Peptide Substrate', *Structure*, 11(12), pp. 1475–1483. Available at: https://doi.org/10.1016/j.str.2003.10.012.

Li, S.-H. *et al.* (1993) 'Huntington's disease gene (IT15) is widely expressed in human and rat tissues', *Neuron*, 11(5), pp. 985–993. Available at: https://doi.org/10.1016/0896-6273(93)90127-D.

Liberek, K. *et al.* (1991) 'The Escherichia coli DnaK chaperone, the 70-kDa heat shock protein eukaryotic equivalent, changes conformation upon ATP hydrolysis, thus triggering its dissociation from a bound target protein', *Journal of Biological Chemistry*, 266(22), pp. 14491–14496. Available at: https://doi.org/10.1016/S0021-9258(18)98713-2.

Lin, H.-K. *et al.* (2017) 'Fibril polymorphism affects immobilized non-amyloid flanking domains of huntingtin exon1 rather than its polyglutamine core', *Nature Communications*, 8(1), p. 15462. Available at: https://doi.org/10.1038/ncomms15462.

Lin, L.T. *et al.* (2021) 'Hsp90 and its co-chaperone Sti1 control TDP-43 misfolding and toxicity', *The FASEB Journal*, 35(5). Available at: https://doi.org/10.1096/fj.202002645R.

Linse, S., Thalberg, K. and Knowles, T.P.J. (2021) 'The unhappy chaperone', *QRB Discovery*, 2, p. e7. Available at: https://doi.org/10.1017/qrd.2021.5.

Lotz, G.P. *et al.* (2010) 'Hsp70 and Hsp40 Functionally Interact with Soluble Mutant Huntingtin Oligomers in a Classic ATP-dependent Reaction Cycle', *Journal of Biological Chemistry*, 285(49), pp. 38183–38193. Available at: https://doi.org/10.1074/jbc.M110.160218.

Lunkes, A. *et al.* (2002) 'Proteases Acting on Mutant Huntingtin Generate Cleaved Products that Differentially Build Up Cytoplasmic and Nuclear Inclusions', *Molecular*

Cell, 10(2), pp. 259–269. Available at: https://doi.org/10.1016/S1097-2765(02)00602-0.

MacDonald, M., Ambrose, C. and Duyao, M. (1993) 'A novel gene containing a trinucleotide repeat that is expanded and unstable on Huntington's disease chromosomes', *Cell*, 72(6), pp. 971–983. Available at: https://doi.org/10.1016/0092-8674(93)90585-E.

Macias, M.J., Wiesner, S. and Sudol, M. (2002) 'WW and SH3 domains, two different scaffolds to recognize proline-rich ligands', *FEBS Letters*, 513(1), pp. 30–37. Available at: https://doi.org/10.1016/S0014-5793(01)03290-2.

Mangiarini, L. *et al.* (1996) 'Exon 1 of the HD Gene with an Expanded CAG Repeat Is Sufficient to Cause a Progressive Neurological Phenotype in Transgenic Mice', *Cell*, 87(3), pp. 493–506. Available at: https://doi.org/10.1016/S0092-8674(00)81369-0.

Mann, D.M.A., Oliver, R. and Snowden, J.S. (1993) 'The topographic distribution of brain atrophy in Huntington's disease and progressive supranuclear palsy', *Acta Neuropathologica*, 85(5). Available at: https://doi.org/10.1007/BF00230496.

Månsson, C. *et al.* (2014) 'Interaction of the Molecular Chaperone DNAJB6 with Growing Amyloid-beta 42 (Aβ42) Aggregates Leads to Sub-stoichiometric Inhibition of Amyloid Formation', *Journal of Biological Chemistry*, 289(45), pp. 31066–31076. Available at: https://doi.org/10.1074/jbc.M114.595124.

Månsson, C. *et al.* (2018) 'Conserved S/T Residues of the Human Chaperone DNAJB6 Are Required for Effective Inhibition of Aβ42 Amyloid Fibril Formation', *Biochemistry*, 57(32), pp. 4891–4902. Available at: https://doi.org/10.1021/acs.biochem.8b00353.

Martin, D.D.O. *et al.* (2015) 'Autophagy in Huntington disease and huntingtin in autophagy', *Trends in Neurosciences*, 38(1), pp. 26–35. Available at: https://doi.org/10.1016/j.tins.2014.09.003.

Marzano, N.R. *et al.* (2022) 'Real-time single-molecule observation of chaperone-assisted protein folding', *Science Advances*, 8(50). Available at: https://doi.org/10.1126/sciadv.add0922.

Mayer, M.P. (2010) 'Gymnastics of Molecular Chaperones', *Molecular Cell*, 39(3), pp. 321–331. Available at: https://doi.org/10.1016/j.molcel.2010.07.012.

Mayer, M.P. and Bukau, B. (2005) 'Hsp70 chaperones: Cellular functions and molecular mechanism', *Cellular and Molecular Life Sciences*, 62(6), pp. 670–684. Available at: https://doi.org/10.1007/s00018-004-4464-6.

Mayer, M.P. and Gierasch, L.M. (2019) 'Recent advances in the structural and mechanistic aspects of Hsp70 molecular chaperones', *Journal of Biological Chemistry*, 294(6), pp. 2085–2097. Available at: https://doi.org/10.1074/jbc.REV118.002810.

Medina, A. *et al.* (2022) 'Prevalence and Incidence of Huntington's Disease: An Updated Systematic Review and Meta-Analysis', *Movement Disorders*, 37(12), pp. 2327–2335. Available at: https://doi.org/10.1002/mds.29228.

Minami, Y. *et al.* (1996) 'Regulation of the Heat-shock Protein 70 Reaction Cycle by the Mammalian DnaJ Homolog, Hsp40', *Journal of Biological Chemistry*, 271(32), pp. 19617–19624. Available at: https://doi.org/10.1074/jbc.271.32.19617.

Mitra, R. *et al.* (2022) 'ATP-Independent Chaperones', *Annual Review of Biophysics*, 51(1), pp. 409–429. Available at: https://doi.org/10.1146/annurev-biophys-090121-082906.

Mitsui, K. *et al.* (2002) 'Purification of polyglutamine aggregates and identification of elongation factor-1alpha and heat shock protein 84 as aggregate-interacting proteins.', *The Journal of neuroscience : the official journal of the Society for Neuroscience*, 22(21), pp. 9267–77. Available at: https://doi.org/10.1523/JNEUROSCI.22-21-09267.2002.

Miyata, Y. *et al.* (2011) 'Molecular chaperones and regulation of tau quality control: strategies for drug discovery in tauopathies', *Future Medicinal Chemistry*, 3(12), pp. 1523–1537. Available at: https://doi.org/10.4155/fmc.11.88.

Monsellier, E. *et al.* (2015) 'Molecular Interaction between the Chaperone Hsc70 and the N-terminal Flank of Huntingtin Exon 1 Modulates Aggregation', *Journal of Biological Chemistry*, 290(5), pp. 2560–2576. Available at: https://doi.org/10.1074/jbc.M114.603332.

Montoya, A. (2006) 'Brain imaging and cognitive dysfunctions in Huntington's disease', *Journal of Psychiatry and Neuroscience* [Preprint].

Moradi, M. *et al.* (2011) 'A Statistical Analysis of the PPII Propensity of Amino Acid Guests in Proline-Rich Peptides', *Biophysical Journal*, 100(4), pp. 1083–1093. Available at: https://doi.org/10.1016/j.bpj.2010.12.3742.

Muchowski, P.J. *et al.* (2000) 'Hsp70 and Hsp40 chaperones can inhibit self-assembly of polyglutamine proteins into amyloid-like fibrils', *Proceedings of the National Academy of Sciences*, 97(14), pp. 7841–7846. Available at: https://doi.org/10.1073/pnas.140202897.

Nachman, E. *et al.* (2020) 'Disassembly of Tau fibrils by the human Hsp70 disaggregation machinery generates small seeding-competent species', *Journal of Biological Chemistry*, 295(28), pp. 9676–9690. Available at: https://doi.org/10.1074/jbc.RA120.013478.

Nakagawa, Y. *et al.* (2022) 'Amyloid conformation-dependent disaggregation in a reconstituted yeast prion system', *Nature Chemical Biology*, 18(3), pp. 321–331. Available at: https://doi.org/10.1038/s41589-021-00951-y.

Nekooki-Machida, Y. *et al.* (2009) 'Distinct conformations of in vitro and in vivo amyloids of huntingtin-exon1 show different cytotoxicity', *Proceedings of the National Academy of Sciences*, 106(24), pp. 9679–9684. Available at: https://doi.org/10.1073/pnas.0812083106.

Newcombe, E.A. *et al.* (2018) 'Tadpole-like Conformations of Huntingtin Exon 1 Are Characterized by Conformational Heterogeneity that Persists regardless of Polyglutamine Length', *Journal of Molecular Biology*, 430(10), pp. 1442–1458. Available at: https://doi.org/10.1016/j.jmb.2018.03.031.

Nillegoda, N.B. *et al.* (2015) ‘Crucial HSP70 co-chaperone complex unlocks metazoan protein disaggregation’, *Nature*, 524(7564), pp. 247–251. Available at: https://doi.org/10.1038/nature14884.

Olzscha, H. *et al.* (2011) ‘Amyloid-like Aggregates Sequester Numerous Metastable Proteins with Essential Cellular Functions’, *Cell*, 144(1), pp. 67–78. Available at: https://doi.org/10.1016/j.cell.2010.11.050.

Österlund, N. *et al.* (2020) ‘Amyloid-β oligomers are captured by the DNAJB6 chaperone: Direct detection of interactions that can prevent primary nucleation’, *Journal of Biological Chemistry*, 295(24), pp. 8135–8144. Available at: https://doi.org/10.1074/jbc.RA120.013459.

Pan, T. *et al.* (2008) ‘The role of autophagy-lysosome pathway in neurodegeneration associated with Parkinson’s disease’, *Brain*, 131(8), pp. 1969–1978. Available at: https://doi.org/10.1093/brain/awm318.

Pandey, N.K. *et al.* (2018) ‘The 17-residue-long N terminus in huntingtin controls stepwise aggregation in solution and on membranes via different mechanisms’, *Journal of Biological Chemistry*, 293(7), pp. 2597–2605. Available at: https://doi.org/10.1074/jbc.M117.813667.

Park, S.-H. *et al.* (2013) ‘PolyQ Proteins Interfere with Nuclear Degradation of Cytosolic Proteins by Sequestering the Sis1p Chaperone’, *Cell*, 154(1), pp. 134–145. Available at: https://doi.org/10.1016/j.cell.2013.06.003.

Pemberton, S. *et al.* (2011) ‘Hsc70 Protein Interaction with Soluble and Fibrillar α-Synuclein’, *Journal of Biological Chemistry*, 286(40), pp. 34690–34699. Available at: https://doi.org/10.1074/jbc.M111.261321.

Perales-Calvo, J., Muga, A. and Moro, F. (2010) ‘Role of DnaJ G/F-rich Domain in Conformational Recognition and Binding of Protein Substrates*’, *Journal of Biological Chemistry*, 285(44), pp. 34231–34239. Available at: https://doi.org/10.1074/jbc.M110.144642.

Perutz, M.F. *et al.* (1994) ‘Glutamine repeats as polar zippers: their possible role in inherited neurodegenerative diseases.’, *Proceedings of the National Academy of Sciences*, 91(12), pp. 5355–5358. Available at: https://doi.org/10.1073/pnas.91.12.5355.

Peskett, T.R. *et al.* (2018) ‘A Liquid to Solid Phase Transition Underlying Pathological Huntingtin Exon1 Aggregation’, *Molecular Cell*, 70(4), pp. 588-601.e6. Available at: https://doi.org/10.1016/j.molcel.2018.04.007.

Peters, M.F. *et al.* (1999) ‘Nuclear Targeting of Mutant Huntingtin Increases Toxicity’, *Molecular and Cellular Neuroscience*, 14(2), pp. 121–128. Available at: https://doi.org/10.1006/mcne.1999.0773.

Piccioni, F. *et al.* (2002) ‘Androgen receptor with elongated polyglutamine tract forms aggregates that alter axonal trafficking and mitochondrial distribution in motoneuronal processes’, *The FASEB Journal*, 16(11), pp. 1418–1420. Available at: https://doi.org/10.1096/fj.01-1035fje.

Pigazzini, M.L. *et al.* (2021) 'An Expanded Polyproline Domain Maintains Mutant Huntingtin Soluble in vivo and During Aging', *Frontiers in Molecular Neuroscience*, 14. Available at: https://doi.org/10.3389/fnmol.2021.721749.

Pircs, K. *et al.* (2018) 'Huntingtin Aggregation Impairs Autophagy, Leading to Argonaute-2 Accumulation and Global MicroRNA Dysregulation', *Cell Reports*, 24(6), pp. 1397–1406. Available at: https://doi.org/10.1016/j.celrep.2018.07.017.

Poirier, M.A. *et al.* (2002) 'Huntingtin Spheroids and Protofibrils as Precursors in Polyglutamine Fibrilization', *Journal of Biological Chemistry*, 277(43), pp. 41032–41037. Available at: https://doi.org/10.1074/jbc.M205809200.

Rampelt, H. *et al.* (2012) 'Metazoan Hsp70 machines use Hsp110 to power protein disaggregation', *The EMBO Journal*, 31(21), pp. 4221–4235. Available at: https://doi.org/10.1038/emboj.2012.264.

Ransome, M.I., Renoir, T. and Hannan, A.J. (2012) 'Hippocampal Neurogenesis, Cognitive Deficits and Affective Disorder in Huntington's Disease', *Neural Plasticity*, 2012, pp. 1–7. Available at: https://doi.org/10.1155/2012/874387.

Ray, S. *et al.* (2020) 'α-Synuclein aggregation nucleates through liquid–liquid phase separation', *Nature Chemistry*, 12(8), pp. 705–716. Available at: https://doi.org/10.1038/s41557-020-0465-9.

Riguet, N. *et al.* (2021) 'Nuclear and cytoplasmic huntingtin inclusions exhibit distinct biochemical composition, interactome and ultrastructural properties', *Nature Communications*, 12(1), p. 6579. Available at: https://doi.org/10.1038/s41467-021-26684-z.

Roos, R.A. (2010) 'Huntington's disease: a clinical review', *Orphanet Journal of Rare Diseases*, 5(1), p. 40. Available at: https://doi.org/10.1186/1750-1172-5-40.

Rosenzweig, R. *et al.* (2019) 'The Hsp70 chaperone network', *Nature Reviews Molecular Cell Biology*, 20(11), pp. 665–680. Available at: https://doi.org/10.1038/s41580-019-0133-3.

Rüdiger, S., Schneider-Mergener, J. and Bukau, B. (2001) 'Its substrate specificity characterizes the DnaJ co-chaperone as a scanning factor for the DnaK chaperone', *The EMBO Journal*, 20(5), pp. 1042–1050. Available at: https://doi.org/10.1093/emboj/20.5.1042.

Ryder, B.D. *et al.* (2022) 'Chaperoning shape-shifting tau in disease', *Trends in Biochemical Sciences*, 47(4), pp. 301–313. Available at: https://doi.org/10.1016/j.tibs.2021.12.009.

Sakono, M. *et al.* (2008) 'Formation of highly toxic soluble amyloid beta oligomers by the molecular chaperone prefoldin', *The FEBS Journal*, 275(23), pp. 5982–5993. Available at: https://doi.org/10.1111/j.1742-4658.2008.06727.x.

Santra, M., Farrell, D.W. and Dill, K.A. (2017) 'Bacterial proteostasis balances energy and chaperone utilization efficiently', *Proceedings of the National Academy of Sciences*, 114(13). Available at: https://doi.org/10.1073/pnas.1620646114.

Saudou, F. and Humbert, S. (2016) 'The Biology of Huntingtin', *Neuron*, 89(5), pp. 910–926. Available at: https://doi.org/10.1016/j.neuron.2016.02.003.

Scheibel, T., Weikl, T. and Buchner, J. (1998) ‘Two chaperone sites in Hsp90 differing in substrate specificity and ATP dependence’, *Proceedings of the National Academy of Sciences*, 95(4), pp. 1495–1499. Available at: https://doi.org/10.1073/pnas.95.4.1495.

Scherzinger, E. *et al.* (1999) ‘Self-assembly of polyglutamine-containing huntingtin fragments into amyloid-like fibrils: Implications for Huntington’s disease pathology’, *Proceedings of the National Academy of Sciences*, 96(8), pp. 4604–4609. Available at: https://doi.org/10.1073/pnas.96.8.4604.

Schneider, J.L. *et al.* (2015) ‘Loss of hepatic chaperone-mediated autophagy accelerates proteostasis failure in aging’, *Aging Cell*, 14(2), pp. 249–264. Available at: https://doi.org/10.1111/acel.12310.

Schneider, M.M. *et al.* (2021) ‘The Hsc70 disaggregation machinery removes monomer units directly from α-synuclein fibril ends’, *Nature Communications*, 12(1), p. 5999. Available at: https://doi.org/10.1038/s41467-021-25966-w.

Schulte, J. and Littleton, J.T. (2011) ‘The biological function of the Huntingtin protein and its relevance to Huntington’s Disease pathology.’, *Current trends in neurology*, 5, pp. 65–78.

Scior, A. *et al.* (2018) ‘Complete suppression of Htt fibrilization and disaggregation of Htt fibrils by a trimeric chaperone complex’, *The EMBO Journal*, 37(2), pp. 282–299. Available at: https://doi.org/10.15252/embj.201797212.

Seidel, K. *et al.* (2012) ‘Cellular protein quality control and the evolution of aggregates in spinocerebellar ataxia type 3 (SCA3)’, *Neuropathology and Applied Neurobiology*, 38(6), pp. 548–558. Available at: https://doi.org/10.1111/j.1365-2990.2011.01220.x.

Shaner, L. *et al.* (2005) ‘The Yeast Hsp110 Sse1 Functionally Interacts with the Hsp70 Chaperones Ssa and Ssb’, *Journal of Biological Chemistry*, 280(50), pp. 41262–41269. Available at: https://doi.org/10.1074/jbc.M503614200.

Sharma, A. *et al.* (2023) ‘Molecular Chaperones as Therapeutic Target: Hallmark of Neurodegenerative Disorders’, *Molecular Neurobiology* [Preprint]. Available at: https://doi.org/10.1007/s12035-023-03846-2.

Sharma, D. and Masison, D. (2009) ‘Hsp70 Structure, Function, Regulation and Influence on Yeast Prions’, *Protein & Peptide Letters*, 16(6), pp. 571–581. Available at: https://doi.org/10.2174/092986609788490230.

Silberg, J.J. *et al.* (2004) ‘Regulation of the HscA ATPase Reaction Cycle by the Co-chaperone HscB and the Iron-Sulfur Cluster Assembly Protein IscU’, *Journal of Biological Chemistry*, 279(52), pp. 53924–53931. Available at: https://doi.org/10.1074/jbc.M410117200.

Sinnige, T., Yu, A. and Morimoto, R.I. (2020) ‘Challenging Proteostasis: Role of the Chaperone Network to Control Aggregation-Prone Proteins in Human Disease’, in *Advances in Experimental Medicine and Biology,* pp. 53–68. Available at: https://doi.org/10.1007/978-3-030-40204-4_4.

Söderberg, C.A.G. *et al.* (2018) ‘Structural modelling of the DNAJB6 oligomeric chaperone shows a peptide-binding cleft lined with conserved S/T-residues at the dimer interface’, *Scientific Reports*, 8(1), p. 5199. Available at: https://doi.org/10.1038/s41598-018-23035-9.

Steffan, J.S. *et al.* (2000) 'The Huntington's disease protein interacts with p53 and CREB-binding protein and represses transcription', *Proceedings of the National Academy of Sciences*, 97(12), pp. 6763–6768. Available at: https://doi.org/10.1073/pnas.100110097.

Sudhakar, S., Manohar, A. and Mani, E. (2023) 'Liquid–Liquid Phase Separation (LLPS)-Driven Fibrilization of Amyloid-β Protein', *ACS Chemical Neuroscience*, 14(19), pp. 3655–3664. Available at: https://doi.org/10.1021/acschemneuro.3c00286.

Tam, S. *et al.* (2009) 'The chaperonin TRiC blocks a huntingtin sequence element that promotes the conformational switch to aggregation', *Nature Structural & Molecular Biology*, 16(12), pp. 1279–1285. Available at: https://doi.org/10.1038/nsmb.1700.

Thakur, A.K. *et al.* (2009) 'Polyglutamine disruption of the huntingtin exon 1 N terminus triggers a complex aggregation mechanism', *Nature Structural & Molecular Biology*, 16(4), pp. 380–389. Available at: https://doi.org/10.1038/nsmb.1570.

Thulasiraman, V. and Matts, R.L. (1998) 'Luciferase Renaturation Assays of Chaperones and Chaperone Antagonists', in *Bioluminescence Methods and Protocols*. New Jersey: Humana Press, pp. 129–141. Available at: https://doi.org/10.1385/0-89603-520-4:129.

Tittelmeier, J., Nachman, E. and Nussbaum-Krammer, C. (2020) 'Molecular Chaperones: A Double-Edged Sword in Neurodegenerative Diseases', *Frontiers in Aging Neuroscience*, 12. Available at: https://doi.org/10.3389/fnagi.2020.581374.

Vale, T.C. and Cardoso, F. (2015) 'Chorea: A Journey through History.', *Tremor and other hyperkinetic movements (New York, N.Y.)*, 5. Available at: https://doi.org/10.7916/D8WM1C98.

Vilchez, D., Saez, I. and Dillin, A. (2014) 'The role of protein clearance mechanisms in organismal ageing and age-related diseases', *Nature Communications*, 5(1), p. 5659. Available at: https://doi.org/10.1038/ncomms6659.

Vonsattel, J.-P. *et al.* (1985) 'Neuropathological Classification of Huntington's Disease', *Journal of Neuropathology and Experimental Neurology*, 44(6), pp. 559–577. Available at: https://doi.org/10.1097/00005072-198511000-00003.

Wacker, J.L. *et al.* (2004) 'Hsp70 and Hsp40 attenuate formation of spherical and annular polyglutamine oligomers by partitioning monomer', *Nature Structural & Molecular Biology*, 11(12), pp. 1215–1222. Available at: https://doi.org/10.1038/nsmb860.

Wagner, A.S. *et al.* (2018) 'Self-assembly of Mutant Huntingtin Exon-1 Fragments into Large Complex Fibrillar Structures Involves Nucleated Branching', *Journal of Molecular Biology*, 430(12), pp. 1725–1744. Available at: https://doi.org/10.1016/j.jmb.2018.03.017.

Wall, D., Zylicz, M. and Georgopoulos, C. (1994) 'The NH2-terminal 108 amino acids of the Escherichia coli DnaJ protein stimulate the ATPase activity of DnaK and are sufficient for lambda replication.', *The Journal of biological chemistry*, 269(7), pp. 5446–51.

Wellington, C.L. *et al.* (2002) ‘Caspase Cleavage of Mutant Huntingtin Precedes Neurodegeneration in Huntington’s Disease’, *The Journal of Neuroscience*, 22(18), pp. 7862–7872. Available at: https://doi.org/10.1523/JNEUROSCI.22-18-07862.2002.

Wentink, A., Nussbaum-Krammer, C. and Bukau, B. (2019) ‘Modulation of Amyloid States by Molecular Chaperones’, *Cold Spring Harbor Perspectives in Biology*, 11(7), p. a033969. Available at: https://doi.org/10.1101/cshperspect.a033969.

Wentink, A.S. *et al.* (2020) ‘Molecular dissection of amyloid disaggregation by human HSP70’, *Nature*, 587(7834), pp. 483–488. Available at: https://doi.org/10.1038/s41586-020-2904-6.

Wexler, A. (2010) ‘Stigma, history, and Huntington’s disease’, *The Lancet*, 376(9734), pp. 18–19. Available at: https://doi.org/10.1016/S0140-6736(10)60957-9.

Williamson, T.E. *et al.* (2010) ‘Modulation of Polyglutamine Conformations and Dimer Formation by the N-Terminus of Huntingtin’, *Journal of Molecular Biology*, 396(5), pp. 1295–1309. Available at: https://doi.org/10.1016/j.jmb.2009.12.017.

Wittung-Stafshede, P. *et al.* (2003) ‘The J-Domain of Hsp40 Couples ATP Hydrolysis to Substrate Capture in Hsp70’, *Biochemistry*, 42(17), pp. 4937–4944. Available at: https://doi.org/10.1021/bi027333o.

Xing, Y. *et al.* (2021) ‘Amyloid Aggregation under the Lens of Liquid–Liquid Phase Separation’, *The Journal of Physical Chemistry Letters*, 12(1), pp. 368–378. Available at: https://doi.org/10.1021/acs.jpclett.0c02567.

Yan, W. and Craig, E.A. (1999) ‘The Glycine-Phenylalanine-Rich Region Determines the Specificity of the Yeast Hsp40 Sis1’, *Molecular and Cellular Biology*, 19(11), pp. 7751–7758. Available at: https://doi.org/10.1128/MCB.19.11.7751.

Yu, L. *et al.* (2019) ‘Association of Cortical β-Amyloid Protein in the Absence of Insoluble Deposits with Alzheimer Disease’, *JAMA Neurology*, 76(7), p. 818. Available at: https://doi.org/10.1001/jamaneurol.2019.0834.

Zhang, H. *et al.* (2023) ‘Effect of evolution of the C-terminal region on chaperone activity of Hsp70’, *Protein Science*, 32(1). Available at: https://doi.org/10.1002/pro.4549.

Zhang, Z. *et al.* (2023) ‘Amyloid Aggregation and Liquid–Liquid Phase Separation from the Perspective of Phase Transitions’, *The Journal of Physical Chemistry B*, 127(28), pp. 6241–6250. Available at: https://doi.org/10.1021/acs.jpcb.3c01426.

Zhuravleva, A., Clerico, E.M. and Gierasch, L.M. (2012) ‘An Interdomain Energetic Tug-of-War Creates the Allosterically Active State in Hsp70 Molecular Chaperones’, *Cell*, 151(6), pp. 1296–1307. Available at: https://doi.org/10.1016/j.cell.2012.11.002.

Zuiderweg, E.R.P. *et al.* (2012) ‘Allostery in the Hsp70 Chaperone Proteins’, in *Topics in Current Chemistry*, pp. 99–153. Available at: https://doi.org/10.1007/128_2012_323.

9. List of tables and figures

10. List of Abbreviations

°C	Degree Celsius
AB	Antibody
ADP	Adenosine diphosphate
ALS	Amyotrophic lateral sclerosis
ANOVA	Analysis of variance
APS	Ammoniumperoxodisulfat
α-Syn	Alpha-synuclein
ATP	Adenosine triphosphate
Aβ	Amyloid beta peptide
BSA	Bovine serum albumin
C. elegans	*Caenorhabditis elegans*
CAG	Cytosine, Adenine, Guanine
Cryo-EM	Cryogenic electron microscopy
Cryo-ET	Cryogenic electron tomography
CTD	C-terminal domain
CyPET	Cyan fluorescent Protein for energy transfer
DD	Dimerization domain
ddH_2O	Double-distilled water
DNA	Deoxyribonucleic acid
DTT	Dithiothreitol
E. coli	*Escherichia coli*
ECL	Enhanced chemiluminescence

EDTA	Ethylenediaminetetraacetic acid
EM	Electron microscopy
Emλ	Emission wavelength
ER	Endoplasmic reticulum
Exλ	Excitation wavelength
FRET	Forster resonance energy transfer
g (µg, mg)	gram (microgram, milligram)
G/F region	Glycine and phenylalanine-rich region
GFP	Green fluorescent protein
GST	Glutathione-S-transferase
h	Hour
HBM	Huntingtin binding motif
HD	Huntington´s Disease
HEAT	**H**untingtin, **E**longation factor 3, protein phosphatase 2**A**, **T**OR1
Hepes	4-(2hydroxyethyl)-1-piperazineethanesulfonic acid
HRPO	Horseradish peroxidase
Hsc	Heat shock cognate protein
Hsp	Heat Shock protein
HTT	Referred to full-length Huntingtin protein in the Introduction section and the following sections referred to Huntingtin Exon1
HTTEx1	Huntingtin Exon1
IPTG	Isopropyl b-D-1-thiogalactopyranoside

JDP	J-domain protein
kDa	Kilodalton
l, (µl, ml)	Liter (microliter, milliliter)
LB	Luria broth
LLPS	Liquid-liquid phase separation
LSM	Laser scanning microscopy
M (nM, µM, mM)	Molar (nanomolar, micromolar, millimolar)
m (nm, µm, mm)	Meter (nanometer, micrometer, millimeter)
MBP	Maltose binding protein
min.	Minute
MWCO	Molecular weight cut-off
n.s.	Not significant
N17	N-terminal 17-residue-long region
NBD	Nucleotide binding domain
NEF	Nucleotide exchange factor
Ni-NTA	Nickel-nitrilotriacetic acid
NMR	Nuclear magnetic resonance
OD	Optical density
PEP	Phosphoenolpyruvic acid
PhoA	Alkaline phosphatase
PMSF	Phenylmethylsulfonyl fluoride
PN	Proteostasis network
PRD	Proline rich domain
rpm	Revolutions per minute

RT	Room temperature
s / sec	Second
S/T motif	Serine/threonine
SBD	Substrate binding domain
SD	Standard deviation
SDS	Sodium dodecyl sulphate
SDS-PAGE	SDS-polyacrylamide gel electrophoresis
SOC	Super Optimal broth with Catabolite repression
SUMO	Small ubiquitin-related modifier
t	Time
T1/2	Half-life time
TBS-(T)	Tris buffered saline (with Tween 20)
TCEP	*Tris(2-carboxyethyl) phosphine*
TDP-43	Transactive response DNA binding protein of 43 kDa
TEM	Transmission Electron Microscopy
TEMED	Tetramethylethylenediamine
TRIC	T-complex protein-1 ring complex
Tris	Tris(hydroxymethyl)aminomethane
UPS	Ubiquitin-proteasome system
V	Volt
w/v	Weight per volume
WB	Western blot
wt	Wild type

XL-MS	Cross-linking mass spectrometry
YPET	Yellow fluorescent Protein for energy transfer
ZFLR	Zinc finger like region

11. Declaration

Versicherung an Eides Statt

Name, Vorname	Özel, Merve

Ich, Merve Özel

versichere an Eides Statt durch meine Unterschrift, dass ich die vorstehende Arbeit selbständig und ohne fremde Hilfe angefertigt und alle Stellen, die ich wörtlich dem Sinne nach aus Veröffentlichungen entnommen habe, als solche kenntlich gemacht habe, mich auch keiner anderen als der angegebenen Literatur oder sonstiger Hilfsmittel bedient habe.
Ich versichere an Eides Statt, dass ich die vorgenannten Angaben nach bestem Wissen und Gewissen gemacht habe und dass die Angaben der Wahrheit entsprechen und ich nichts verschwiegen habe.
Die Strafbarkeit einer falschen eidesstattlichen Versicherung ist mir bekannt, namentlich die Strafandrohung gemäß § 156 StGB bis zu drei Jahren Freiheitsstrafe oder Geldstrafe bei vorsätzlicher Begehung der Tat bzw. gemäß § 161 Abs. 1 StGB bis zu einem Jahr Freiheitsstrafe oder Geldstrafe bei fahrlässiger Begehung.

Ort, Datum / Unterschrift

12. Acknowledgement

First and foremost, I would like to thank my supervisor Prof. Dr. Janine Kirstein for giving me the opportunity to do my PhD in her research group and always supporting and encouraging me throughout all the ups and downs along the way.

I thank Prof. Dr. Erich Wanker for kindly accepting to review my thesis.

I would like to express my gratitude to all the previous and current members of the Kirstein Lab, for being amazing colleagues whom I have learned a lot from and always felt their support. Thanks to Dr. Sara Ayala Mariscal and Dr. Maria Lucia Pigazzini, for sharing their experiences and suggestions especially at the beginning of my PhD. I thank to Regina Nahrstedt and Verena Fischer for always being there whenever I needed help from them. Special thanks to Dr. Annette Peter for always providing insightful guidance and opinions especially during the microscopy sessions in my last year. I would like to acknowledge and thank my close colleague Dr. Yasmin Richter whom I have worked with side by side for four years and exchanged endless ideas. Thanks to my colleague Sabrina Montresor, who closely accompanied me especially throughout the writing process.

Lastly, I thank my family and friends who has always supported and comforted me not only through PhD, but for my whole life, I feel extremely lucky to have you.